AFML-TR-68-334, Part II

MECHANISMS OF DEGRADATION OF POLYMERIC THERMAL CONTROL COATINGS

PART II. EFFECTS OF RADIATION ON SELECTED PIGMENTS

T. E. Firle and T. M. Flanagan
Gulf General Atomic Incorporated

TECHNICAL REPORT AFML-TR-68-334, Part II
March 1970

Air Force Materials Laboratory
Air Force Systems Command
Wright-Patterson Air Force Base, Ohio 45433

AFML-TR-68-334, Part II

MECHANISMS OF DEGRADATION OF POLYMERIC THERMAL CONTROL COATINGS

PART II. EFFECTS OF RADIATION ON SELECTED PIGMENTS

T. E. Firle and T. M. Flanagan
Gulf General Atomic Incorporated

AFML-TR-68-334
Part II

FOREWORD

This report was prepared by Gulf General Atomic Incorporated, and the Space Sciences Laboratory of General Dynamics, Convair Division, under Air Force contract F33615-69-C-1055. This contract was initiated under Project No. 7342, "Fundamental Research on Macromolecular Materials and Lubrication Phenomena," Task No. 734202, "Studies on the Structure-Property Relationship of Polymer Materials." This work was administered under the direction of the Elastomers and Coatings Branch, Nonmetallic Materials Division, Air Force Materials Laboratory, with Mr. Carl P. Boebel as Project Engineer. This report describes work conducted between 4 September 1968 through 3 September 1969.

This report was released by the authors in November 1969 for publication as a Technical Report.

This technical report has been reviewed and is approved.

WARREN P. JOHNSON, Chief
Elastomers and Coatings Branch
Nonmetallic Materials Division
Air Force Materials Laboratory

ABSTRACT

An investigation has been conducted on the mechanisms of degradation of pigments and polymeric coatings for thermal control applications exposed to ultraviolet (uv) and electron irradiation. The materials investigated were rutile (titanium dioxide) and strontium titanate ($SrTiO_3$). The effects of treating the pigments by heating in various gas ambients at elevated temperatures were studied using gas chromatography and electrical conductivity measurements. Significant changes in the surface characteristics were found to result from these treatments. A comparison was made between the reflectance degradation in binderless pigments and silicone-binder coatings exposed to uv light, to energetic electrons, and simultaneously to uv light and electrons. Evidence for stabilization of defect sites by charge capture was discovered in the binderless pigment experiments. This mechanism for defect stabilization does not appear as prevalent in the silicone-binder coatings, since the binder apparently passivates the pigment surface to some extent. The fluence dependence of the degradation and the recovery of the damage in vacuum and in the presence of various gas ambients were also studied.

CONTENTS

CONTENTS (Continued)

FIGURES

FIGURES (Continued)

FIGURES (Continued)

FIGURES (Continued)

TABLES

SECTION I

INTRODUCTION

Thermal control coatings form an essential element in modern spacecraft technology; their degradation by sunlight and by other components of the space environment has been extensively studied. Most of these studies have generally, of necessity, been of an empirical nature and have proved reasonably successful as an aid in developing coatings with satisfactory performance and lifetime.

Some preliminary fundamental studies have been started recently, and it is clear that a study of the mechanisms by which damage occurs is now needed. Better understanding in this area would accomplish three things:

1. Provide a scientific framework for the interpretation of test results

2. Make it possible to devise more reliable simulation procedures for the space environment, for example, by clarifying dose rate effects and detailing the wavelength dependence, thus making possible more accurate predictions of the performance of coatings during specific missions

3. Lead to control of damage mechanisms and hence to improved materials

The pigments selected for the present study consisted of rutile (titanium dioxide) with different impurity levels and highly purified strontium titanate. Most of the work was conducted using the same source material in the form of either binderless specimens or pigments incorporated in a silicone binder.

The irradiation programs were designed to treat both types of specimens with similar electron irradiations, exposure to solar radiation, or combined environments.

Electrical conductivity measurements and gas evolution experiments under exposure to uv excitation were conducted to investigate the role of the surface of the pigment particles.

To obtain information on damage mechanisms, optical reflectance degradation and recovery characteristics were measured using as parameters both irradiation conditions and time. Postirradiation recovery kinetics were also examined in vacuum and with the specimens exposed to various ambient gases.

SECTION II

SAMPLE PREPARATION

Reproducible and known materials and starting conditions are essential for meaningful experiments. This requirement becomes of paramount importance when intercomparisons between materials are to be attempted.

SOURCE MATERIALS

The primary pigment material studied in this program has been rutile (titanium dioxide) powder. Powder (pigmentary) rutile was obtained from a number of sources. A 1-lb sample of high-purity rutile made by a proprietary colloidal process was supplied at no cost by the Research Division of W. R. Grace and Company. A spectrographic analysis of this sample (experimental lot No. 5037-30A) showed 220 ppm silicon, 60 ppm aluminum, 100 ppm nickel, and 10 ppm magnesium. The specific surface area, determined using a BET method with nitrogen, was approximately 1 sq m/g. X-ray diffraction analysis showed the powder to be of rutile phase with a crystallite size greater than approximately 1150 A, approaching the limit of this method when KCl is used for comparison. This material is slightly off-white (yellow tinged) and does not change color when heated to 100 to 120 C.

Stabilized rutile pigments (E. I. DuPont Ti-Pure Type R910) was also used in some of the work reported here. Emission spectroscopy analysis of this pigment (lot No. 4392) showed approximately 4000 ppm aluminum, 1000 ppm silicon, and 10 ppm magnesium. An additional analysis for carbon, made in view of the importance of carbonaceous impurities in the oxygen loss process, yielded a carbon content of 87 ppm. A similar analysis of the W. R. Grace material showed 21 ppm carbon. This constituent is organic carbon (determined by inducing total oxidation and subtracting a value for the inorganic carbonate CO_2 released on acidification).

Strontium titanate pigment was also supplied at no cost by W. R. Grace. This material (experimental lot No. 5069-10) has particles 0.2 to 3 micrometers in size and a surface area, determined by the BET method, of approximately 22 sq m/g. Principal impurities are silicon (in the 1000-ppm range) and lower concentrations of aluminum, barium, copper, iron, and magnesium. The material was not calcined.

SPECIMENS

Binderless Samples

The preparation of binderless specimen coupons, for studying the response of pigment by itself, requires special techniques. Various

methods such as spraying, cold pressing, hot pressing, pressing and sintering, and casting have been used. The most desirable method of sample preparation is one which yields a mechanically strong compact, thick enough to ensure that the substrate will not influence the reflectance and with reasonably good reflectance properties that are relatively insensitive to small variations in the preparation parameters.

For "pigment-only" samples, two methods were used: spraying and casting. With both techniques, water was used an an intermediate vehicle which was removed during or after deposition. Ethyl alcohol was also tried for a few samples.

In the spray technique, a slurry of the pigment is dispersed through an atomizer onto a heated substrate. The critical parameters are pigment purity, particle size, slurry consistency, degree of homogenization, atomizing efficiency of the nozzle, driving force, spray arrival conditions, substrate material, and surface roughness and temperature.

As an alternative to the spray technique, a casting method was developed. In this method, the pigment slurry is put into a die and the vehicle is evaporated. Slurry consistency is critical, but the die material and geometry, the amount of die loading, and the rate of evaporation are also of great importance.

The criteria for judging the specimens are mechanical integrity, surface roughness, microcracks, ease of preparation, reproducibility, similarity of reflectance characteristics, and inherent chemical cleanliness of method. Although from a mechanical standpoint the spray technique has proved more successful, the layers produced are thin and not sufficiently controllable. This is undesirable since layers should be thick enough to represent "bulk" pigment to both the particle and the uv irradiation and allow no optical "shine-through"; i.e., the results should be substrate-independent.

The casting technique has the basic advantage that its parameters are experimentally easier to control and are reproducible once the right set of conditions has been found. The coupons obtained have a thickness of about 1 mm, which easily constitutes bulk pigment. In fact, one of the difficulties has been to cast thin enough cakes to fit through the entrance slit of the integrating sphere of the diffuse reflectance apparatus. Thin coupons have a tendency to crack and curl up during the evaporation phase. Mechanical thinning procedures and coupon to sample-holder bonding methods have been only partially successful. Bonding proved to be surprisingly difficult, owing to the necessity for the adhesive to be compatible with a vacuum environment and noncontaminating with respect to the pigment.

Titanium dioxide from two sources and strontium titanate were used as pigment material for cast and spray coupon preparation. The pigments have been previously characterized as to their material parameters (Ref. 1).

Another set of specimens was prepared from the high-purity titanium dioxide obtained from W. R. Grace (Ref. 1). The samples were formed by compression and compacted to an effective density of 1.5 g/cu cm. A specially designed aluminum sample holder, which doubles as a compression die, makes it possible to transport and mount the coupons repeatedly and reliably in different experimental apparatus. After the conditions for specimen preparation were established, the dry technique yielded higher quality and more reproducible binderless samples than earlier methods.

Pigment-Silicone Samples

A number of specimens were prepared using titanium dioxide pigments in a polymer. The first group consisted of samples of titanium dioxide pigment, SR 125 (General Electric) resin, and A1100 (Union Carbide) adhesive silane. Specimens with these constituents were given only a preliminary evaluation. The system was changed to titanium dioxide as pigment, RTV 602 (General Electric) silicone, and tetramethyl guanidine, TMG (Eastman Organic Chemicals), as the curing agent.[1] Compositions centered around a 1:1 pigment-to-silicone ratio by weight with four drops of TMG for each 50 g of preparation (0.0122 g/drop).

Although a number of pigment-resin-catalyst combinations were tried with both oven cures and vacuum deaeration, using the 1:1 ratio subjected to air drying at room temperature resulted in reproducible specimens with diffuse reflectance values consistently in the 90 percent range.

Results obtained using samples prepared by these various methods are reported in Section IV.

[1]The Air Force Materials Laboratory recommended that this system be studied because it would permit better integration with results obtained in other investigations.

SECTION III

EXPERIMENTAL APPARATUS

This section briefly describes the experimental apparatus developed and used for the present program (a comprehensive description is given in Ref. 1). Two facilities have been utilized:

1. A combined facility at Gulf General Atomic for gas chromatographic, optical, and electrical characterization of pigments enables their reactions and properties to be measured while the pigments are in a stream of ultrapure helium gas. This permits close control of their surface condition.

2. A facility at General Dynamics, Convair Division, makes possible the irradiation of coatings in vacuum with combined uv light and particulate radiation and the in-situ measurement of their reflectance properties without removal from the vacuum system.

GAS CHROMATOGRAPH

General Objectives

A gas chromatograph (GC) is used to identify and measure the gas or gases evolved when pigments are irradiated with uv light or charged particles. The powdered material is permeated by a flow of ultrapure helium gas, which is used as the carrier gas for the chromatograph. Electrical and optical measurements can be made on the sample while it is in the apparatus. The system can also be used to expose a sample to short-duration pulses of other gases, such as oxygen, so that the changes produced in the electrical and optical properties can be measured.

Experimental Procedures

After a sample has been placed in the cell, the apparatus is purged with helium (generally overnight) and the trap is baked out. Bypassing the sample cell and trap, a sample gas mixture is injected to give a quantitative calibration of the gas chromatograph. The trap is then placed on-stream and cooled to liquid nitrogen temperatures, and the background impurities in the helium gas stream are condensed for a suitable time, typically 30 min. Typical background concentrations are: O_2, 18 parts per billion (ppb); N_2, 20 ppb; CO_2, not measurable (less than 1 ppb); CO, not measurable (less than 2 ppb). Background concentrations are repeatable but appear to arise from small, probably virtual, leaks. They can be reduced to negligible values by using an additional trap (a molecular sieve

cooled with liquid nitrogen) just ahead of the sample cell. Typical concentrations of O_2 and N_2 are then less than 2 ppb. The sample cell is then introduced into the line, and a check is made to determine that the background with the sample in the line is the same as that without the sample. The sample may then be irradiated (with uv light, for example), following which the evolved gases are collected for 30 min in the cooled trap, then dumped by warming the trap, and measured by the gas chromatograph. Typical sensitivities are 10^{-8} moles of most gases. Since a 0.1- or 0.01-mole sample can be used, a gas evolution of 10^{-6} or 10^{-7} of the sample weight can be studied.

Multistation Gas Chromatograph Facility

Time utilization is usually poor with gas chromatographic equipment, since gas collection and analysis are restricted to one experimental setup. Design criteria were therefore reviewed to provide for the selection of a number of experimental stations. This simple requirement presented a real design challenge owing to the extreme sensitivity of the system to contamination, pressure changes, leakage, etc. After a number of components for this type of application had been tested, it was found that both flexible lines and reliable, low-leakage couplings could be obtained, although some have a short service life.

An analysis of the principal switching requirements for the gas flow circuits was carried out. Two independent supply sources of helium carrier gas are required and must be coupled reliably and functionally to the multiple experiment access, gas-collection, and GC analysis sections. The gas switching is accomplished by providing seven high-quality multiport valves, specifically designed for GC use and proved reliable in the field.

The new multistation gas chromatograph reflectance (MSGCR) system which resulted is highly sensitive and has excellent reproducibility and flexibility. This instrument permits rapid connection of a variety of independent experimental stations without requiring that one experiment be physically removed to permit analysis of another. The system has a number of subsections: carrier gas supplies, calibration gas supplies and metering, purification station ports for mating to experimental cells, gas accumulation traps, flow monitoring and control, and a two-column GC analyzer with strip chart recorder and disc integrator. Provisions have been made for effective interfacing of the experimental cell with the diffuse reflectance measurement apparatus and the uv irradiation source.

The carrier gas purification section consists of a molecular sieve trap in series with an activated charcoal trap which can be independently chilled by liquid nitrogen. Both the primary and secondary helium carrier gas circuits have their own independent purification trains.

The analysis section consists of a GC driving a strip chart recorder with a disc integrator. This section also contains the valve which connects the input of the GC to the multistation loop. The design is such that the primary carrier always flows past the detectors; the secondary carrier is

always excluded from the detectors (see Figure 1). However, selection permits either carrier circuit to flow through the multistation loop. One of the resulting features is that the analyzing section can be calibrated independently of any system connected to the multistation loop. Further, a number of experimental systems can be connected to the various stations and purged or otherwise tested using the secondary carrier or an attached vacuum system. This feature also protects the GC analyzer from being inadvertently saturated or contaminated.

The multistation section presently accommodates four pairs of fittings connected to four multiport valves. These four stations are series connected and provide the input to the GC analyzer as selected by its main valve.

An example of the operational capabilities of the MSGCR is given in Table I. Station 1 is used here to insert a "pretrap." This trap contains silica gel and when chilled removes contamination from either virtual leaks or desorbing species from the line. Its function is to obtain the purest possible carrier gas for the experimental cell. This function is important, especially if one is concerned with catalytic or synergistic effects. Station 2 connects the experimental cell into the line. This experimental cell loop can be part of a reflectivity measurement apparatus or, alternatively, can be an electrical conductivity cell permitting other measurements to be carried out simultaneously with the gas analysis. Stations 3 and 4 are used in this example with identical accumulation traps. These traps vastly increase the basic sensitivity of the GC, particularly for small quantities of gases evolving at slow rates. Utilizing two traps allows the collection of two gas samples at two different times without interruption of the experiment, and thus provides an efficient way to survey evolution rates. When appropriate, the initial gas portion can be analyzed while the second one is being collected.

The sample shown in Table I represents the flow patterns and utilization of the various stations in a real experimental situation. Others can be used or developed.

ELECTRICAL CONDUCTIVITY APPARATUS

Changes in the electrical conductivity of pigments are associated with the changes produced in their optical properties by irradiation and are expected to provide a very sensitive and useful technique for the study of the fundamental changes produced in thermal coating materials by irradiation. By inducing changes by different but controlled means--as, for instance, chemical reduction or irradiation by uv light or charged particles--response can be measured and compared to give a clue to the determining primary mechanisms. However, measurements on powders using dc techniques are complicated by such effects as packing of the powder and are difficult to reproduce or interpret. Measurements using ac techniques make it possible to separate out contact effects and also yield information on frequency dependence.

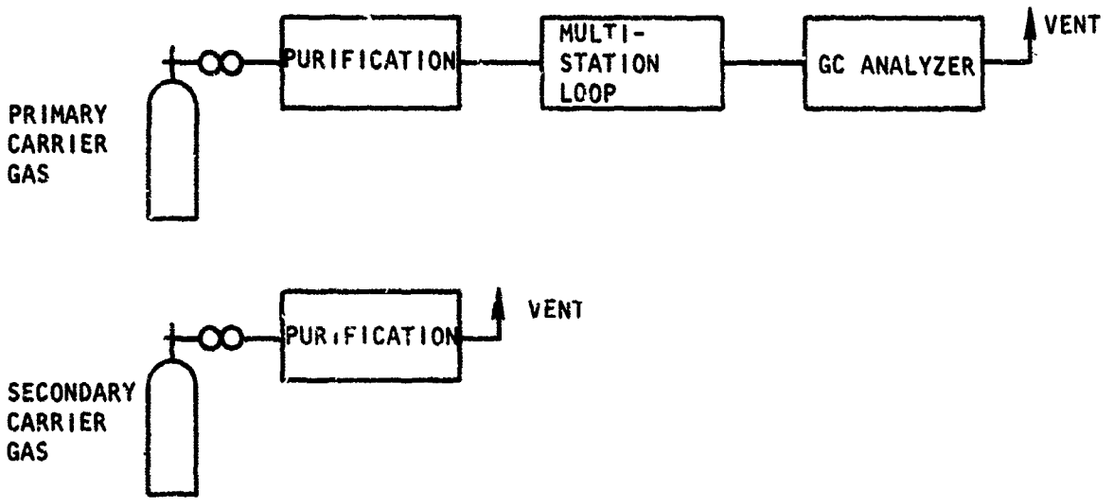

(a) Carrier circuits during analysis

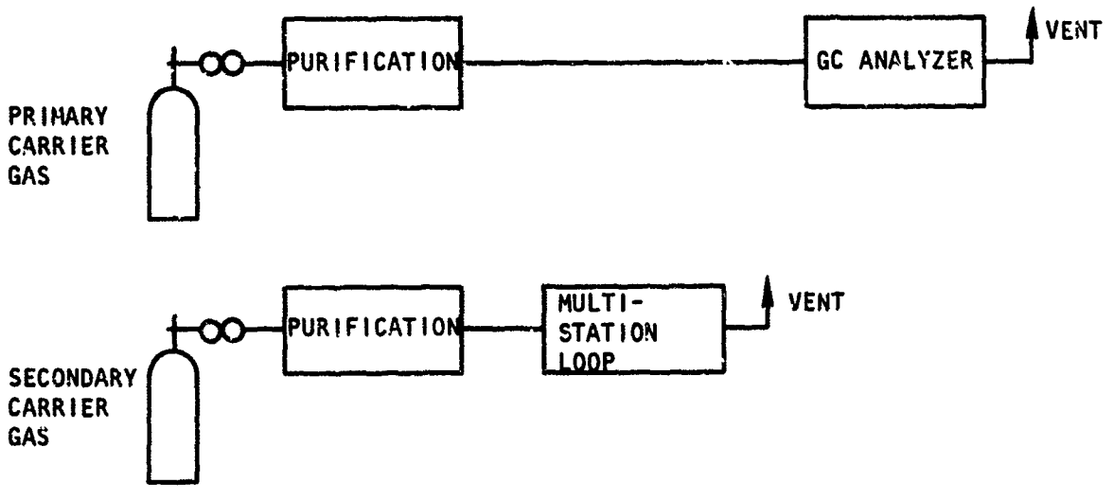

(b) Carrier circuits for preanalysis or postanalysis treatment

Figure 1. Carrier Gas Circuits

TABLE I
EXAMPLE OF OPERATIONAL FUNCTIONS OF MSGCR

Input[a]	Sta. 1 Pre-trap[b]	Sta. 2 Exp Cell[c]	Sta. 3 Accum Trap[d]	Sta. 4 Accum Trap[d]	Link Vent	GC Mode (Identification and Quantity)	Vent Flow-meter	Principal Objective for Operation
2	—	—	—	—	↑	1	↑	Flush multistation loop
2	2	2	2	2	↑	1	↑	Flush and check each station first individually, then in combination, then in series
1+ calib	—	—	1 cold	—	—	Monitor	↑	Calibration and collection efficiency (also for No. 4)
1	—	—	1 hot	—	—	Analyze	↑	Determine collection efficiency (also for No. 4)
1	—	—	1 cold	—	—	Monitor	↑	Collect background (also for No. 4)
1	—	—	1 hot	—	—	Analyze	↑	Determine background
1	1 cold	1	—	1 cold	—	Monitor	↑	Accumulate unknown evolving gases
1	1 cold	1	1 cold	1 hot	—	Analyze first gases	↑	While continuing gases collect at station 3, analyze the accumulated first portion
1	1 cold	—	1 hot	—	—	Analyze second portion	↑	Determine rate of gas evolution

NOTE:

1 = primary helium carrier gas
2 = secondary helium carrier gas
calib = calibration gases
cold = chilled by liquid nitrogen
hot = warmed by boiling water
↑ = vent
— = direct transfer; station not in use, bypassed

[a] Selection of carrier gas through multistation loop

[b] Silica gel trap, chilled in LN_2, removes line impurity gases and absorbs virtual leaks

[c] Can be system, located at reflectance apparatus, electrical conductivity bridge, etc.

[d] Used to extend sensitivity, especially for low desorption rates

It is desirable to be able to quantitatively monitor chemical changes which result in the evolution of one or more gaseous reaction products from the specimen. By incorporating the specimen cell used for the measurement of electrical conductivity into the stream of a GC, both qualitative and quantitative studies can be carried out.

At low frequencies ($10^3 \leq f \leq 10^8$ Hz), the cell and sample combination has the characteristic of a lossy capacitor. To determine the loss (and hence the conductivity), the sample cell is placed in parallel with the tuning capacitor of a Q-meter and the resonant capacitance is adjusted to obtain a resonance condition. Details of the experimental apparatus and theory are given in Ref. 1. Experimental results are discussed in Section IV.

DUAL-BEAM REFLECTOMETER FOR USE WITH GAS CHROMATOGRAPH

A special optical apparatus enables changes in the reflectance of samples to be measured while the samples are in the helium stream of the GC. This inert chemical ambient is necessary since exposure to air is known to bleach the changes in the reflectance. The sample is in the form of a powder contained in a quartz cell. The powder is viewed from beneath and can be exposed to uniform irradiation by a uv lamp through the bottom of a rectangular quartz cell.

The optical arrangement is shown in Figure 2. Light from a single source is allowed to follow one of two optical paths, depending upon the position of a mechanical chopper. When the light beam traverses one path, it is reflected from the surface of a reference specimen; when the light traverses the other path, it is reflected from the surface of the test sample. Both light paths converge on the entrance slit of a scanning monochromator, traverse the monochromator, and then fall on a photomultiplier mounted at the exit slit of the monochromator. The light falling on the photomultiplier comes alternately from the control and test specimens. After electronic shaping and processing, the difference signal between the sample and the optical reference channel can be plotted on an X-Y recorder against a monochromator dial reading (related to wavelength).

IN-SITU APPARATUS

An in-situ apparatus was used for measuring reflectance changes in coatings after exposure to either separate or combined uv and particulate irradiation. This equipment, designed and built by Convair, enables eight samples to be mounted in a vacuum chamber, to be exposed one at a time, or both at once, to either uv or charged particle irradiation, and to have their reflectance measured over the range from 0.23 to 2.3 micrometers without removal from the vacuum system.

The apparatus consists of a horizontal 12-in.-diameter vacuum chamber incorporating an integrating sphere, particulate beam tube, sample-cooling thermostat, and sample wheel as shown schematically in Figure 3. The samples are mounted on a central axle and may be rotated 180 degrees from the irradiation position into the integrating sphere for reflectance

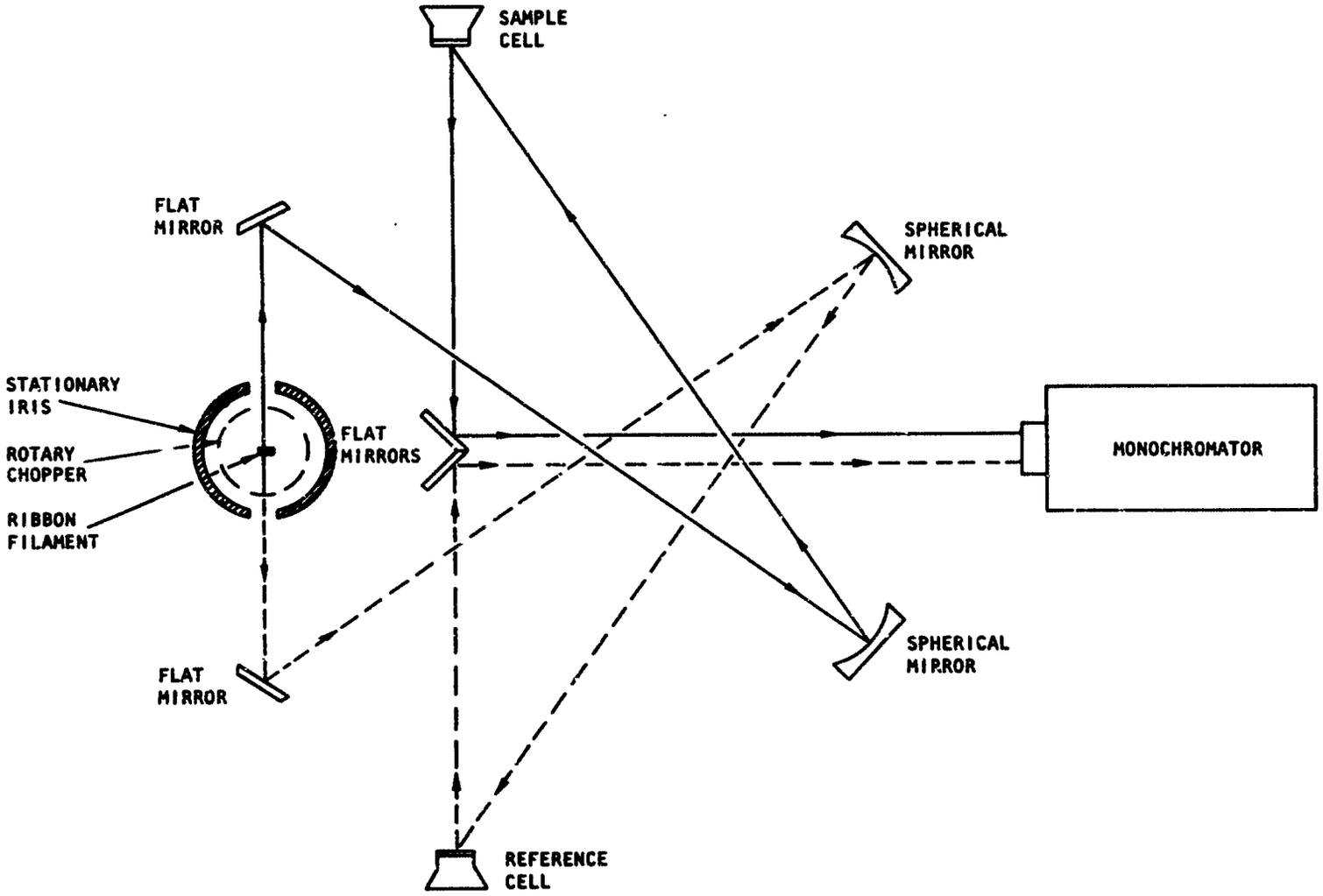

Figure 2. Schematic of Dual-Beam Reflectometer

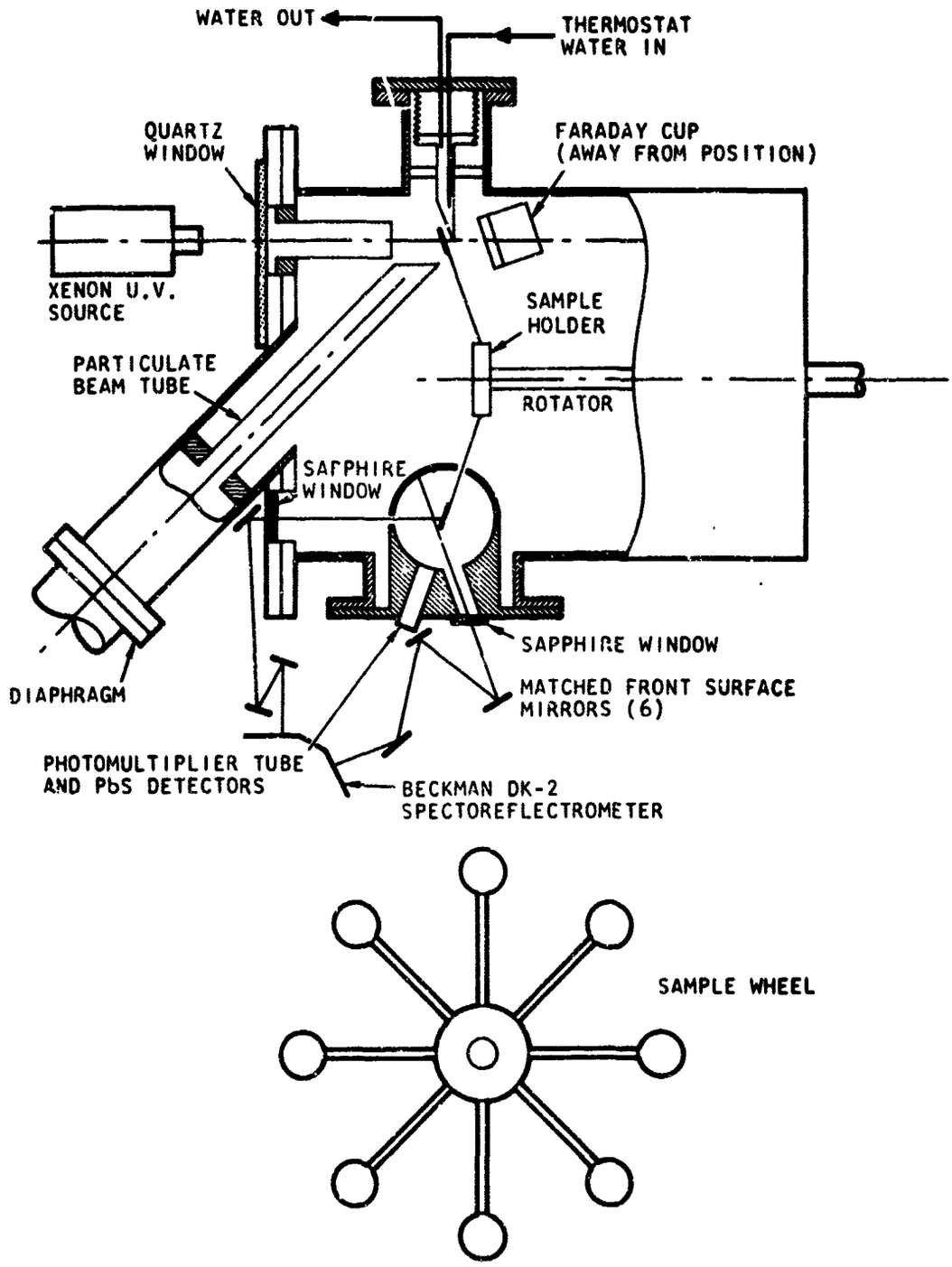

Figure 3. Diagram of In-Situ Apparatus

measurements. Monochromatic beams are provided by a Beckman DK-2 spectrophotometer and are made incident to the sphere by transfer optics as shown in Figure 3. In the present work, uv radiation was obtained from a Spectrolab X-25 Solar Simulator, and electrons were provided by a Radiation Dynamics Dynamitron at the Convair accelerator facility.

A Beckman DK-2 spectrophotometer was employed to provide light dispersion, detection, and recording. This dual-beam instrument ordinarily is used to measure percent absorption as a function of wavelength but can be readily adapted to the requirements of reflectance measurements, since it is a ratio recording device. With the present arrangement, it was necessary to "reverse" the beams, i.e., make the sample beam follow the path conventionally followed by the reference beam, and vice versa. This "reversal" was accomplished by a simple modification of the instrument electronics. The instrument scans the full spectrum and provides readout on a chart.

The transfer optics for the sample and reference beams between the spectrophotometer and the integrating sphere consist of six front-surfaced aluminized mirrors and two sapphire windows. The sapphire windows are a matched pair. Each beam employs one concave mirror and two plain mirrors and one window which serves to admit the beam to the vacuum tank. The full set of six mirrors were aluminized at one time to ensure uniformity between the two beams.

The integrating sphere employs a center-mounted sample and requires no reference sample. The inside diameter is 5 in., and the inner surface is coated with 2 mm of MgO.

Monochromatic sample and reference beams enter the sphere through openings as shown schematically in Figure 3. The sample beam strikes the sample in the center of the sphere. The reference beam strikes the sphere wall at approximately the same position as a specularly reflected beam from the sample would strike the wall. This optical arrangement helps greatly to eliminate errors due to non-uniform illumination of the sphere. The trace corresponding to 100 percent reflectance is obtained by rotating the sample out of position, so that the sample beam strikes the sphere wall at a point approximately opposite that at which the reference beam strikes the wall.

The detectors are mounted so as to view symmetrically the point at which the sample and the reference beam strike the sphere. A photomultiplier tube is used from 0.23 to 0.6 micrometer, and a lead sulfide cell is used from 0.6 to 2.3 micrometers. The face of the end-on photomultiplier tube and the face of the lead sulfide cell mount on the surface of the sphere.

Samples are attached to a sample wheel which is mounted to a central axle in the chamber. The sample wheel can accommodate 1-in.-diameter samples; one sample at a time can be irradiated. Samples are placed in the irradiation position for application of a radiation flux and are placed in the measurement position for determination of reflectance characteristics. Placement is accomplished by rotating the sample wheel using a cylindrical magnet.

A sample being irradiated requires cooling to dissipate the heat deposited in it. The metal bellows arrangement, shown in Figure 3, can be used to provide thermostatting of the sample. After a sample is rotated into position, a 1-in.-diameter metal tube, cooled by a constant flow of water, is moved inward to a point where the angled surface is in full contact with the sample backing. This provides temperature control throughout the irradiation of the samples. After an irradiation is complete, the cooling device is moved away from the sample to allow the wheel to be rotated.

In the ideal case, the particulate and uv radiations should strike the sample simultaneously and from the same direction, but practical and economic constraints imposed upon our laboratory simulation apparatus preclude this procedure since one radiation beam would have to be transmitted through the source of the other. To cause both beams to impinge on the sample as close to normal as possible, it was decided to have the beams 45 degrees apart, with the sample positioned so that each beam would strike the sample with one half of this angle from the normal.

When positioned for irradiation, the sample is at an angle of 22.5 degrees from the normal for the flux of ionizing radiation and also for the flux of uv light. This geometrical arrangement makes possible simultaneous irradiations with uv and charged particles. Both the charged particle beam and the uv beam are confined by the internal defining tubes shown in Figure 3 so as to prevent radiation from striking samples other than the sample in the irradiation position.

The vacuum for the in-situ apparatus is obtained with an ion pump suspended below the tank. Four cryogenic sorption pumps mounted on a manifold can be used individually or together for initial pumping from atmospheric pressure.

Plasma discharge during ion pump startup can cause significant changes in sample properties. This problem is avoided by ensuring that the pressure in the tank is reduced to a level below the Paschen region before the gate valve is opened to the ion pump. Further, an ion reflection system consisting of alternately charged grids in the throat of the in-situ apparatus tank prevents ion penetration from this source into the working region.

The oil-pumped accelerator vacuum system is separated from the ultra-high-vacuum system of the reflectance chamber by a 0.002-in. aluminum window. To obtain an energy of 1 MeV after passage through the window, 1.025-MeV electrons must be used. A collimating aperture is provided beyond the window to eliminate the scattered beam and provide a well-defined area.

Electrons generated and accelerated in the Dynamitron are directed down a beam tube to a deflection magnet where the beam is deflected 90 degrees into the in-situ apparatus, through the 2-mil aluminum diaphragm. Flux measurements are made at the sample position using a Faraday cup with an opening the same size as the sample. The Dynamitron can provide electrons in the energy range from 0.4 to 2.5 MeV.

SECTION IV

RESULTS

INTRODUCTION

Various experiments have been carried out in which diffuse reflectance spectra, gas chromatographic analyses, electrical conductivity, and other measurements have been obtained. In most cases, specimens have been subjected to various controlled ambient conditions and exposed to uv or electron irradiation. The response of the samples is dependent on many environmental variables, including time. Because of the complexity of even our simple pigment formulations or pigment-binder systems, multiple samples and controls were used in the experimental work whenever feasible.

Many of the experiments were relatively self-contained and are reported below as units or grouped together by subject.

COMBINED ELECTRICAL CONDUCTIVITY AND GAS EVOLUTION

Electrical conductivity is a characteristic of the state of a specimen, and hence can be used to identify mechanisms in conjunction with reflectance degradation under uv and particle irradiation. Previous work on other oxides has shown the high sensitivity of electrical conductivity changes to gas evolution (Ref. 2). In the present program, electrical conductivity measurements combined with simultaneous monitoring of gas evolution using a gas chromatograph were made while subjecting the pigments to purging with helium gas at both room temperature and 200 C. The objective of these experiments was to observe (1) changes in electrical conductivity following the initial flushing of the pigment with purified helium gas at room temperature, (2) changes in electrical conductivity due to the desorption of gas when heating the material, (3) the amount and species of evolved gases, (4) the desorption rate at elevated temperature, (5) the stability of resulting room temperature electrical conductivity, and (6) the degree of completion of desorption.

The chronological relationship between the temperature and gas ambient changes is important. A typical series of experimental measurement events is shown schematically in Figures 4 and 5 for two different titanium dioxide powder charges. Elapsed time is indicated in hours between gas chromatograph analyses; in-situ electrical conductivity measurements are represented by "σ." The carrier gas was purified helium, except for the initial room temperature electrical conductivity measurements

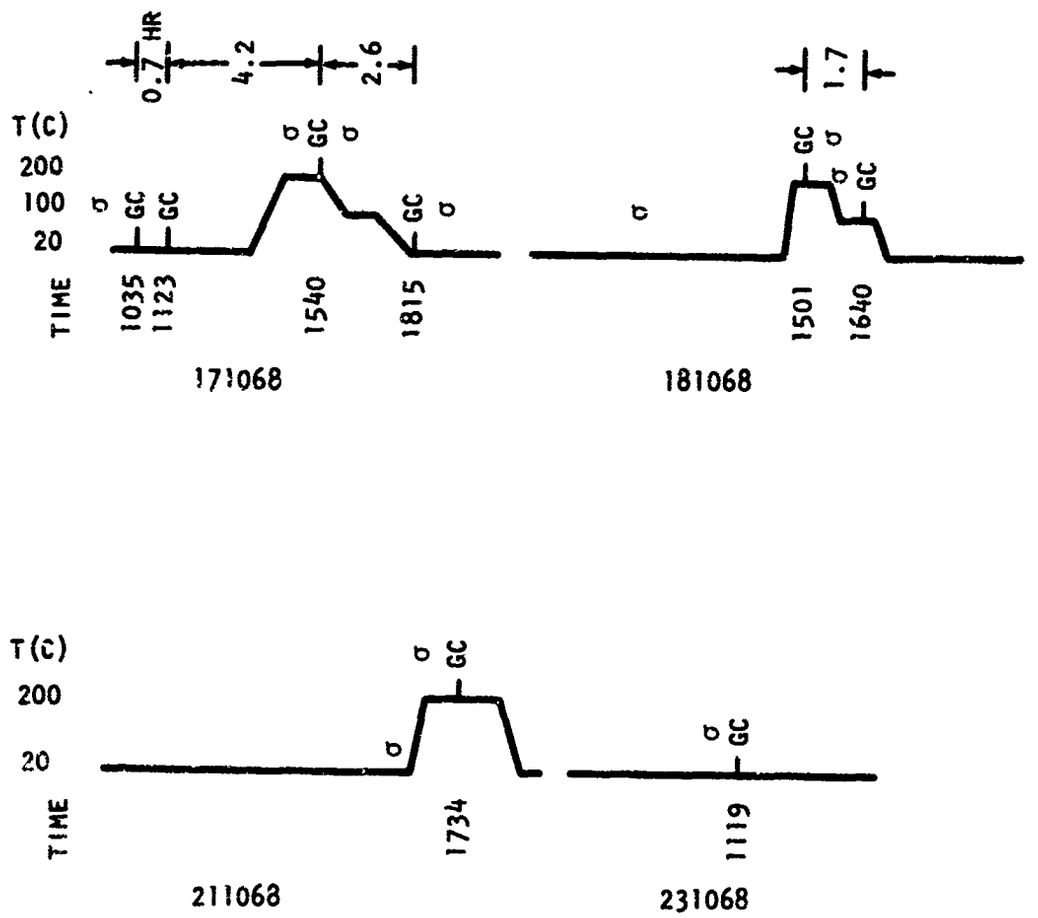

Figure 4. Heating and Measurement Chronology for TiOx(R910)/L13.1, No Binder

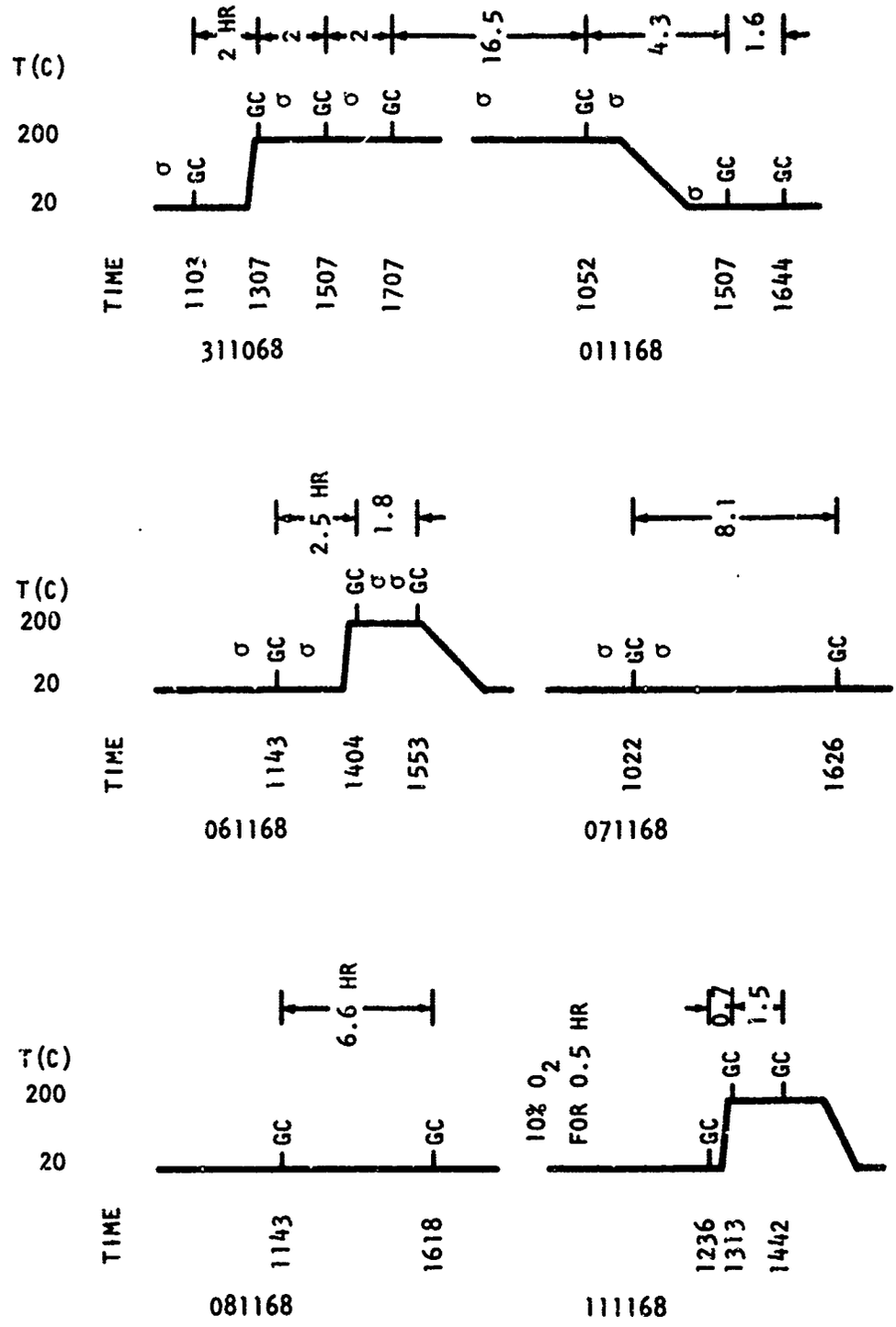

Figure 5. Heating and Measurement Chronology for TiOx(R910)/L23.13, No Binder

in air or backfilling with a 10 percent oxygen/90 percent helium mixture as noted. Electrical conductivity measurements were also made on strontium titanate in air, but this material was not heat-treated.

Electrical Conductivity

Electrical resistance was measured as a function of frequency for two powder charges of titanium dioxide and one of strontium titanate. Curve 1 of Figure 6 is a plot of log cell resistance versus log frequency for the initial state of TiOx(R910)/L13.1 in air. The air was then purged from the cell with purified helium gas and the cell heated to 200 C; the heat-treatment and measurement history is shown in Figure 4. The electrical resistance as determined at the elevated temperature is shown by curve 2 of Figure 6. Upon cooling to room temperature, the material was remeasured and the data plotted in curve 3 were obtained.

These results indicate that a rather large change in state had occurred, which might have been caused either by the heat treatment or by a permanent desorption. To investigate this effect, the cell was recycled from room temperature to 200 C and then remeasured. The results are given in Figure 7, where the room temperature values were determined just before and after the heating period. The shift to higher resistance indicates that heating continues to have an effect although it is smaller than the original change. Since the cell had not been further exposed to any ambient other than pure helium gas, the question regarding the effect of displacing the initial "as-received" air by helium at room temperature was left open.

To determine whether the pigment state had been stabilized, recycling to 200 C was undertaken. The results are given in Figure 8, where powder is seen to have reached a condition of stability since the room temperature resistance remained unchanged. Temperatures of less than 200 C (for times on the order of hours) are therefore not expected to change the conductance of the pigment. This is important since maximum (surface) temperatures during irradiation are below 200 C.

The question concerning the effect of the initial purging was examined using fresh material from the same source (specimen designated TiOx(R910)/L23.13). Measurements of the as-received electrical resistance in air and after purging with purified helium gas were performed. The results are plotted in curves 1 and 2 of Figure 9, respectively. These results demonstrate clearly that purging at room temperature produces changes similar to those observed with higher-temperature purging. (Since the powder charges differed, the actual resistance values should not be compared directly with those of the previous figures.)

To obtain a stable state, this powder charge was cycled to 200 C according to the schedule illustrated by Figure 5. After having been treated for a total of approximately 25 hr at 200 C in helium, the charge had the final room temperature resistance shown by curve 3 of Figure 9.

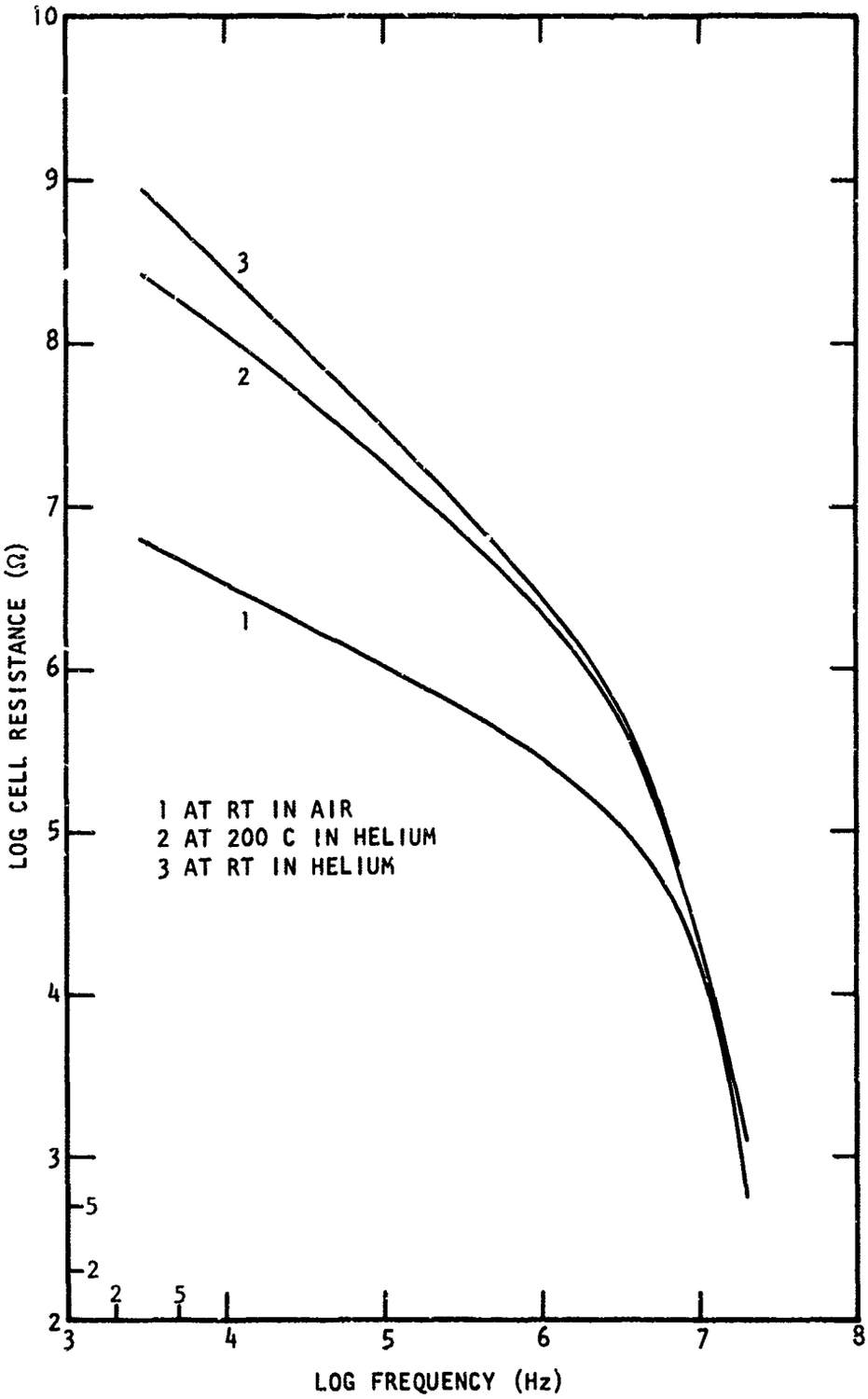

Figure 6. Cell Resistance Versus Frequency (TiOx(R910)/L13.1, No Binder)

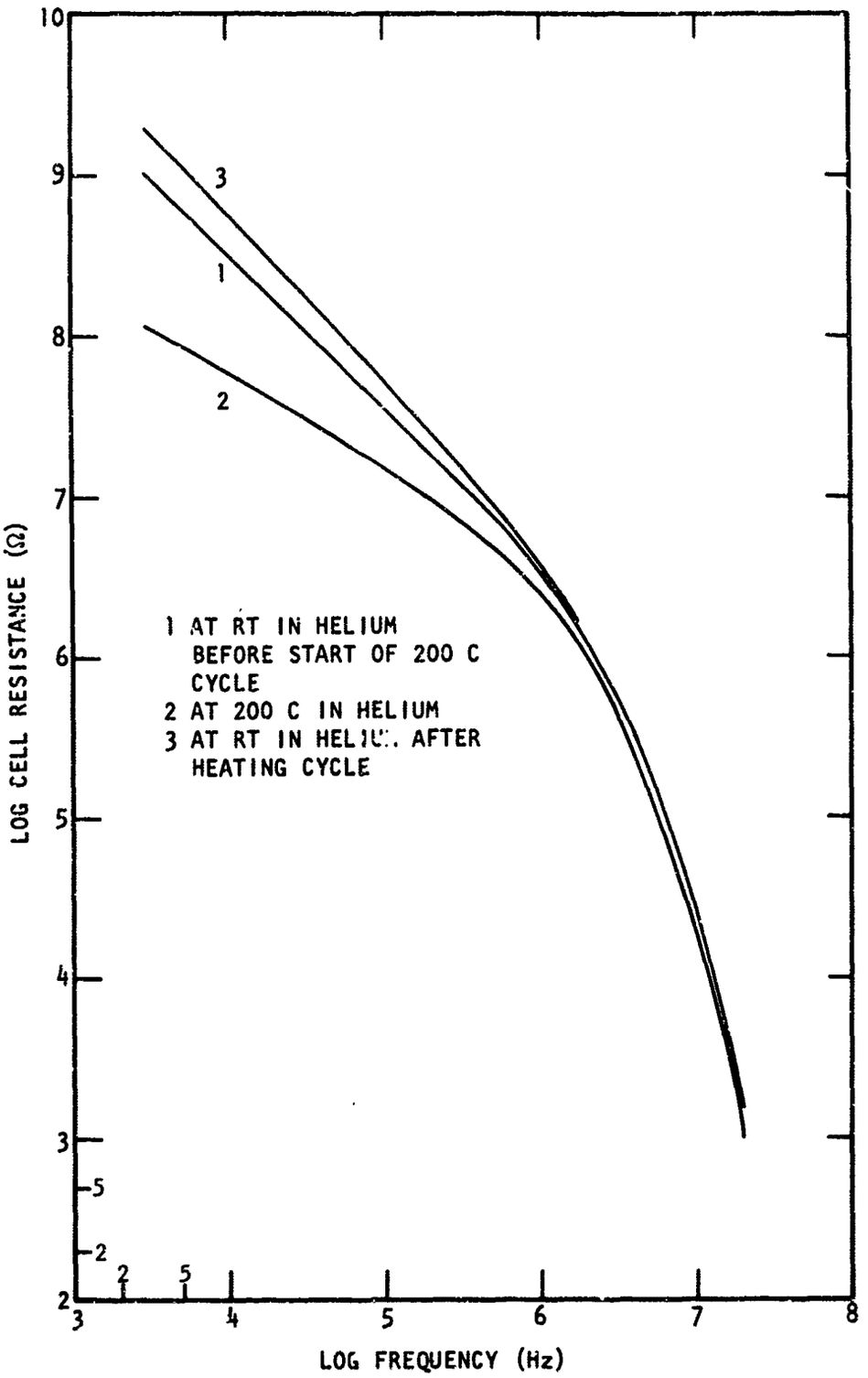

Figure 7. Cell Resistance Versus Frequency After Recycling to 200 C (TiOx(R910)/L13.1, No Binder)

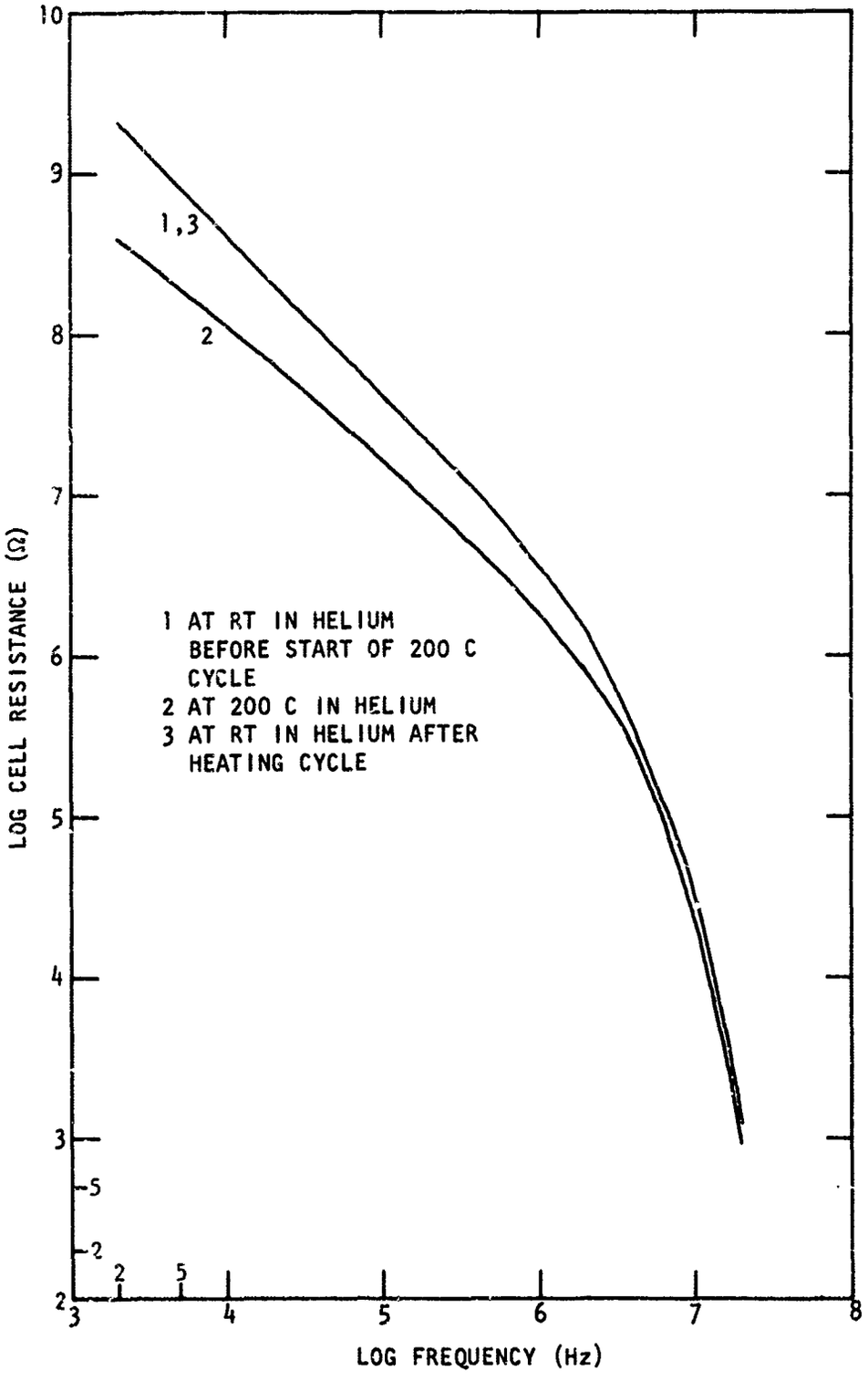

Figure 8. Cell Resistance Versus Frequency After Further Recycling to 200 C (TiOx(R910)/L13.1, No Binder)

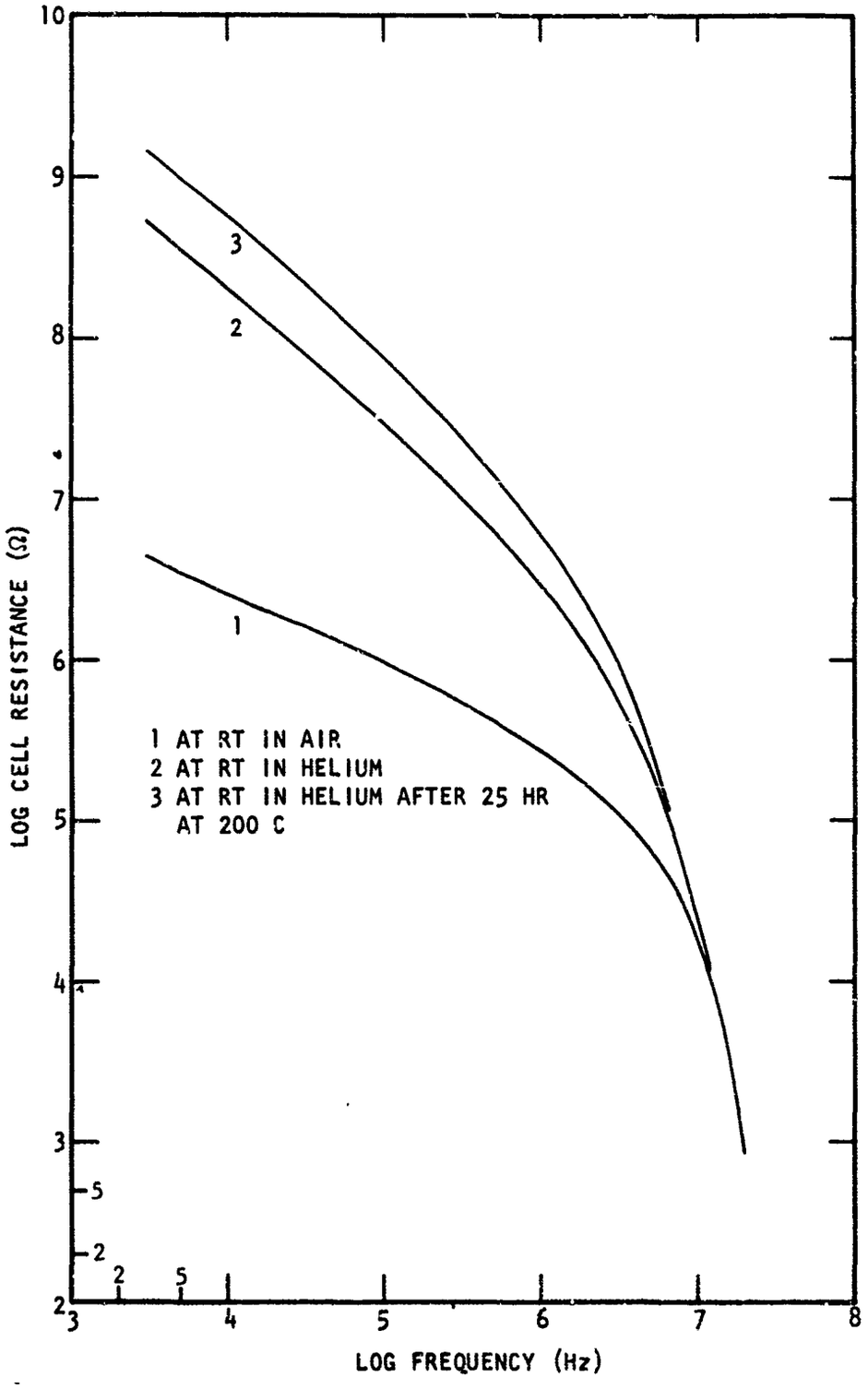

Figure 9. Cell Resistance Versus Frequency in Air and after Purging with Helium (TiOx(R910)/L2?.13, No Binder)

The heat treatment thus does have an additional effect. Readmitting air to the cell and then letting the cell stand for a few weeks brings the room temperature resistance partially back toward its starting condition, but this sorption effect could not be examined further.

Progressive changes in conductivity, measured at 200 C with time-at-temperature as a parameter, are shown in Figure 10. It is interesting to note that overnight treatment at 200 C resulted primarily in a bulge in the intermediate frequency region.

Some experiments were made on two strontium titanate charges in the as-received state. The results are plotted in Figure 11. The separation between the two lower curves can be accounted for by the difference in amount, and therefore distribution, of pigment material. The upper curve shows the results of a titanium dioxide charge for comparison. If the two pigment species are in equivalent as-received states, as far as adsorbed gases and water vapor are concerned, then the strontium titanate has a considerably lower intrinsic resistivity than the titanium dioxide powder.

Gas Chromatograph Analysis

The evolution of gases was studied in conjunction with electrical conductivity measurements for three different powder charges of titanium dioxide. The heating and measurement chronology of two of these samples has been given in Figures 4 and 5, and the electrical conductivity results were discussed above. The third charge demonstrated the same general behavior.

After installation of the electrical conductivity cell containing the pigment in the sample loop of the gas chromatograph, purified helium gas was used to purge the sample of those gaseous constituents which would desorb at room temperature at a helium gas pressure of about 2 atm. The general procedure consisted of making simultaneous gas chromatograph and electrical conductivity measurements. The gases were collected on a chilled accumulation trap for a 30-min interval under standard flow conditions, since gas evolution is in the parts-per-billion range. The powder charge, packing, and particle size all affect the carrier gas through-put. Since the through-put can be varied over only a relatively small range, the actual collection times used were adjusted instead. All data were normalized to a trapping time of 30 min, which is the interval used with the standard gases in the calibration procedure.

The only gas species observed were oxygen, nitrogen, and carbon dioxide, although had they been present, carbon monoxide and low-molecular-weight hydrocarbons could readily have been detected. The results obtained for pigment charge TiO_2(R910)/L13.1 are presented in Table II. Room temperature analyses yielded both oxygen and nitrogen in amounts greater than had been observed as "background" from an empty cell. When the charge was heated to 200 C, carbon dioxide appeared in fairly large amounts.

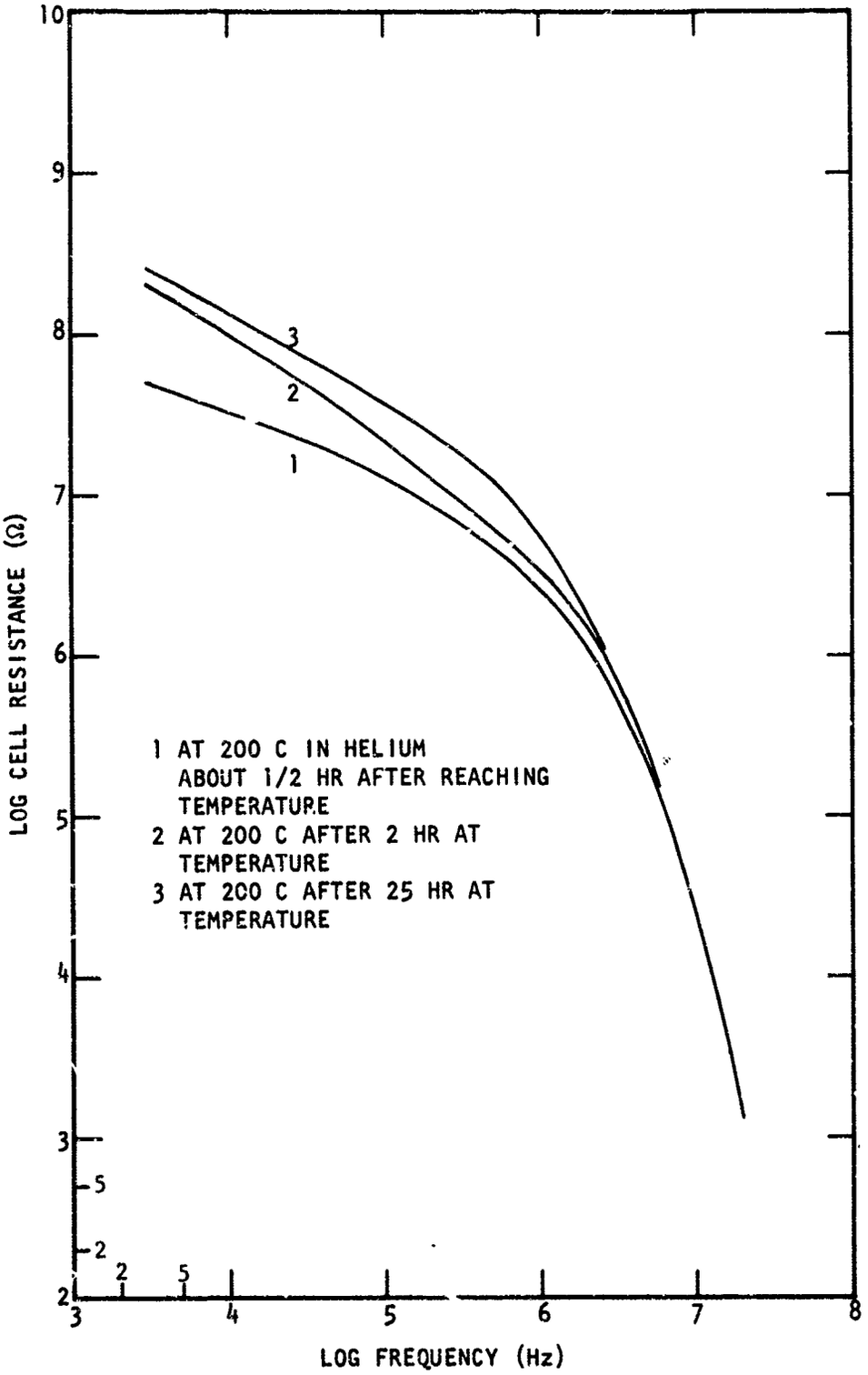

Figure 10. Cell Resistance Versus Frequency after Cycling to 200 C (TiOx (R910)/L23.13, No Binder)

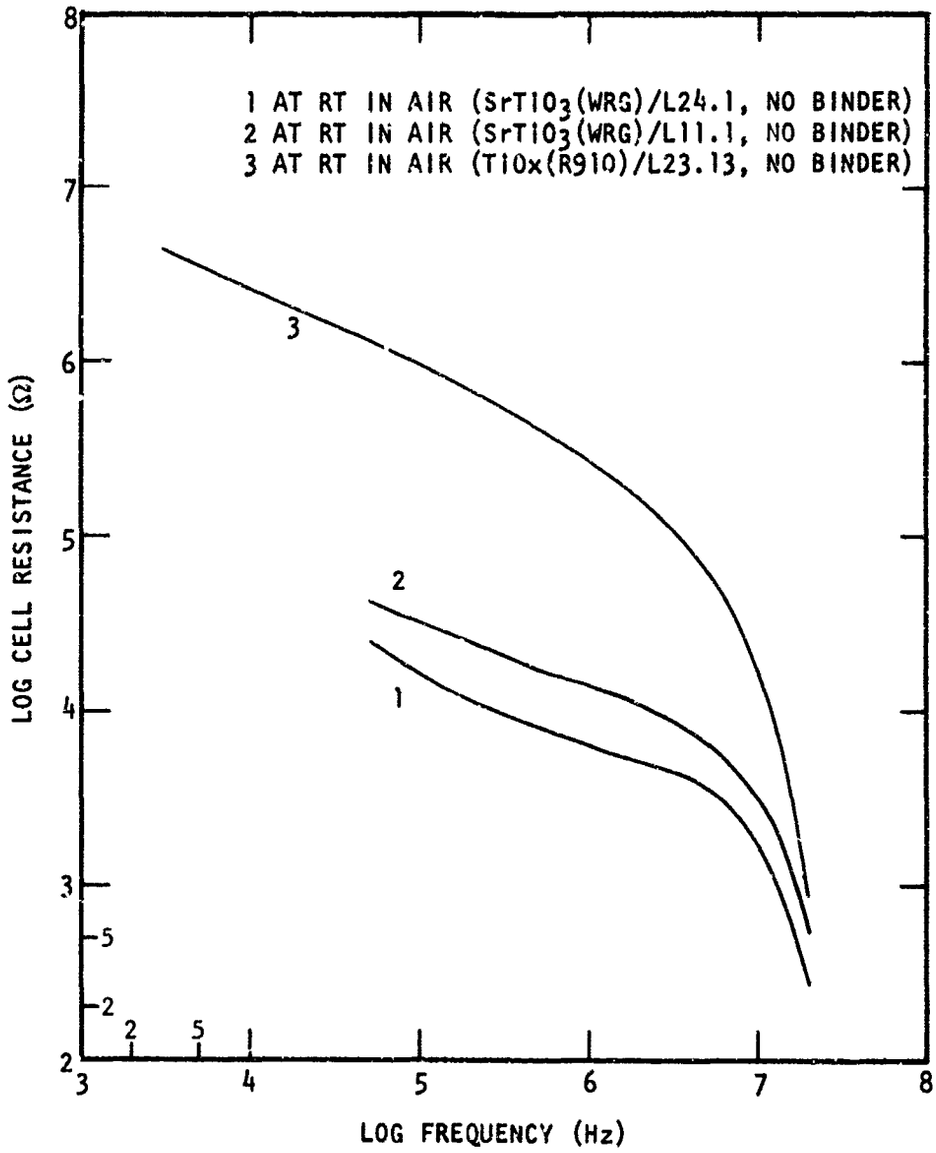

Figure 11. Cell Resistance Versus Frequency for Two Strontium Titanate and One Titanium Dioxide Charges

TABLE II

EVOLVED GASES FOR HEATING RUNS (TiOx-D/L13.1)

O_2 ($\times 10^{-9}$)[a]	N_2 ($\times 10^{-9}$)[a]	N_2/O_2	CO_2 ($\times 10^{-9}$)[a]	Condition[b]	Code	
					Date	Time
23	64	2.8	<1	Typical empty cell background		
63	150	2.4	<1	Room temperature	171068	1035
40	250	6.3	1670	Heated to 200 C	171068	1540
64	118	1.9	<1	Cooled to 100 C, then measured at room temperature	171068	1815
42	221	5.3	113	200 C	181068	1501
41	234	5.7	41	100 C	181068	1640
23	240	11.0	210	200 C	211068	1734
94	221	2.4	<1	Room temperature	231068	1119

[a] Moles per 30-min collection time

[b] See also the temperature chronology shown in Figure 4.

Evolution of carbon dioxide stopped when the temperature was lowered first to 100 C and then to room temperature. Additional carbon dioxide was observed when the powder was reheated to 200 C; however, the evolution took place at a lower rate.

Thus, for the carbon dioxide evolution, one observes that (1) most of the gas is released during the warming period, (2) evolution is a strong function of temperature, and (3) reheating to 200 C results in additional evolution, given heating times on the order of hours.

The significance of the oxygen and nitrogen and their ratio is not clear. It appears that heating increases nitrogen evolution while the oxygen concentration is actually falling below the room temperature value, which would indicate that some of the background oxygen is removed from the carrier gas stream. This may be due to oxidation of the stainless steel cell or may be a reaction of the titanium dioxide. If the room temperature background oxygen and nitrogen are due to a small or virtual leak, then the N_2/O_2 ratio should not have increased on heating. Attempts at balancing the oxygen concentration, assuming that either leaked or entrapped air has provided the oxygen necessary to yield the observed carbon dioxide from postulated carbonaceous impurities, lead to the conclusion that a definite oxygen shortage exists.

The same type of experiment was repeated using pigment charge TiOx-D/L23.13 with the heating and measurement schedule shown in Figure 5. The objectives of this particular experiment were (1) to separate gas evolution during the initial heating for each cycle, (2) to determine the desorption dynamics by sampling the rate of gas evolution at various times at elevated temperature, (3) to determine if there were subsequent changes at room temperature, and (4) to observe the effect of flushing the powder with oxygen after heating.

Results of the gas chromatograph analyses for TiOx-D/L23.13 are given in Table III. Behavior similar to that observed in the first test generally prevailed. The amount of carbon dioxide evolved initially was larger in this test. Keeping the sample at 200 C for more than 20 hr showed that the evolution proceeded at a rate which was approximately inversely proportional to time. Flushing with a 10 percent oxygen/90 percent helium mixture about doubled the carbon dioxide concentration on subsequent heating to 200 C. However, the amount evolved was much less than that initially evolved.

OPTICAL MEASUREMENTS

Specimen Evaluation

To evaluate samples prepared by various methods, particularly by spraying and casting, diffuse reflectance measurements were made using a Cary 14 spectrophotometer with an integrating sphere attachment. The spectral response of the individual coupons was obtained to determine reproducibility between samples of the same batch. The differences in the optical properties due to using the spray technique or casting the same source material were established.

TABLE III
EVOLVED GASES FOR HEATING RUNS (T10x-D/L23.15)

O_2 ($\times 10^{-9}$)[a]	N_2 ($\times 10^{-9}$)[a]	N_2/O_2	CO_2 ($\times 10^{-9}$)[a]	Condition[b]	Code	
					Date	Time
23	64	2.8	<1	Typical empty cell background		
361	1018	2.7	62	Room temperature	311068	1103
252	888	3.5	9450	Heated to 200 C	311068	1307
265	672	2.5	266	At 200 C	311068	1507
232	568	2.5	129	At 200 C	311068	1707
224	766	3.4	24	At 200 C	011168	1052
300	741	2.5	<1	Room temperature	011168	1507
284	822	2.9	<1	Room temperature	061168	1143
255	706	2.8	<1	Heated to 200 C	061168	1404
164	659	4.0	104	At 200 C	061168	1553
219	731	3.3	<1	Room temperature	071168	1022
348	951	2.7	<1	Room temperature	081168	1143
Flush with 10% O_2/90% He for 30 min					111168	1143
228	741	3.1	<1	Room temperature	111168	1236
322	912	2.8	263	Heated to 200 C	111168	1313
150	621	4.1	155	At 200 C	111168	1442

[a]Moles per 30-min collection time

[b]See also the temperature chronology shown in Figure 5.

Diffuse reflectance versus wavelength is plotted in Figure 12 for rutile titanium dioxide pigment (DuPont R910). The wavelength range is divided into two sections: from 0.3 to 0.6 micrometer and, on a more compressed scale, from 0.6 to 2.0 micrometers. Three cast coupons are represented by curve 1 and two sprayed samples by curve 2. Maximum spread within the group of cast coupons is less than 0.3 percent. The sprayed specimens differed from each other by less than 1 percent over the entire spectral range.

A comparison of the cast and the sprayed samples shows that (1) in the short-wavelength visible region the agreement is very good, and (2) with increasing wavelength (greater than 0.6 micrometer), the reflectance of the sprayed samples falls further and further below that of the cast specimens. It appears that the second result is due to "shine-through"; i.e., the pigment layer is too thin to scatter longer-wavelength incident radiation back out and it is instead absorbed by the substrate.

Samples of titanium dioxide from another source (W. R. Grace) have been similarly prepared in cast and sprayed form. Generally, the preparation of samples of this material was more difficult. In Figure 13 the spectral response of the samples is shown. The sprayed samples had a maximum spread (at 2 micrometers) of approximately 4 percent; only one cast specimen was mounted successfully. The same features can be noted as for the DuPont material: the cast specimen reflectance is above that of the sprayed material, with divergence occurring even near the absorption edge. Some further absorption near the short-wave visible region is evident, which correlates with the slightly "off-white" appearance of the pigment.

Specimens of strontium titanate gave the spectral response shown in Figure 14. Agreement for the three cast coupons was excellent. The four sprayed samples group into two pairs, and the typical spectrum for each pair is given in the figure. The maximum difference (at 2 micrometers) was about 4 percent, while agreement within each pair was very good. This division into pairs was due to the spray preparation: the outermost samples in the spray pattern gave the lower reflectance, and the two inner samples grouped to give the higher response. It is believed that the inner specimen received slightly more pigment material, resulting in less "shine-through."

Ethanol was used as the vehicle for spraying the strontium titanate because water was not successful. Since there was concern about the possible residuum of carbonaceous impurities left in the pigment, an analysis for organic carbon was made, which showed only about 50 ppm. The cast specimens were prepared from a water slurry.

From Figure 14 it should also be noted that the high reflectance region extends to lower wavelengths as compared with titanium dioxide: the absorption edge of the strontium titanate powder appears at 0.36 micrometer.

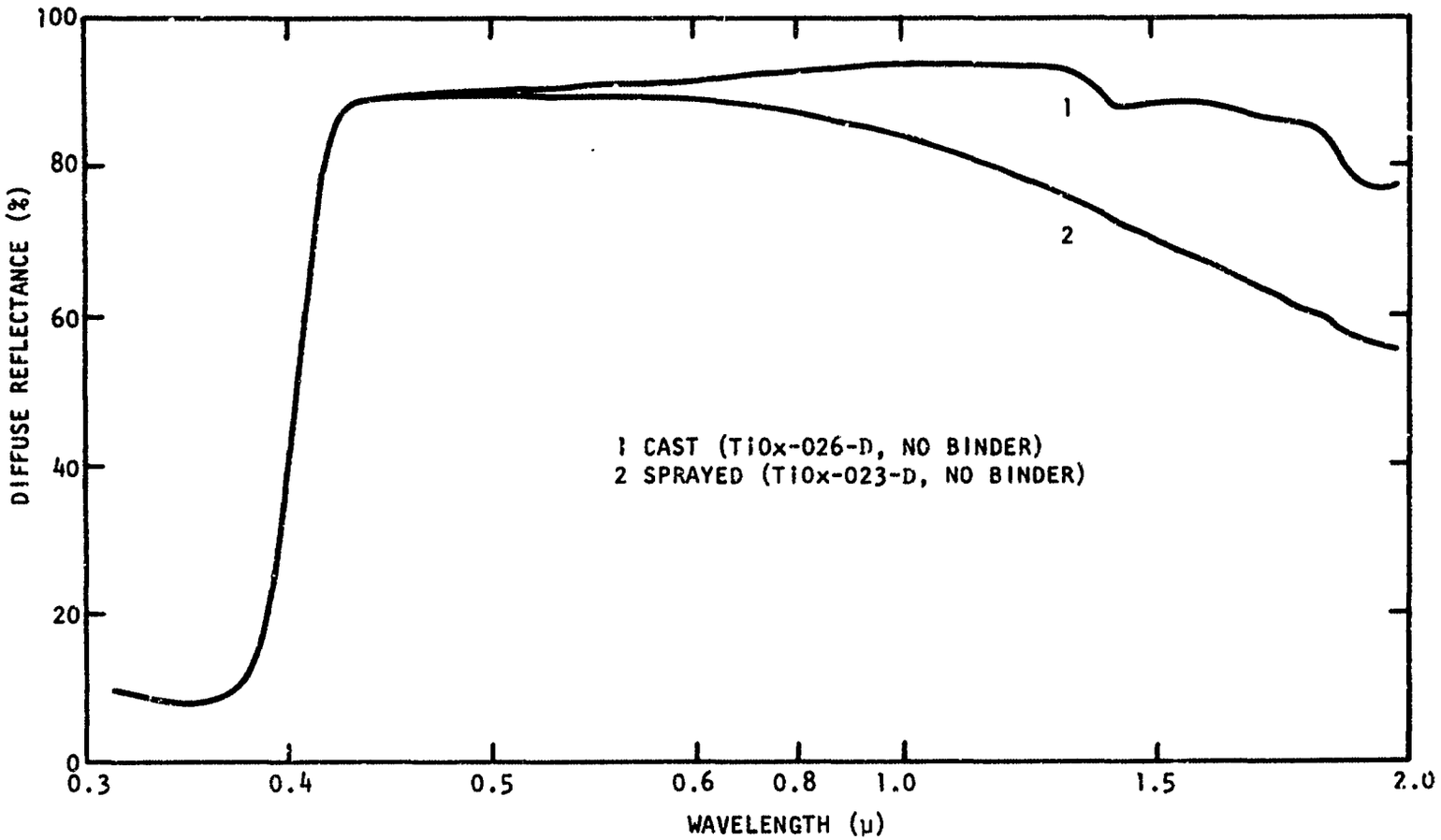

Figure 12. Diffuse Reflectance Spectra for Cast and Sprayed Titanium Dioxide

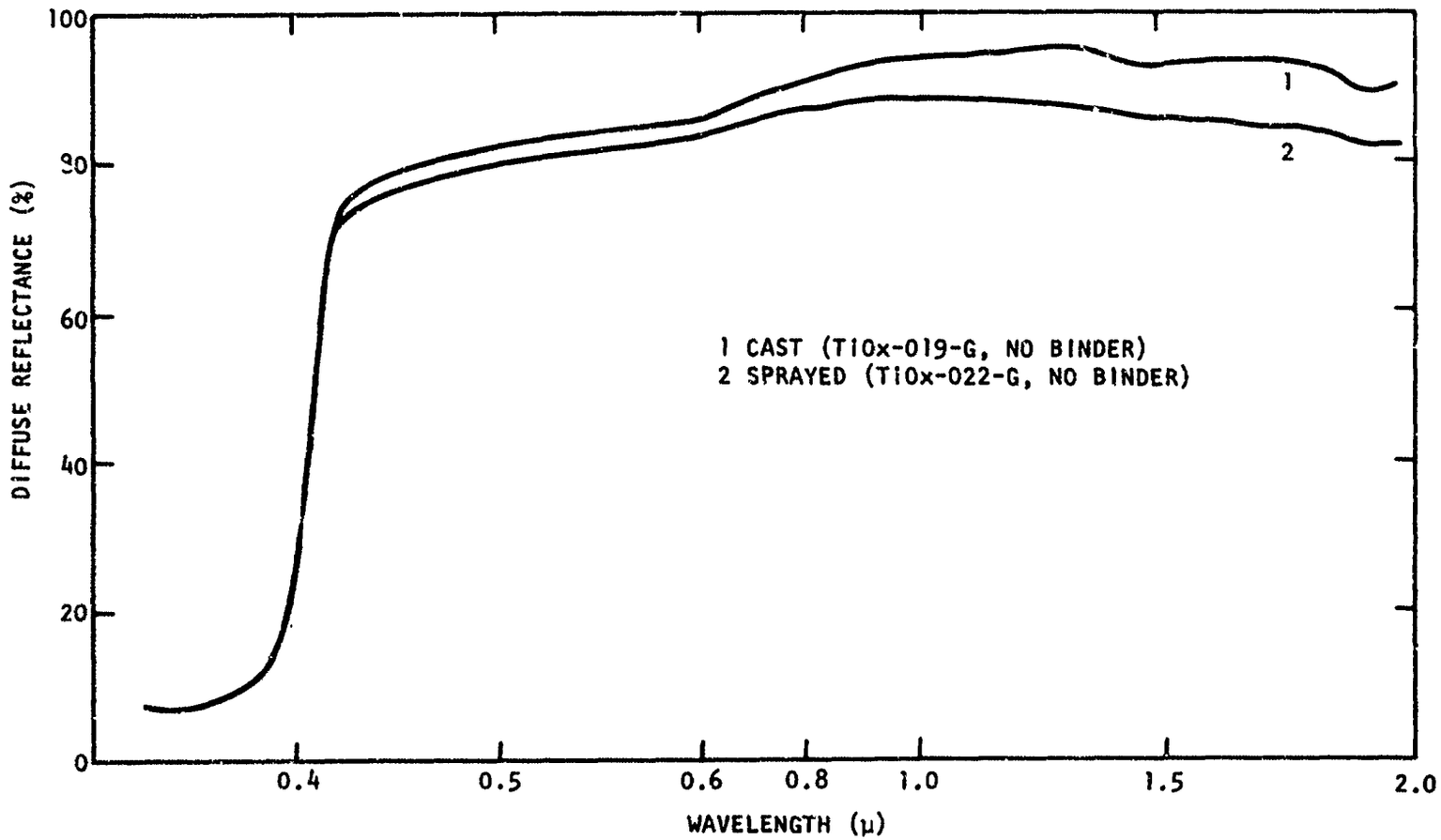

Figure 13. Diffuse Reflectance Spectra for Cast and Sprayed Titanium Dioxide from Another Source

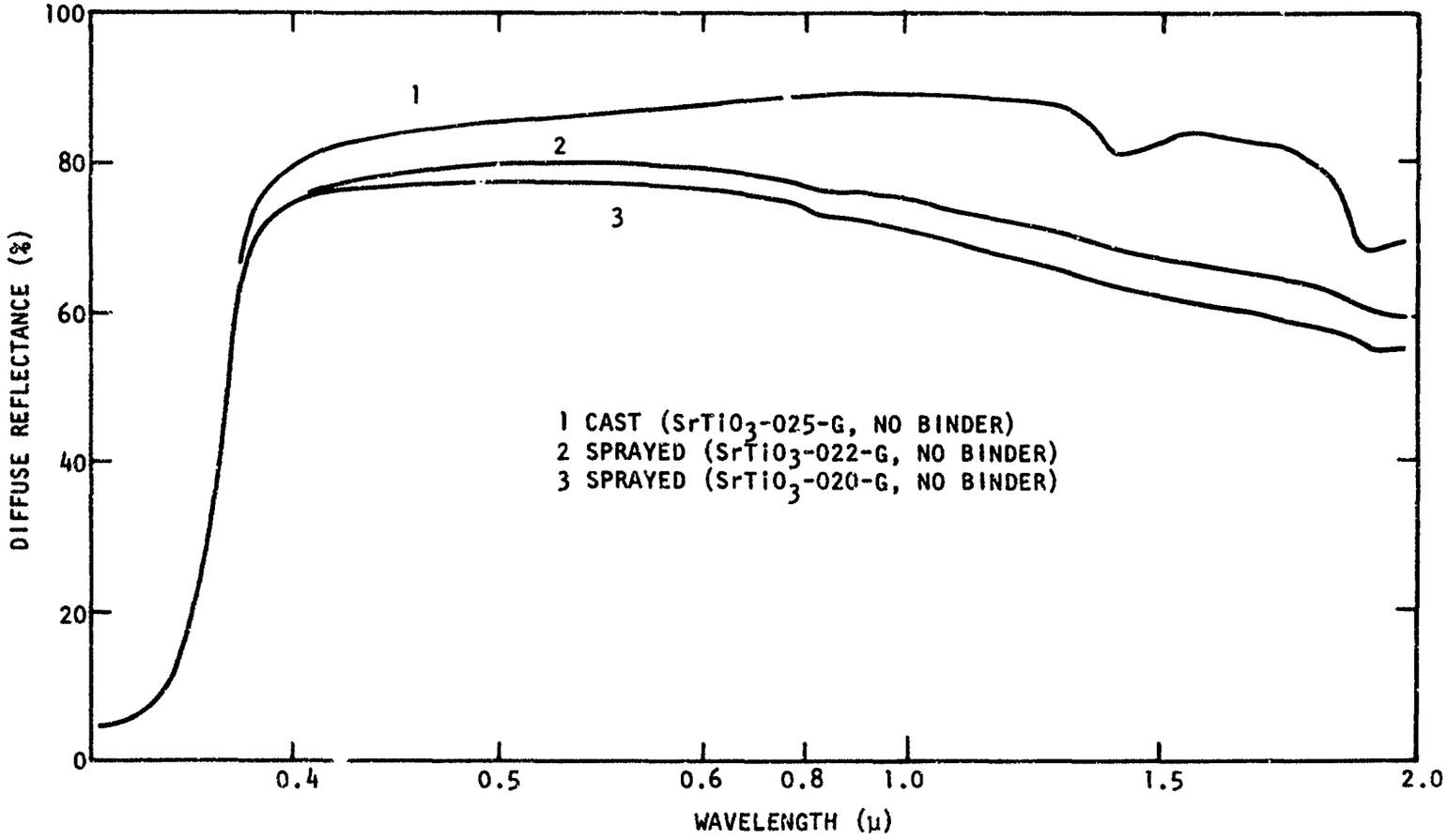

Figure 14. Diffuse Reflectance Spectra for Cast and Sprayed Strontium Titanate

From these reflectance spectra it is concluded that (1) the casting technique yields highly reproducible specimens, (2) sprayed samples must be checked for "shine-through" if comparisons with bulk pigments are to be made, (3) reproducibility among sprayed samples is achievable, and (4) for degradation experiments, both sample preparation techniques can be used for binderless specimens.

Transmittance of Silicone Binder

In the experimental specimens prepared with RTV 602 silicone, the changes in spectral response differed from those of binderless specimens. Experiments were therefore carried out to obtain information about possible degradation of the binder itself under equivalent irradiation conditons.

Specimens were prepared by casting the resin (with appropriate catalyst) into an annular mold with a removable bottom plug. Since a transmission sample was desired, the optical properties of both surfaces of the silicone "disc" had to be comparable. A technique was developed for casting the resin which permitted the mold liner to subsequently be cleanly peeled off. Without the liner, partial adhesion to the bottom plug had initially resulted in a mottled surface. The use of chemicals to solve the initial sticking problem would not have been acceptable because of the possibility of surface interactions during subsequent irradiation treatments. The surface appearance of the bottom of the disc is excellent, showing replication of the foil, including occasional microscopic draw marks. Discs typically have a 7/8-in. diameter and a 0.1-in. thickness. The ring mold was designed to double as sample holder.

Optical response was measured by transmission. The in-situ apparatus was used in the following manner to obtain the results reported below. A reference was established in the usual way on the Beckman DK-2 spectrophotometer. The transmission sample was then inserted in one light path of the transfer optics between the spectrophotometer and the in-situ vacuum chamber. The resulting spectrum thus showed absorption characteristics of the binder similar to the diffuse reflectance of in-situ specimens. Using the same instrument made direct comparison of induced changes possible. Reflection losses were assumed to be constant, and only transmission of the light beam normal to the silicone specimen surface was determined.

Six specimens which had cured in air for 47 hr were examined. Differences in their overall characteristics were less than 5 percent. When an individual specimen was rotated, while being kept normal to the light beam, a polarization-like effect was observed with maximum-to-minimum transmission spectra differing by as much as 15 percent. The transmission maximum is broad and was chosen for later comparisons.

Exposure to Ultraviolet

One sample was exposed to the Spectralab X-25 solar simulator for 30 min at a distance equal to that used for the in-situ reflectance specimens. Since no compensating sapphire window was used for the silicone transmission

specimen, its equivalent exposure is expected to be somewhat greater than 2 esh. There was no observable change over the entire spectral range from 0.35 to 2.1 micrometers. Exposure was carried out in air. Spectrum measurements started within 2 min after the uv irradiation was stopped.

Electron Irradiation

For the electron irradiation of the silicone transmission specimens, a special tube section was inserted in the Dynamitron beam tube. The machine was disconnected from the in-situ apparatus during these experiments, but the individual ambient vacuum conditions were maintained. A collimator confined the electron beam to the sample area. The total electron density was determined with a Faraday cup. The experimental conditions were chosen to match those used for the high incremental fluence measurements with the reflectance samples. The flux was varied to check for rate effects. Since there was concern about a possible change in transmittance caused by additional curing of the silicone resin under vacuum conditions (or just with time), a control sample was included in the specimen chamber. This sample was wrapped in metal foil to shield it from stray electron irradiation. Further, a control sample was maintained unirradiated in air to monitor for changes with time.

In the experimental procedure initially followed, spectra of the specimen to be irradiated and of the control sample were taken; then the specimen was mounted in the irradiation section, and the control was placed in the chamber. The chamber was then evacuated and electron irradiation was begun. After the irradiation was completed, the reference on the spectrophotometer was reestablished before the irradiated specimen and control were removed from the vacuum chamber. By this means, the time between vent-up and start of spectrum measurements was kept to about 2 to 3 min. Therefore, possible unobservable recovery effects were limited to times on the order of a minute.

In Figure 15, the transmittance of an RTV 602 silicone specimen is shown as a function of electron irradiation. Curve 1 represents the initial spectrum; curves 2, 3, and 4 show the response after equal increments in fluence of 50×10^{14} e/sq cm. The flux was deliberately varied over a range similar to that used for the in-situ pigmented specimens. With the same setup, curve 5, which overlays the last irradiation curve, was taken after the specimen had been in air for 47 hr. A spectrum taken with the Cary 14 spectrophotometer 12 days later shows similar values.

The most striking observation is the deterioration in the uv, which is considerably larger than the overall across-the-spectrum decrease. This degradation sensitivity may be very significant in the coating of specimens where the absorption edge of the pigments is below the one used in our titanium dioxide, namely, about 0.42 micrometer. In oxides where the edge is near or below 0.3 micrometer, a paint compounded with this type of silicone may well show coating degradation caused by binder deterioration. For the titanium dioxide pigment specimens reported in this investigation,

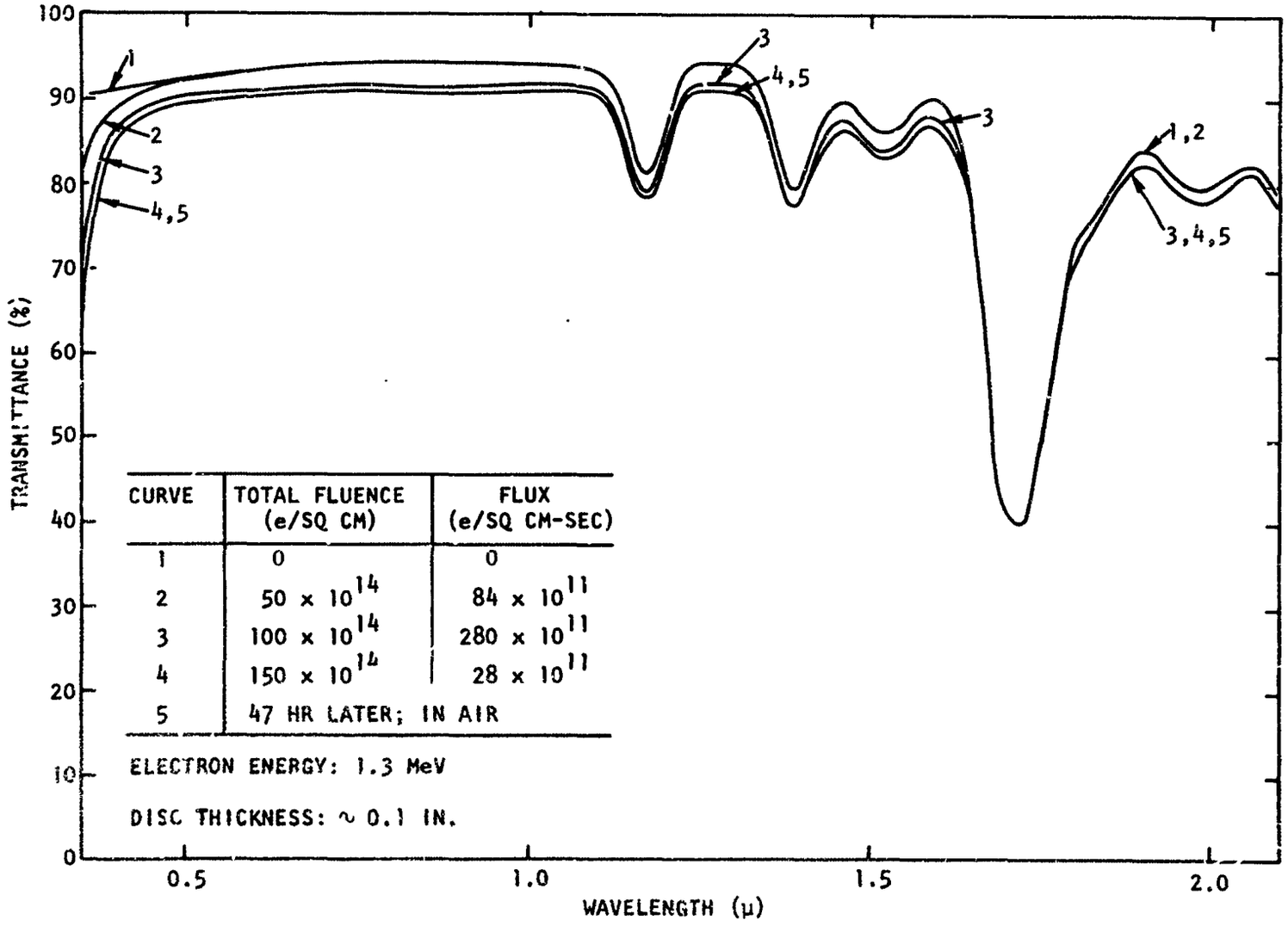

Figure 15. Transmittance of RTV Disc Versus Electron Irradiation (RTV/T3)

the binder deterioration is negligible: the intrinsic pigment band edge is above the region of highest binder degradation sensitivity. Further, the effective path length in our reflectance specimens is at least an order of magnitude shorter than for the transmission discs.

Binder recovery was not observed on a time scale of days. If the binder is indeed irreversibly damaged, then the lack of binder recovery would be significant for long-term irradiations. For example, coating analysis after a space mission may show a certain "unrecoverable" portion when the coating is reexposed to atmosphere.

Irradiation of Sprayed and Cast Specimens

Five specimens prepared by either the spray or cast technique were installed in the in-situ apparatus. Two were of high-purity titanium dioxide which was sprayed, using ethanol, on stainless steel paddles; two consisted of experimental strontium titanate (also ethanol sprayed); and one was a coupon cast from a water slurry of commerical rutile pigment. The materials and the preparation methods used are described in detail in Section II. One specimen of titanium dioxide and one of strontium titanate were electron-irradiated, and one specimen of each material was kept as a control within the same ambient environment; no control was available for the cast coupon.

The entire diffuse reflectance spectrum for each specimen was taken before and after each change. All specimens had been first characterized in air using the Cary 14 spectrophotometer with the diffuse reflectance integrating sphere attachment. The samples were then transferred and installed in the in-situ apparatus attached to the electron accelerator. The diffuse reflectance spectrum for all specimens was then obtained, again in air, with the Beckman DK-2 spectrophotometer, modified to work with the integrating sphere of the in-situ apparatus. This measurement quantitatively relates the two instruments. In Figure 16, the ratio of the measured reflectance of the Cary 14 to that of the DK-2 is plotted as a function of wavelength. The in-situ instrument gives numerically higher values than the Cary 14; this difference has been examined before (Ref. 1) and was not pursued further, since primary interest is in relative changes under irradiation in the in-situ apparatus.

Reflectance spectra taken for the specimens after evacuation indicate primarily the removal of water absorption bands in the IR region without major change in the overall specimen characteristics. The stability of the reflectance spectra in vacuum was established by monitoring for about 4 weeks. Three of the five specimens were subsequently electron-irradiated with 1.5-MeV electrons to 10^{11} e/sq cm. The irradiation had no apparent effect on the ethanol-sprayed, high-purity titanium dioxide and the ethanol-sprayed strontium titanate specimens.

However, the spectrum for the water-cast titanium dioxide coupon (R910) indicates a large degradation, as shown in Figure 17. The upper trace shows the reflectance spectrum obtained in vacuum before the 10^{11}

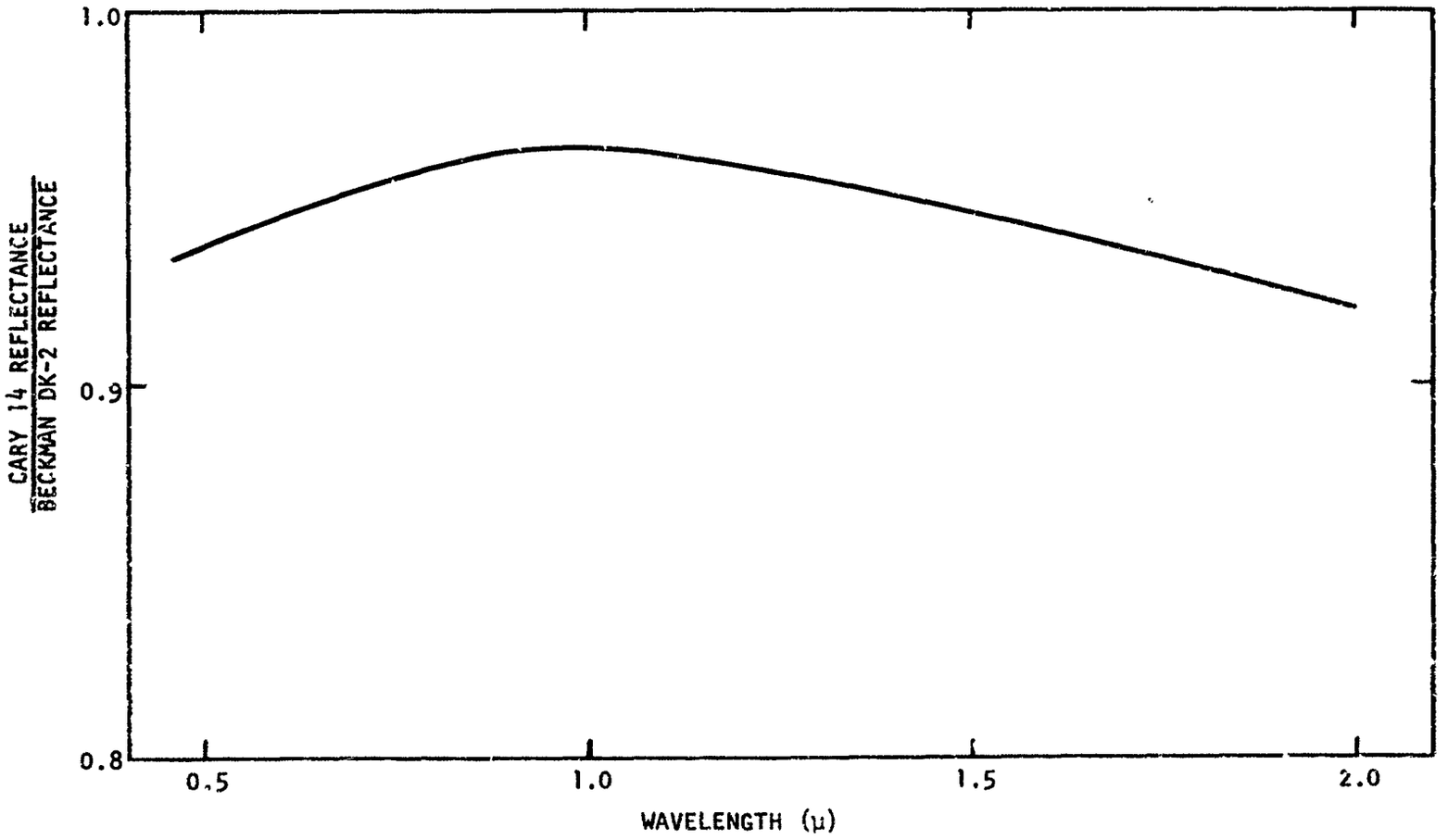

Figure 16. Relationship Between Cary 14 Response and Response of Beckman DK-2 In-Situ Spectrophotometer

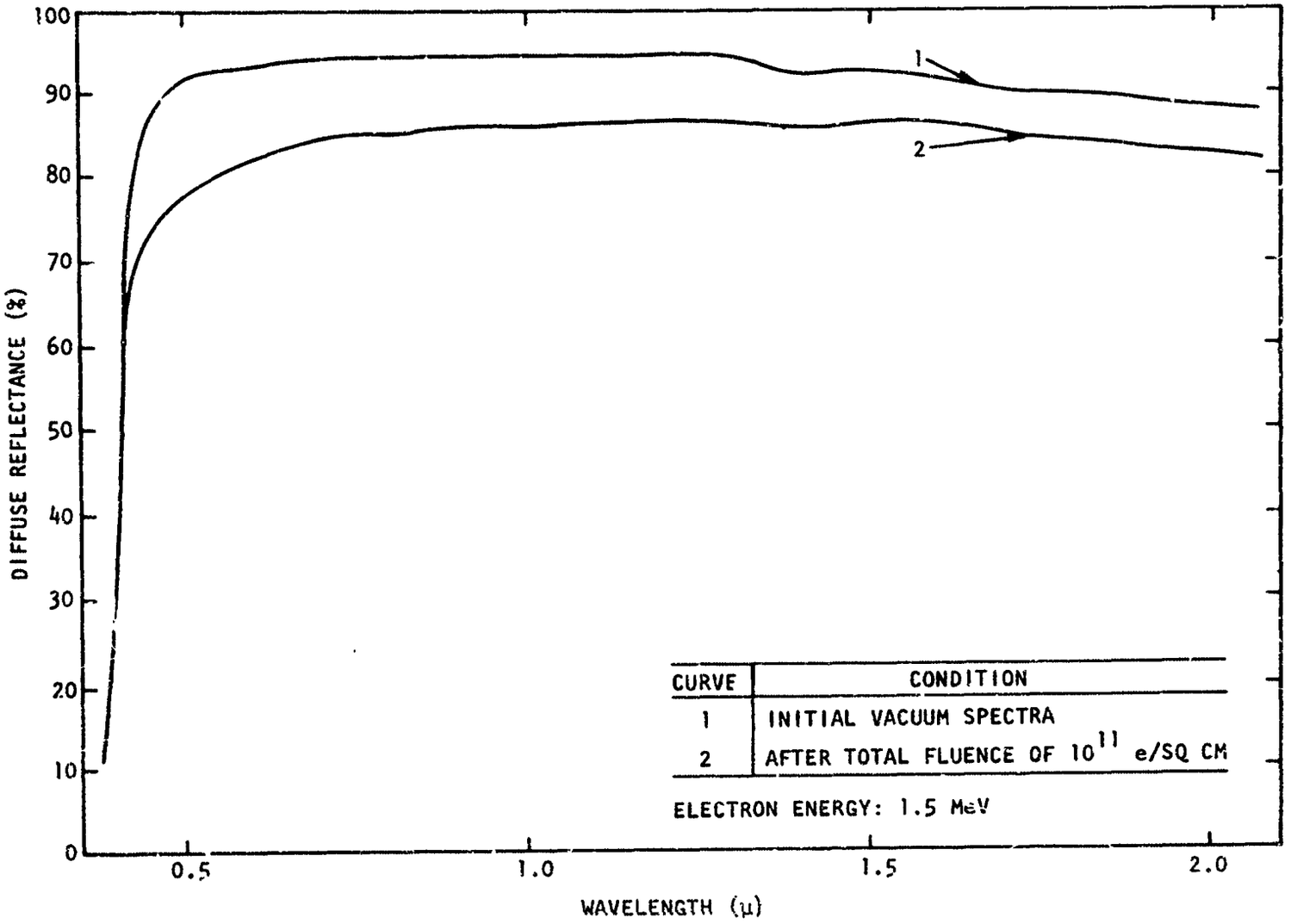

Figure 17. Reflectance Versus Electron Irradiation for Cast Commercial Rutile (TiOx-023-D, No Binder)

e/sq cm irradiation, which produced the new state shown by the lower trace. The cause of the large degradation was not ascertained since the material was relatively impure (Ref. 1) and the cast coupon technique was discontinued. Some recovery took place in the visible region in the 3 weeks subsequent to the electron irradiation. Exposure of the specimen to a dry nitrogen atmosphere produced no further change.

Ultraviolet and Electron Irradiation of Dry-Pressed Binderless Specimens

Initial Characterization

A set of dry-pressed binderless titanium dioxide specimens was prepared as described above. Similarity among specimens and surface uniformity was ascertained by comparing the relative diffuse reflectance spectra of the freshly prepared samples. For each acceptable sample, the absolute spectrum was then determined using the Cary 14 spectrophotometer with the integrating sphere attachment. For five specimens installed in the in-situ apparatus, the spectra were then measured with the Beckman DK-2. If the samples had remained unchanged in transit, the two measurements are related very much as shown in Figure 16, where the ratio of the reflectance measured with the Cary 14 to that measured with the DK-2 is plotted as a function of wavelength. The correspondence of the two instruments is close to that observed earlier but differs somewhat in absolute value owing to realignments of the DK-2. All the initial characterizations were carried out in air.

Irradiation Program

The objective of this portion of the experimental program was to provide comparative information about the changes in the diffuse reflectance spectrum brought about by exposing identical specimens to uv and electron irradiation, both separately and simultaneously. This information, obtained for binderless pigments, also provides the reference to which the polymeric pigment systems can be related.

From the work reported above, it had become clear that (1) specimens should be closely matched and similarly prepared from the same material, (2) at least one control sample should be subjected to the same ambient environment but not irradiated, and (3) recovery of damage can be expected to be time-dependent. With these requirements in mind, an irradiation program matrix was developed. The program steps and actual conditions for binderless specimens are presented in simplified form in Table IV. After the irradiation chamber was evacuated, the spectra for all specimens were determined in vacuum. Since differences from the "in air" graphs were observed, the sample reflectances were monitored for several days to ascertain that a new equilibrium state had been established. The steady-state vacuum spectrum was then taken as the reference spectrum for subsequent treatment of the individual specimens.

When the five specimens had been installed, assignments were made as follows: one specimen would receive uv exposure only; one specimen would receive electron irradiation only; one specimen would receive

TABLE IV

EXPERIMENTAL PROGRAM SEQUENCE AND IRRADIATION MATRIX FOR BINDERLESS DRY-PRESSED SPECIMENS

ALL FIVE SPECIMENS

Prepare specimens

Measure spectra with Cary 14 - in air

Mount in in-situ apparatus

Measure spectra with DK-2 - in air

Evacuate sample chamber

Monitor spectra in vacuum for stability

→

	Time Increment (min)	Total Time (min)	Total Exposure (esh)
UV	30	30	2
UV	30	60	4
UV	90	150	10

SPECIMEN NO. TiOx-024-G2

	Time Increment (min)	Total Time (min)	Total Irradiation (e/sq cm)
Electrons	30	30	2×10^{15}
Electrons	30	60	4×10^{15}
	Recovery for 17.5 Hr		
Electrons	90	150	10^{16}

SPECIMEN NO. TiOx-028-G2

Time Increment (min)	Total Time (min)	UV Exposure (esh)	Electron Irradiation e/sq cm)
30	30	2	2×10^{15}
30	60	4	4×10^{15}

SPECIMEN NO. TiOx-026-G2

CONTROL

SPECIMEN NO. TiOx-027-G2

CONTROL
Partly flaked initially

SPECIMEN NO. TiOx-029-G2

→

ALL FIVE SPECIMENS

Expose to dry nitrogen

Measure spectral response

Evacuate nitrogen

Measure spectral response

Expose to dry oxygen

Measure spectral response

Displace oxygen with air

Measure spectral response

Remove specimen from in-situ apparatus

Measure spectra with Cary 14 - in air

simultaneous uv exposure and electron irradiation; one specimen would be studied at a different dose rate; and one specimen would be maintained as a control specimen, since the experimental program extended over several months.

After the completion of the irradiation program, the specimens were to be brought back to atmospheric pressure with dry nitrogen and remeasured; the ambient was then to be replaced by dry oxygen; and, finally, the oxygen was to be replaced by air, as shown in the right-hand block of Table IV. However, after the irradiation program had been completed and while the posttreatment recovery was under way, a power outage resulted in loss of vacuum and prematurely terminated the planned sequence.

Irradiation Effects and Recovery

As had been observed earlier, the spectra of binderless pigment specimens degrade somewhat when the specimens are evacuated. In Figure 18, a typical set of diffuse reflectance spectra is shown. Curve 1 represents the response obtained in air after installation and curve 2 the response after a stable condition had been attained in vacuum. Primarily, the change is in the visible wavelength region; the indication of the moisture bands in the IR region has been erased.

The effect of exposure to uv from an unfiltered xenon arc (Spectralab X-25 solar spectrum simulation source of 4 suns) is illustrated in Figure 19. The highest trace shows the spectrum in vacuum before the exposure. The response after total exposures to 2, 4, and 10 esh is also indicated. The degradation moves rapidly toward saturation after an exposure of about 2 esh. After the specimen had remained in a vacuum (approximately 10^{-6} torr) for 6 days following exposure to uv, its spectrum was remeasured. During this time, an 80-percent recovery of the damage occurred as shown by curve 5 (dashed). Vent-up occurred 53 days later. Final recovery was to better than 1 percent of curve 1.

The effect of irradiation by electrons is shown in Figures 20 and 21. The original spectrum in vacuum is again given as reference. The degradation due to electron irradiations of 20×10^{14} and 40×10^{14} e/sq cm is shown by curves 2 and 3. The second irradiation took place within an hour of the first one and resulted in very little additional degradation, indicating that the specimen did not recover significantly from saturation in 1 hr.

The spectrum was redetermined 17.5 hr after the last irradiation, and is plotted as curve 2 of Figure 21. Recovery was almost complete at 2 micrometers, but very little change had occurred in the short-wavelength visible region. Electron irradiation was then resumed and degraded the spectrum, as shown by curve 3. The additional irradiation of 60×10^{14} e/sq cm, which brought the total fluence since the start of the electron

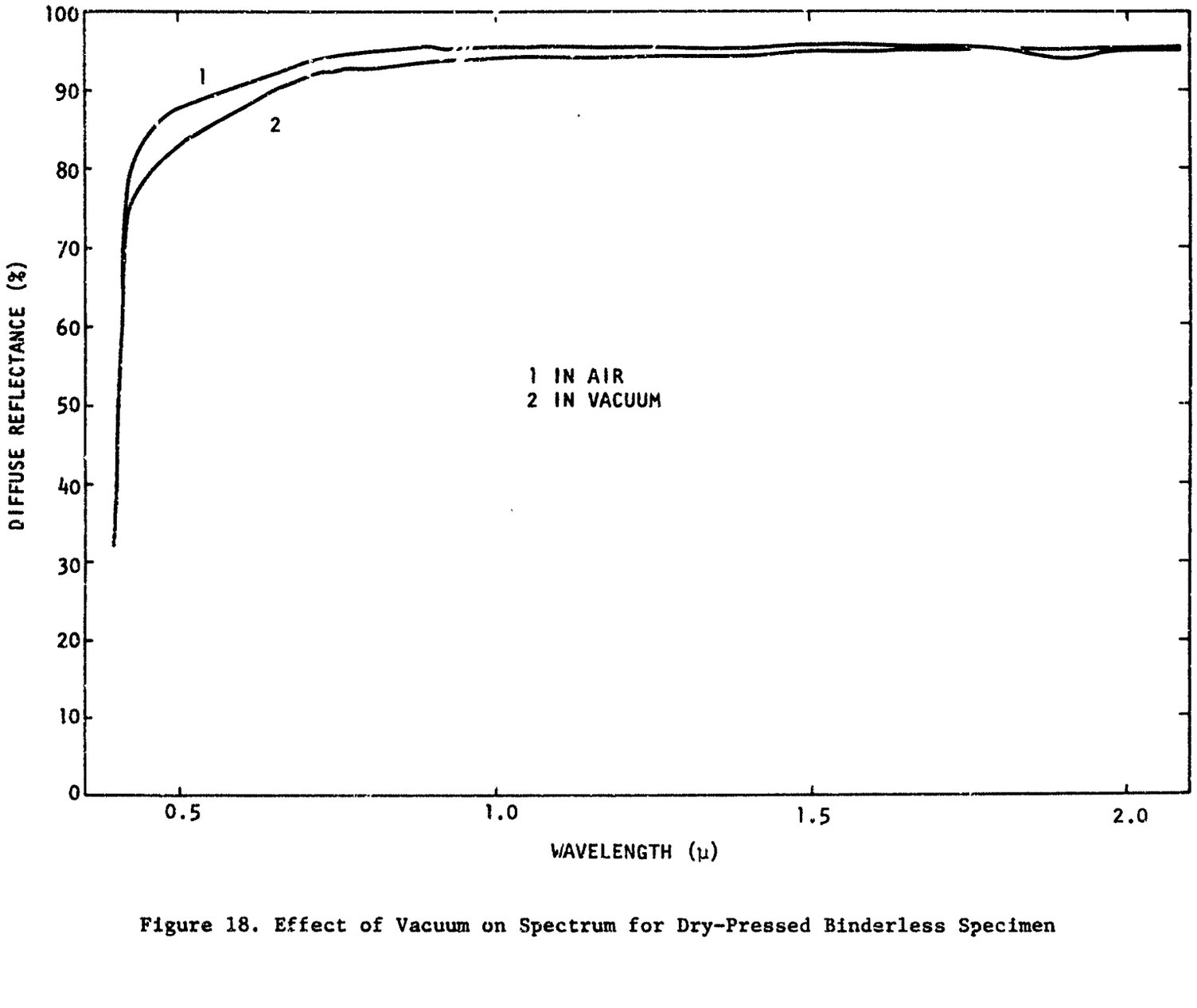

Figure 18. Effect of Vacuum on Spectrum for Dry-Pressed Binderless Specimen

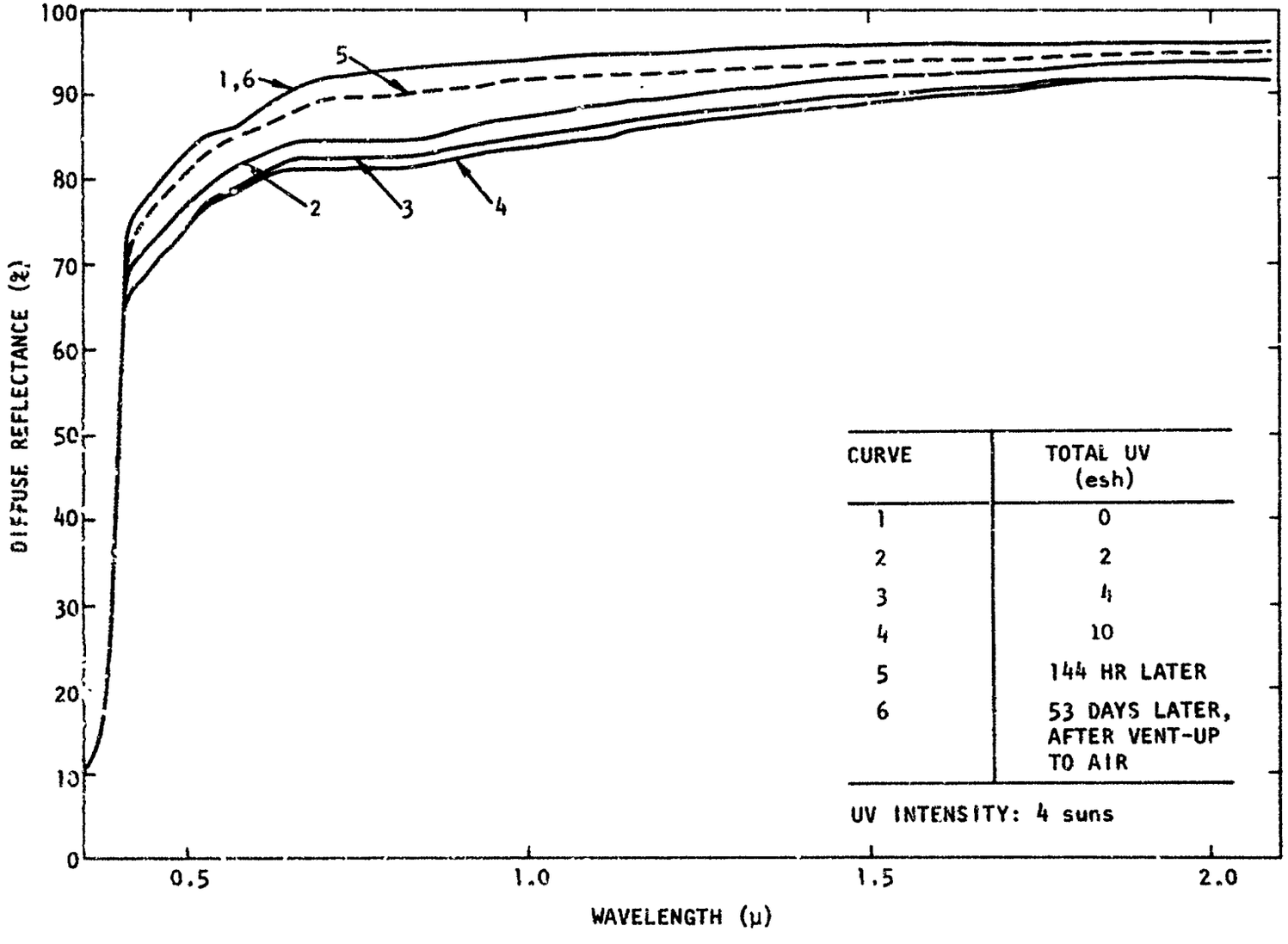

Figure 19. Effect of Exposure to UV and Recovery (TiOx-024-G2, No Binder)

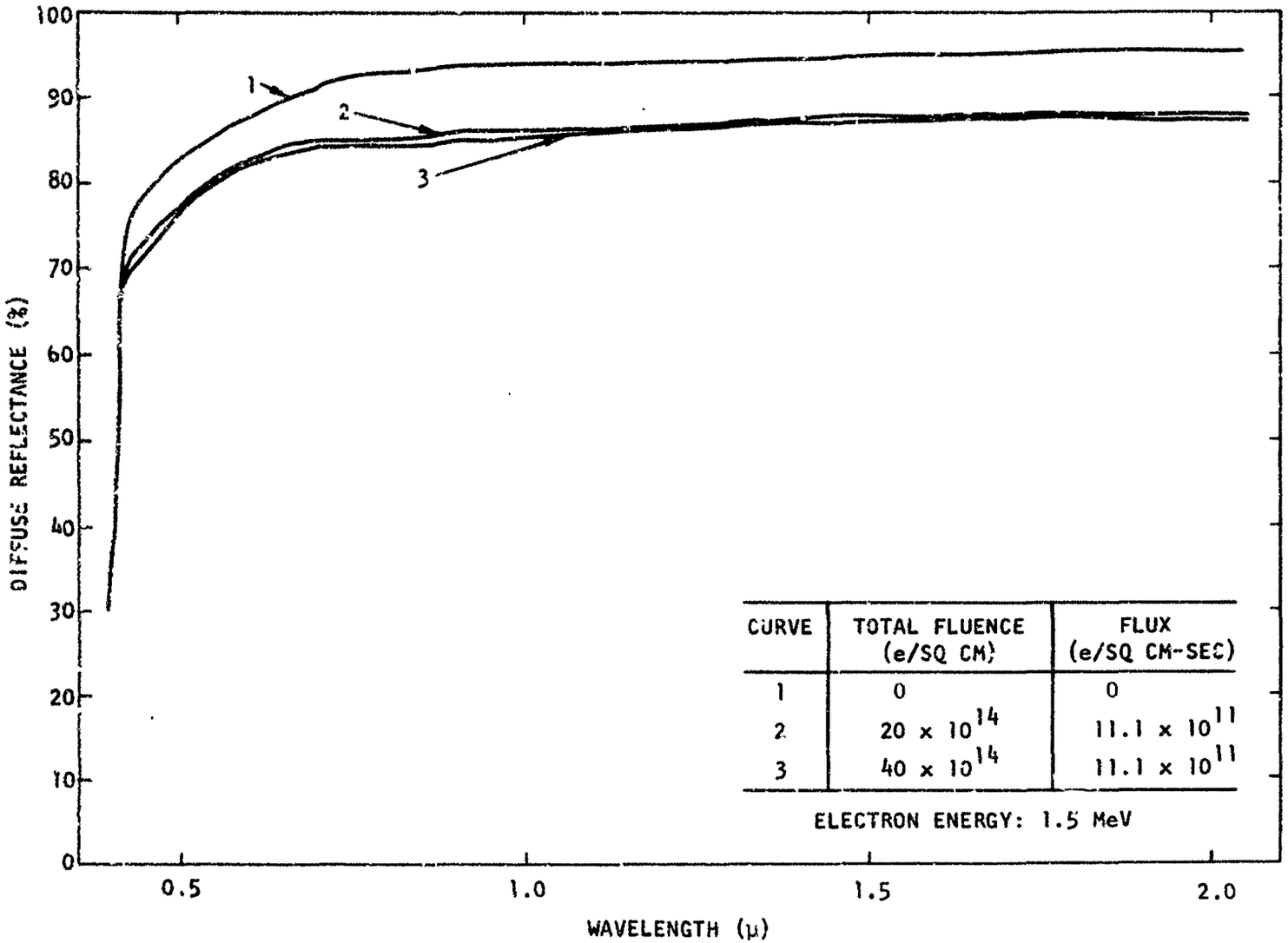

Figure 20. Effect of Electron Irradiation on Dry-Pressed Binderless Specimen (TiOx-028-G2)

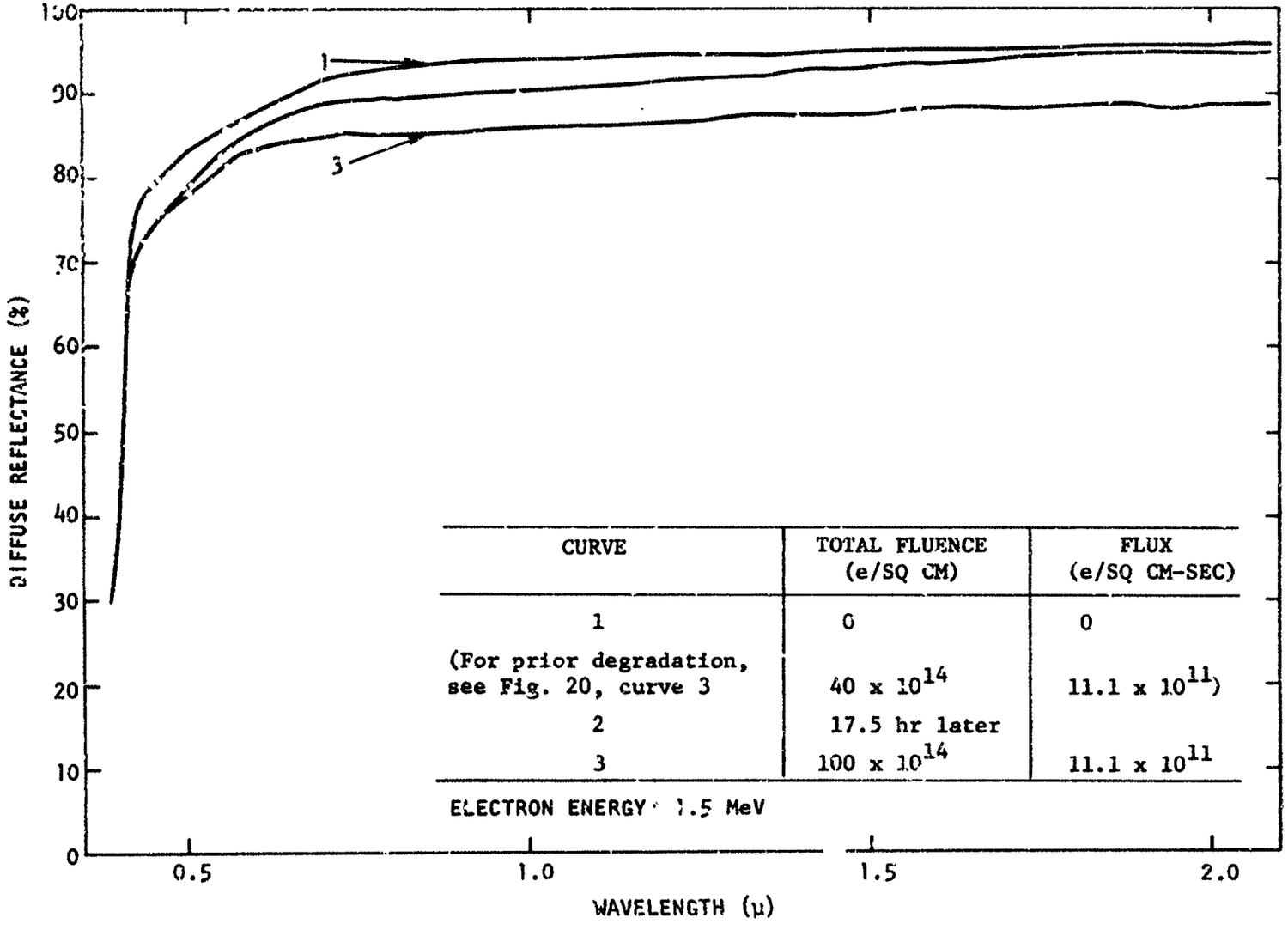

Figure 21. Effect of Further Electron Irradiation on Dry-Pressed Binderless Specimen (TiOx-028-G2)

irradiation to 100 x 10^{14} e/sq cm, erased the recovery. As a result, the response dropped nearly to the level at which it apparently had saturated (shown in Figure 20).

The time dependence of recovery, after electron irradiation to a total fluence of 100 x 10^{14} e/sq cm, is shown in Figure 22. Curve 2, taken after the irradiation had been completed, shows that some additional irreversible damage in the visible region has occurred as compared with the 17.5 hr recovery plotted in Figure 21. The spectra were then redetermined after 1.5, 4.5, and 29 hr. As can be seen from the curve obtained after 1.5 hr, the recovery appears to be considerably more rapid at the long wavelength. That part of the recovery which takes place in vacuum is essentially complete at or before the 4.5 hr point; the 29 hr response overlays it. Recovery after vent-up 53 days later is complete to the initial vacuum state.

The effects of simultaneous exposure to uv and irradiation by electrons are shown in Figures 23 and 24. The conditions chosen were similar to those used for the specimens which were exposed to separate irradiations. The degradation resulting from two equal amounts of simultaneous uv and electron irradiation is shown in Figure 23. For these dry-pressed binderless specimens, the effect of the combined exposure is stronger than that of individual exposures. The saturation of damage observed for uv or electron irradiation alone appears to be absent. Damage continues particularly in the visible and short-wavelength regions, but also near 2 micrometers. The wavelength region near 1 micrometer seems to best resist additional damage.

Recovery from the simultaneous uv and electron irradiations is illustrated in Figure 24. Curve 2 was taken after the specimen had received a total exposure of 4 esh and 40 x 10^{14} e/sq cm. The spectrum obtained after 1 hr showed considerable IR recovery. A measurement made after 24 hr indicated some recovery near 2 micrometers. The final recovery after vent-up to air 53 days following the last exposure is essentially complete to the preirradiation vacuum characteristic.

In general, all final curves show that recovery to the preirradiation vacuum state of all specimens is complete to within about 1 to 2 percent over the entire spectral range from 0.35 to 2.1 micrometers. As pointed out above, the relative effectiveness of recovery with time in vacuum as compared with exposure to air could not be ascertained for binderless samples. It should be noted that recovery is essentially complete only to the spectrum obtained in vacuum before irradiation. Thus, the initial degradation observed as the binderless specimens were first exposed to a vacuum is an irreversible state change, neither recoverable nor affected by the irradiations. The importance of controlling the pigment treatment before paints are formulated is again apparent.

The following qualitative statements can be made on the basis of the results obtained for the dry-pressed binderless specimens:

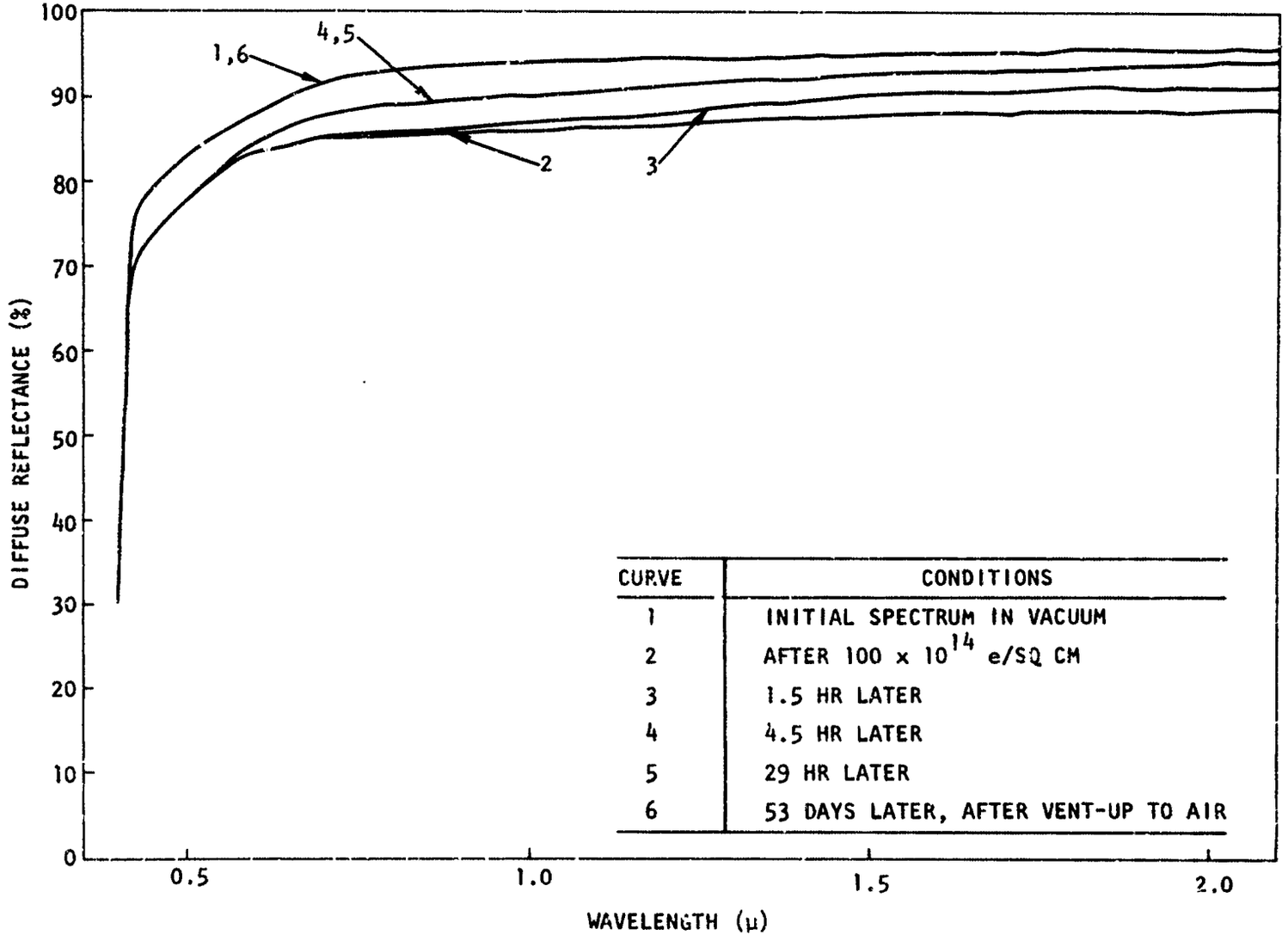

Figure 22. Recovery after Electron Irradiation of Dry-Pressed Binderless Specimen (TiOx-C28-G2)

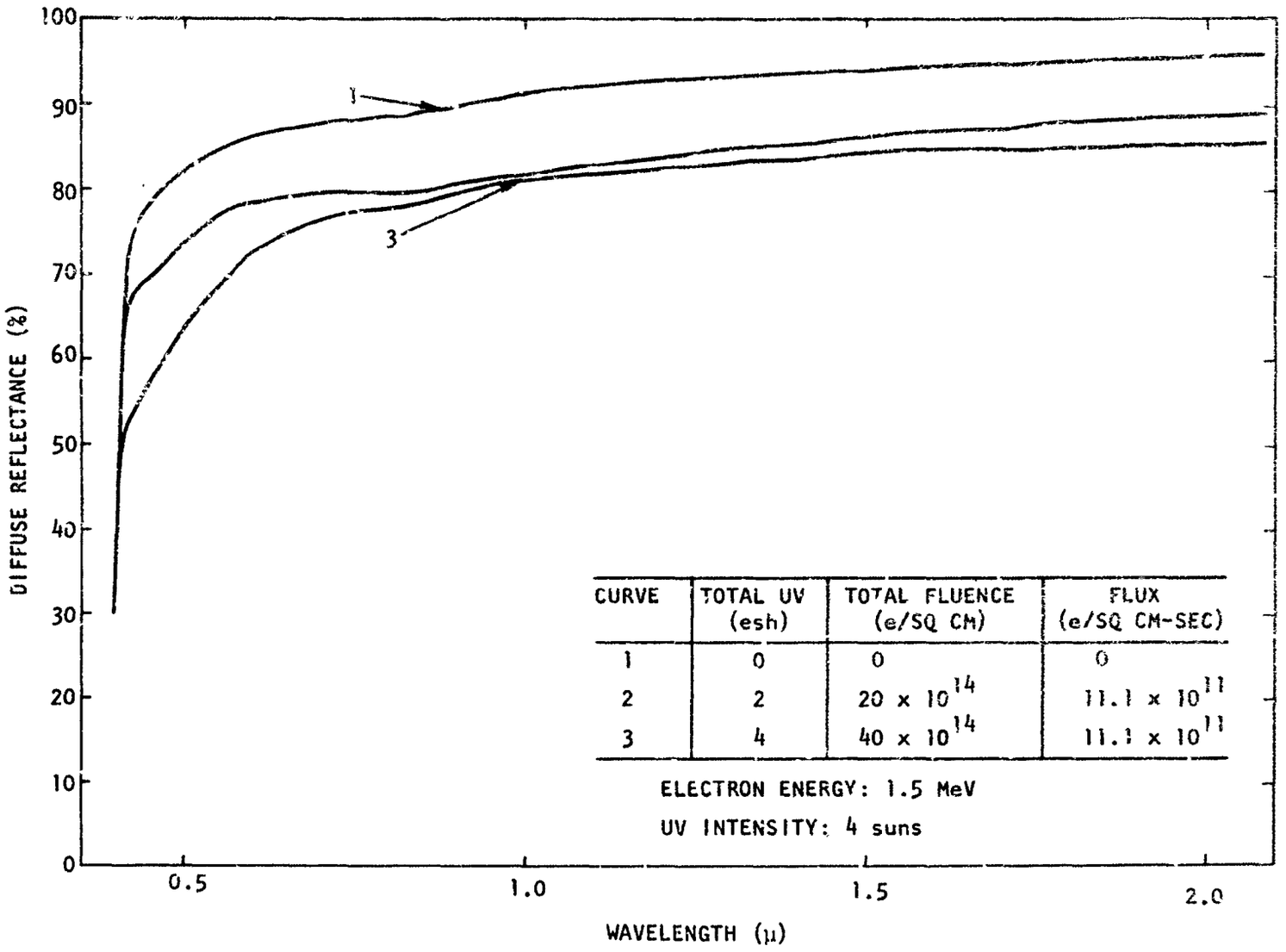

Figure 23. Effect of Simultaneous UV and Electron Irradiation of Dry-Pressed Binderless Specimen (TiOx-026-G2)

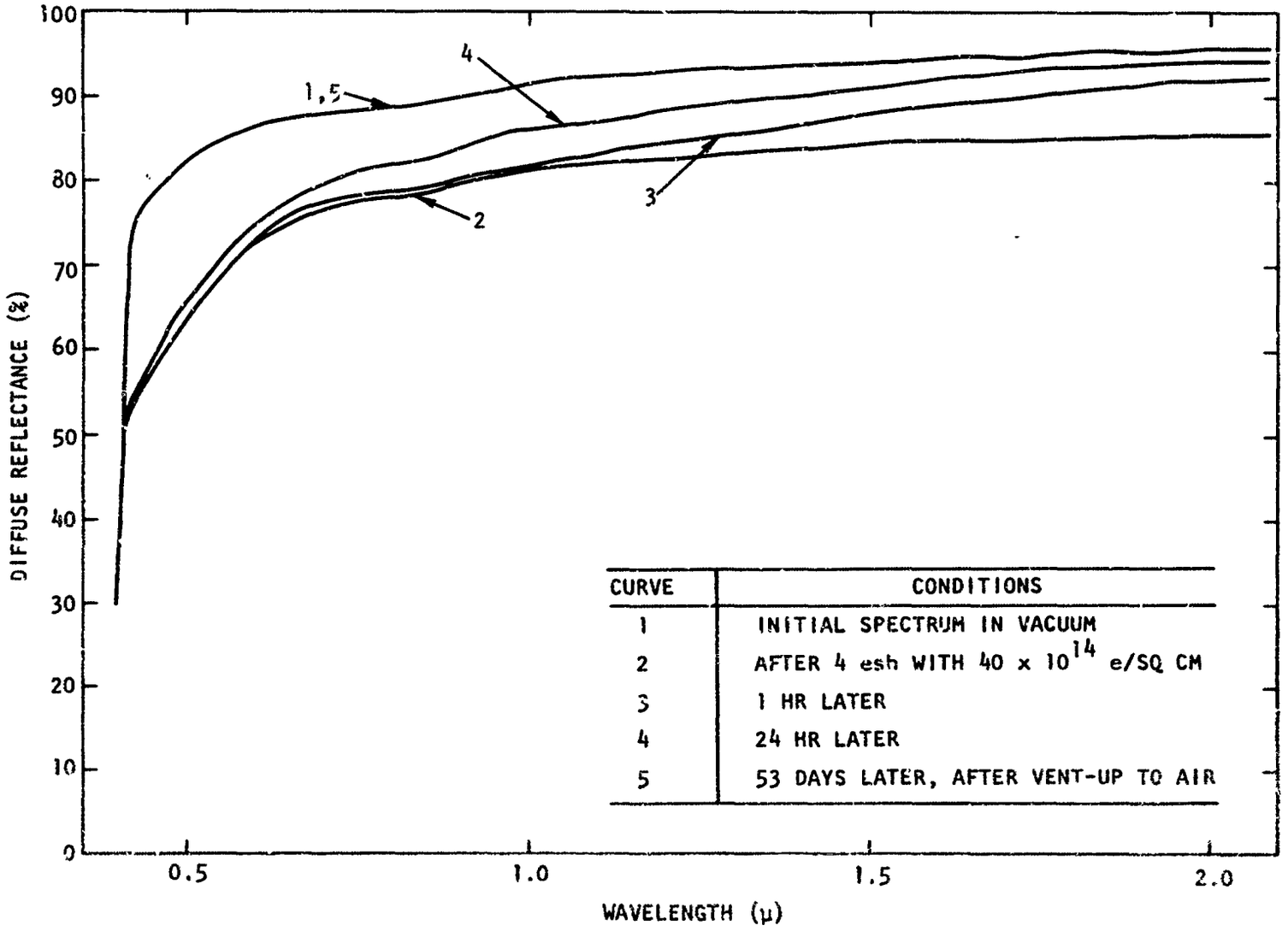

Figure 24. Recovery after Simultaneous UV and Electron Irradiation of Dry-Pressed Binderless Specimen (TiOx-026-G2)

1. The diffuse reflectance spectra of all irradiated specimens degraded.

2. Ultraviolet irradiation produced significantly more degradation in the visible than in the IR region, while electron irradiation produced a relatively uniform degradation across the spectrum.

3. The saturated magnitudes of the uv and electron degradations are about the same.

4. All the damaged samples showed recovery at room temperature in vacuum (about 10^{-6} torr). The uv-damage recovery tends to destroy all the defect centers, whereas the electron-damage recovery is more rapid in the IR and small in the visible region. In both cases, the recovery essentially ceases in about 4 to 6 hr.

5. Renewed irradiation with electrons following recovery produces new absorbing centers in the visible region, but the IR reflectance degradation for the second irradiation is about the same as for the first.

6. Simultaneous uv and electron irradiation results in saturation behavior only near 1 micrometer, indicating a synergistic effect in the IR.

7. Recovery from simultaneous uv and electron bombardment leads to almost complete recovery in the IR within a day, whereas little recovery in the visible is observed at this stage.

8. Recovery after vent-up 53 days later is essentially complete to the preirradiation vacuum characteristic for all specimens.

Ultraviolet and Electron Irradiation of Pigment-Silicone Specimens

To determine the characteristics and response of a coating system which utilizes the pigment characterized previously, the pigment was incorporated into a binder. The first group of samples was prepared using SR 125 resin, but this material was abandoned in favor of RTV 602 silicone after consultation with MANE. The details of specimen preparation are given in Section II.

The irradiation program followed the pattern established for the pigment-only samples, the objective being to have similar experimental conditions so that meaningful comparisons could be made between the two types of systems. Samples were selected for uv exposure alone, for electron irradiation alone, and for combined uv and particle irradiation.

The program carried out on these titanium dioxide RTV binder specimens is outlined in Table V. Preirradiation measurements and treatment are indicated in the box on the left. The postirradiation changes in diffuse

TABLE V

PROGRAM SEQUENCE FOR TITANIUM DIOXIDE SILICONE-BINDER SPECIMENS

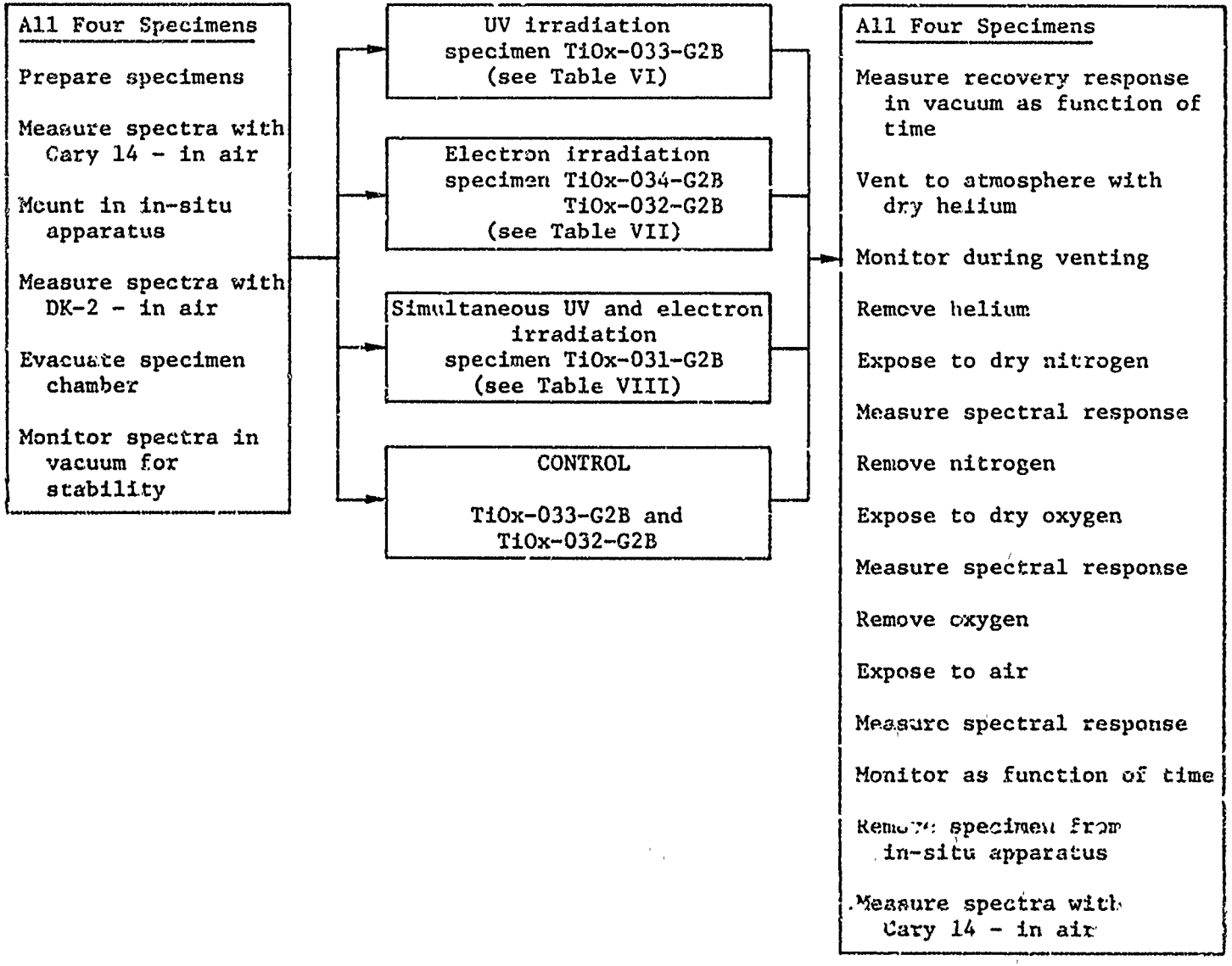

reflectance spectra were monitored in vacuum for weeks, and then all samples were exposed to various gas ambients as shown in the box on the right in Table V. The primary purpose of exposure to various ambients was to determine the relative effectiveness of these environments with respect to recovery from degradation. The central portion of Table V shows the assignment of individual specimens, one being used exclusively for uv exposure, one for simultaneous uv and electron exposure, and two for electron exposure. Originally, it was intended that a ceramic dummy specimen would serve as a calibration reference and one titanium dioxide specimen would be carried from beginning to end as a control. However, since the ceramic calibration control was slightly oversize, it scraped the entrance to the integrating sphere, covering it with various amounts of MgO dust, and thus proved to be unusable. The TiO_2 control (TiOx-032-G2B) showed exceptional reproducibility, which gave confidence that the optical properties of the overall in-situ apparatus were stable with time both on a short- and long-term (week-to-month) basis. When the program had progressed to the point where electron flux dependence was to be investigated, a virgin specimen was desired, and the TiO_2 control sample was therefore used for this purpose. As the specimen exposed to uv (TiOx-033-G2B) had by that time recovered in vacuum to its final in-situ value, it was selected as a new control. This choice was validated by the observation that the specimen's spectrum remained constant until vent-up.

The procedure followed in these irradiations was like the one used for the binderless specimens. First, a complete diffuse reflectance spectrum was obtained from 0.35 to 2.1 micrometers for both the specimen to be irradiated and the control. A reference spectrum was taken on the Beckman DK-2 spectrophotometer for every run to allow proper interpretation of small changes in the "before" and "after" measurements. At the start of every experimental sequence, all specimens were routinely characterized; this is particularly important because of the recovery observed after irradiation.

The major events of the exposure and the irradiation schedules are given in Tables VI, VII, and VIII. Clock time limitation presents a problem both for uv exposures and electron irradiations. The experimental proposal of using high flux density to obtain equivalent long-term exposures in a short time cannot be used if damage mechanisms are dose- and rate-dependent. Since degradation is intensity-sensitive but scaling laws are not even established empirically, the lowest reasonable flux was chosen initially to give definite but small degradation. Since the level at which this might happen was not accurately predictable, the effect of irradiation levels had to be constantly analyzed, which required formidable data documentation. The binder specimen irradiation study alone generated in excess of 280 individual spectral curves.

In Table VI, the uv exposure increments and the accumulated values are indicated for a constant intensity of about 4 suns. In view of the overall objective and scope of this study, no long-time exposures were sought; interest was instead focused on the dynamics of the degradation.

TABLE VI
UV EXPOSURE (TiOx-033-G2B, RTV BINDER)

UV Exposure (esh)	Total Exposure (esh)	UV Intensity
0.5	0.5	4 suns
1.0	1.5	4 suns
0.5	2.0	4 suns
Recovery in vacuum for 19 hr		
2.0	4.0	4 suns
2.0	6.0	4 suns
4.0	10.0	4 suns
Recovery in vacuum for 17.5 hr		
4.0	14.0	4 suns
4.0	18.0	4 suns
4.0	22.0	4 suns
Recovery in vacuum for 945 hr		

TABLE VII
ELECTRON IRRADIATION (TiOx-034-G2B, RTV BINDER AND TiOx-032-G2B, RTV BINDER)

Fluence[a] (e/sq cm)	Total Fluence (e/sq cm)	Flux (e/sq cm-sec)
TiOx-034-G2B, RTV binder		
0.2×10^{14}	0.2×10^{14}	0.111×10^{11}
Recovery in vacuum for 19 hr		
0.4	0.6	0.222
1.0	1.6	0.556
5.0	6.6	2.78
Recovery in vacuum for 144 hr		
5.0	11.6	2.78
5.0	16.6	2.78
Recovery in vacuum for 71.5 hr		
5.0	21.6	2.78
5.0	26.6	2.78
Recovery in vacuum for 20.5 hr		
5.0	31.6	2.78
10.0	41.6	5.56
10.0	51.6	11.1
Recovery in vacuum for 452 hr		
TiOx-032-G2B, RTV binder		
5.0	5.0	2.78
5.0	10.0	27.8
5.0	15.0	8.33
5.0	20.0	4.17
Recovery in vacuum for 46.5 hr		
50	70	83.3
50	120	278
50	170	27.8
Recovery in vacuum for 175 hr		

[a]Electron energy: 1.3 MeV

TABLE VIII
SIMULTANEOUS UV AND ELECTRON IRRADIATION
(TiOx-031-G2B, RTV BINDER)

UV[a] (esh)	Total UV (esh)	Fluence[b] (e/sq cm)	Total Fluence (e/sq cm)	Flux (e/sq cm-sec)
1	1	$1x10^{14}$	$1x10^{14}$	$1.11x10^{11}$
1	2	1	2	1.11
Recovery in vacuum for 53.5 hr				
2	4	4	6	2.22
2	6	4	10	2.22
2	8	4	14	2.22
Recovery in vacuum for 18 hr				
2	10	10	24	5.56
2	12	10	34	5.56
2	14	40	74	22.2
Recovery in vacuum for 18 hr				
2	16	40	114	22.2
2	18	40	154	22.2
2	20	40	194	22.2
Recovery in vacuum for 322 hr				

[a]UV intensity: 4 suns

[b]Electron energy: 1.3 MeV

The schedule of electron irradiations for two specimens is given in Table VII. The detailed irradiation objectives were based on the actual degradation response of the first specimen, from which subsequent fluence and flux levels were determined. In the schedule for the second specimen, fluence increments were kept equal while the flux was changed nonmonotonically. This procedure was then repeated with the fluence increment level raised by an order of magnitude. Other alternatives were considered but could not be carried out because of practical limitations imposed on this program.

The sequence for simultaneous exposure to uv and electrons is given in Table VIII. Conditions paralleled those of the separate uv and electron irradiations. The final irradiation values, i.e., total fluence and total uv exposure, for the simultaneous irradiation are particularly close to those of the separate treatments.

Exposure to Ultraviolet

The diffuse reflectance degradation of the TiO_2-RTV specimen which was exposed to the uv solar simulator is shown in Figure 25. The initial state after stabilization in vacuum is represented by curve 1. Subsequent spectra are given at the total exposures as indicated. As discussed earlier, overnight interruption of the irradiation caused partial recovery of the degradation. It is possible to make a reasonable correction for the recovery in some cases. The set of curves shown in Figure 25 has been adjusted so as to remove, to first approximation, the portion recovered between successive uv exposures. It should be noted that exposure increments are not equal throughout the set. The change of damage with increasing total exposure is analyzed later for two wavelengths, at 0.8 and 2 micrometers. The absorption bands are caused by the RTV binder; if scanned slowly, they show a rich fine-structure which is not, however, pertinent to the present study.

Electron Irradiation

If specimens of TiO_2-RTV which are prepared from the same batch at the same time and show almost identical initial conditions are exposed to 1.3-MeV electrons, as shown in Table VII, the resulting reflectance spectra give a composite picture such as that presented in Figure 26. The recovery characteristics for this specimen were not as clear-cut as in case of uv exposure and therefore no adjustments have been made to graphically remove the recovery contribution. The spectra shown in Figure 26 represent final values for individual irradiation sets; since no recovery adjustments were incorporated, degradation in this figure does not appear monotonic with increasing fluence. A saturation tendency was observable within each individual set and can be observed in the overall composite graph. It must be kept in mind that the electron flux density was increased considerably over the starting value.

To determine the sensitivity to flux, two experiments were run on a fresh sample according to the lower schedule in Table VII. The fluence increment was first kept constant at 5×10^{14} e/sq cm while the flux

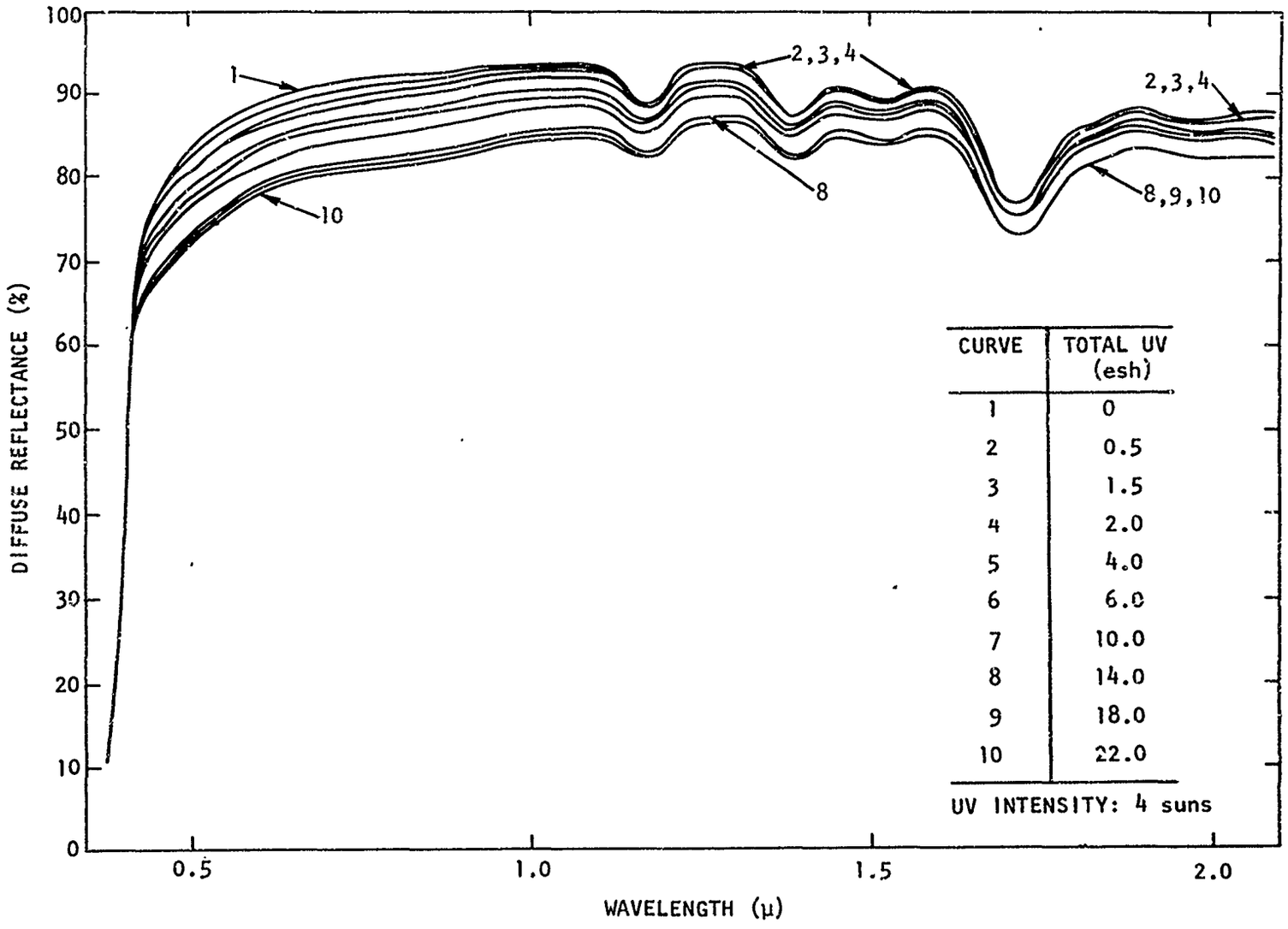

Figure 25. Effect of UV Exposures, Adjusted for Recovery (TiOx-033-G2B, RTV Binder)

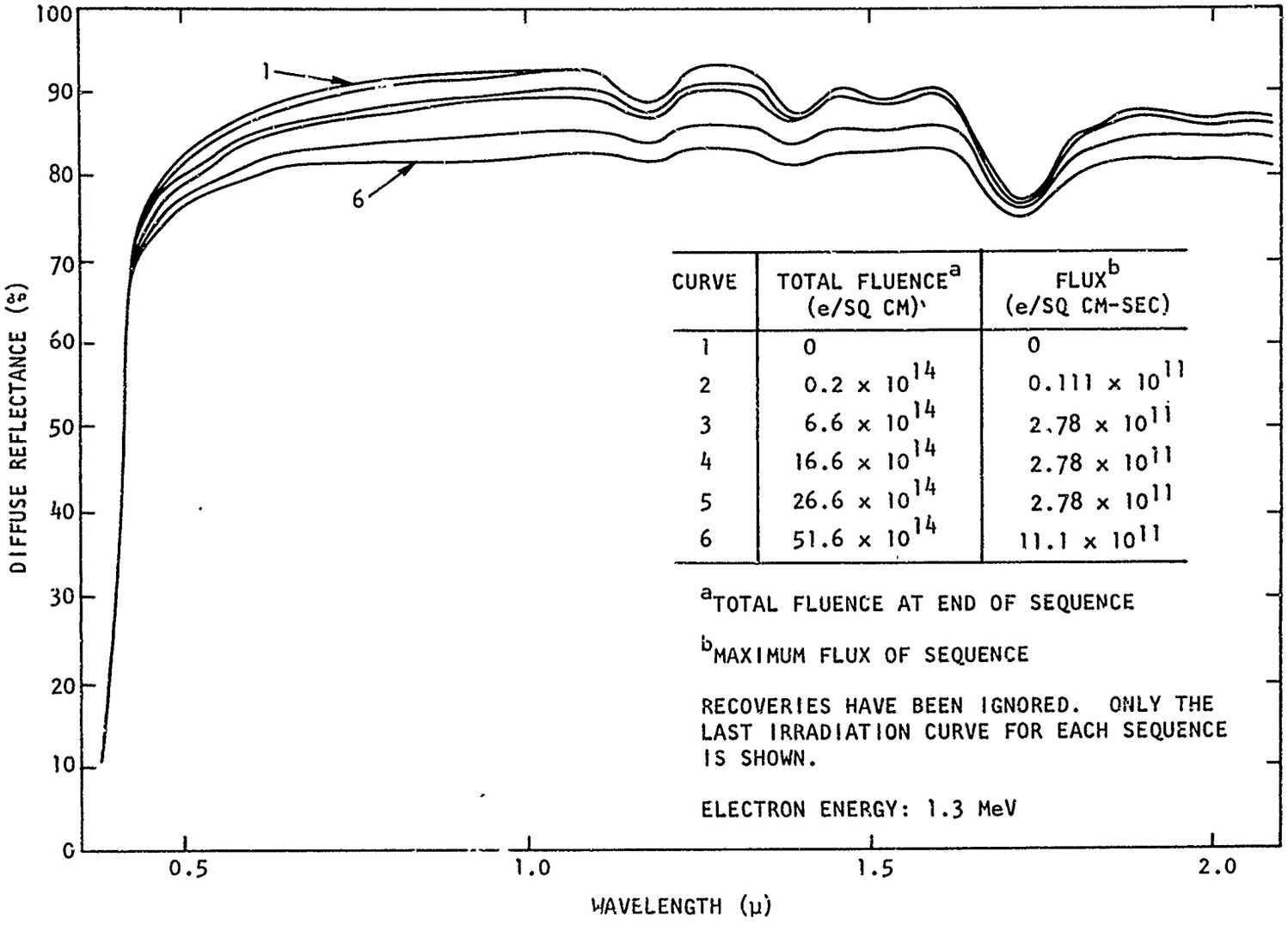

Figure 26. Composite Picture of Effect of Electron Irradiations, No Recovery Adjustments (TiOx-034-G2B, RTV Binder)

varied nonmonotonically over an order of magnitude. The resulting spectra are shown in Figure 27. The trend for the degradation to saturate is evident. These irradiations were carried out with just sufficient time taken between electron bombardments to obtain the spectra for the specimen and control; i.e., less than 1 hr for recovery was allowed between successive irradiations.

The specimen next was left undisturbed for 117 hr in order (1) to obtain recovery data and (2) to reach a new, quasi-steady-state starting condition for a repeat experiment with higher flux and fluence increment levels. (For details, refer to Table VII.) The results of the repeat experiment are shown in Figure 28. Curve 1 shows the spectrum obtained after the specimen had recovered from the prior irradiation. After irradiation at the increased flux and fluence, degradation is severe but still has a tendency to saturate. The contribution to the overall coating reflectance of the two major binder absorption bands below 1.5 micrometers is beginning to disappear, while the band near 1.7 micrometers still remains.

Simultaneous Ultraviolet and Electron Irradiation

As was seen in Figure 22, the simultaneous exposure of the binderless, dry-pressed specimen to uv and electron irradiation had pointed to (1) an absence of saturation effect and (2) increased degradation over that found in the separate irradiations. The question of how the TiO_2-RTV specimen, made using the same pigment material, would behave under similar conditions was therefore investigated. The exposure schedule is indicated in Table VIII. Because of the importance of showing the details of behavior and the difficulty of graphically removing the recoveries (which are wavelength-dependent), the data obtained are presented in a set of figures which give the individual irradiation sequences.

The effect of the initial, mild treatment is shown in Figure 29, where the pertinent experimental conditions are also indicated. Again, relatively greater sensitivity for degradation in the visible and near IR is prominent.

After a recovery period of 90 hr (analyzed separately below), simultaneous irradiation was resumed with the results shown in Figure 30. Increments in this case were the same: it appears as if the first exposure after a "rest" (recovery) period is always very effective in erasing the recovery and bringing the spectrum down to near the prior damage level. After the next exposure the specimen had received nearly 10×10^{14} e/sq cm. From the curves obtained for the irradiation by electrons only, it appears that a change in degradation sensitivity occurs only at perhaps two to four times this dose. The next exposure increment with uv and electrons simultaneously present was considerably more effective in degrading the reflectance. These exposure sequences were made promptly, with just enough time between treatments to permit the taking of curves.

After 18 hr the specimen had recovered to the point illustrated by curve 1 of Figure 31. Again, the first irradiation was very effective in bringing the spectrum back down to the prior level. The increased

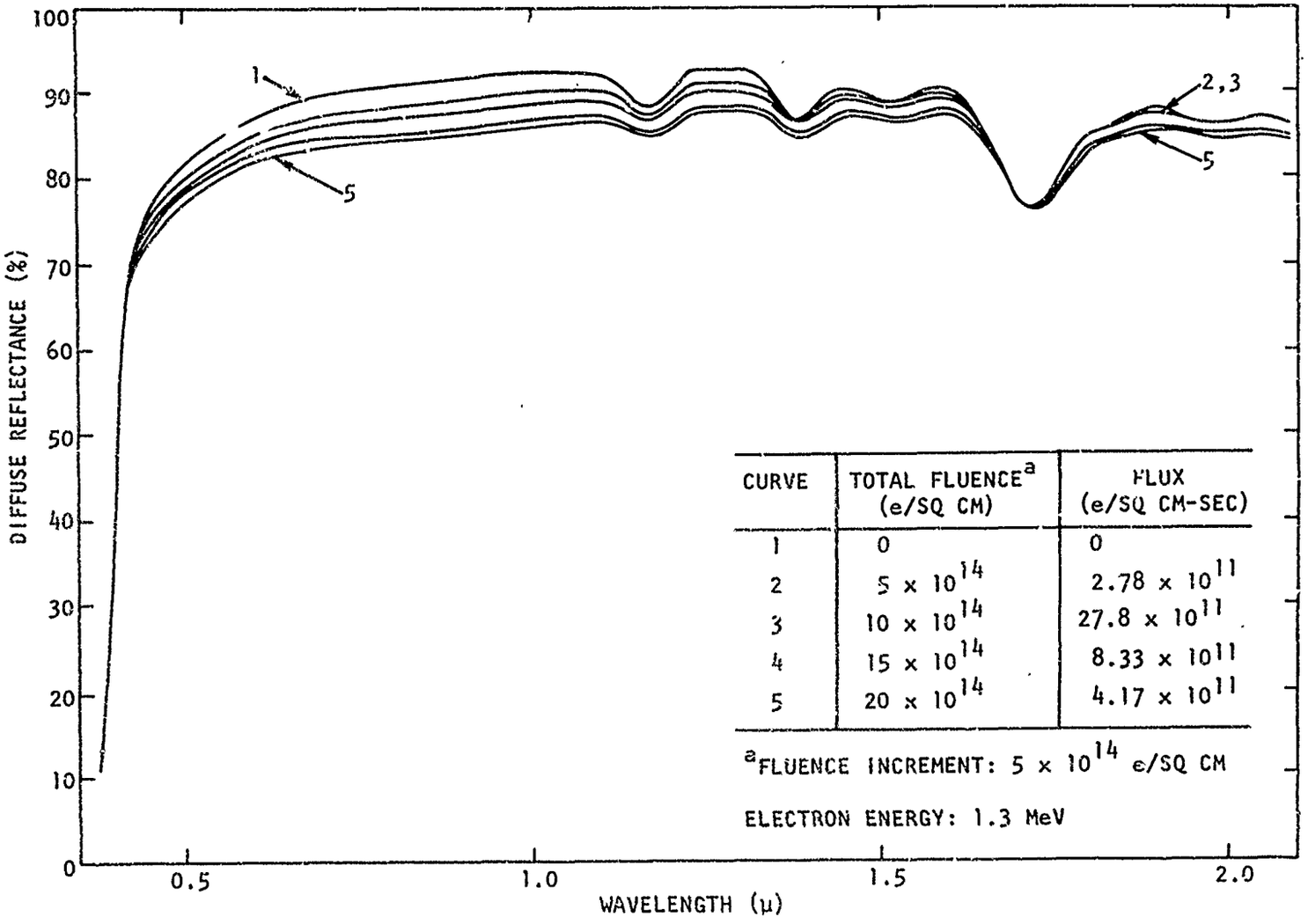

CURVE	TOTAL FLUENCE[a] (e/SQ CM)	FLUX (e/SQ CM-SEC)
1	0	0
2	5×10^{14}	2.78×10^{11}
3	10×10^{14}	27.8×10^{11}
4	15×10^{14}	8.33×10^{11}
5	20×10^{14}	4.17×10^{11}

[a]FLUENCE INCREMENT: 5×10^{14} e/SQ CM

ELECTRON ENERGY: 1.3 MeV

Figure 27. Effect of Electron Irradiation Performed with Constant Fluence and Different Fluxes (TiOx-032-G2B, RTV Binder)

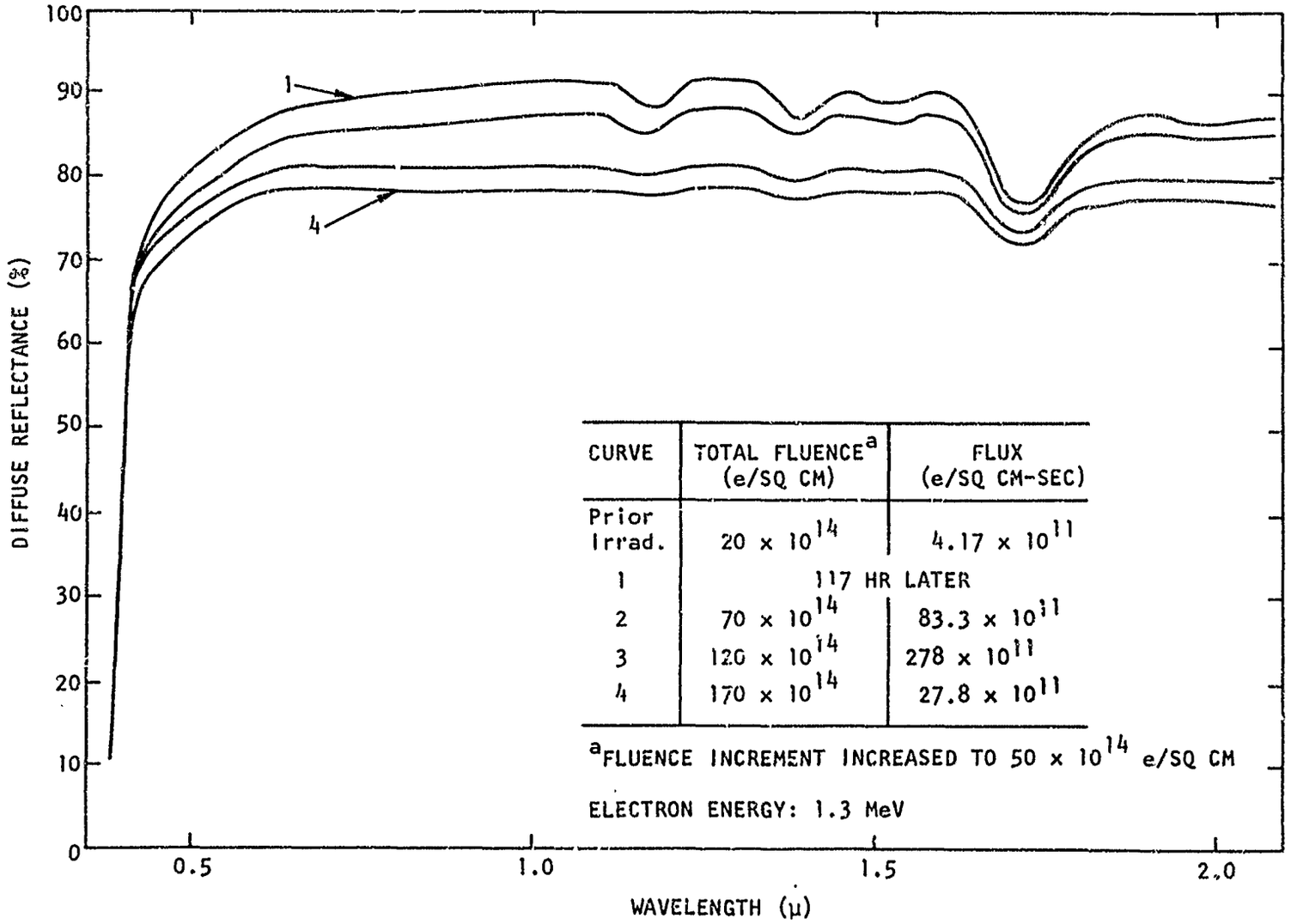

Figure 28. Effect of Further Electron Irradiation Performed with Constant Fluence and Different Fluxes (TiOx-032-G2B, RTV Binder)

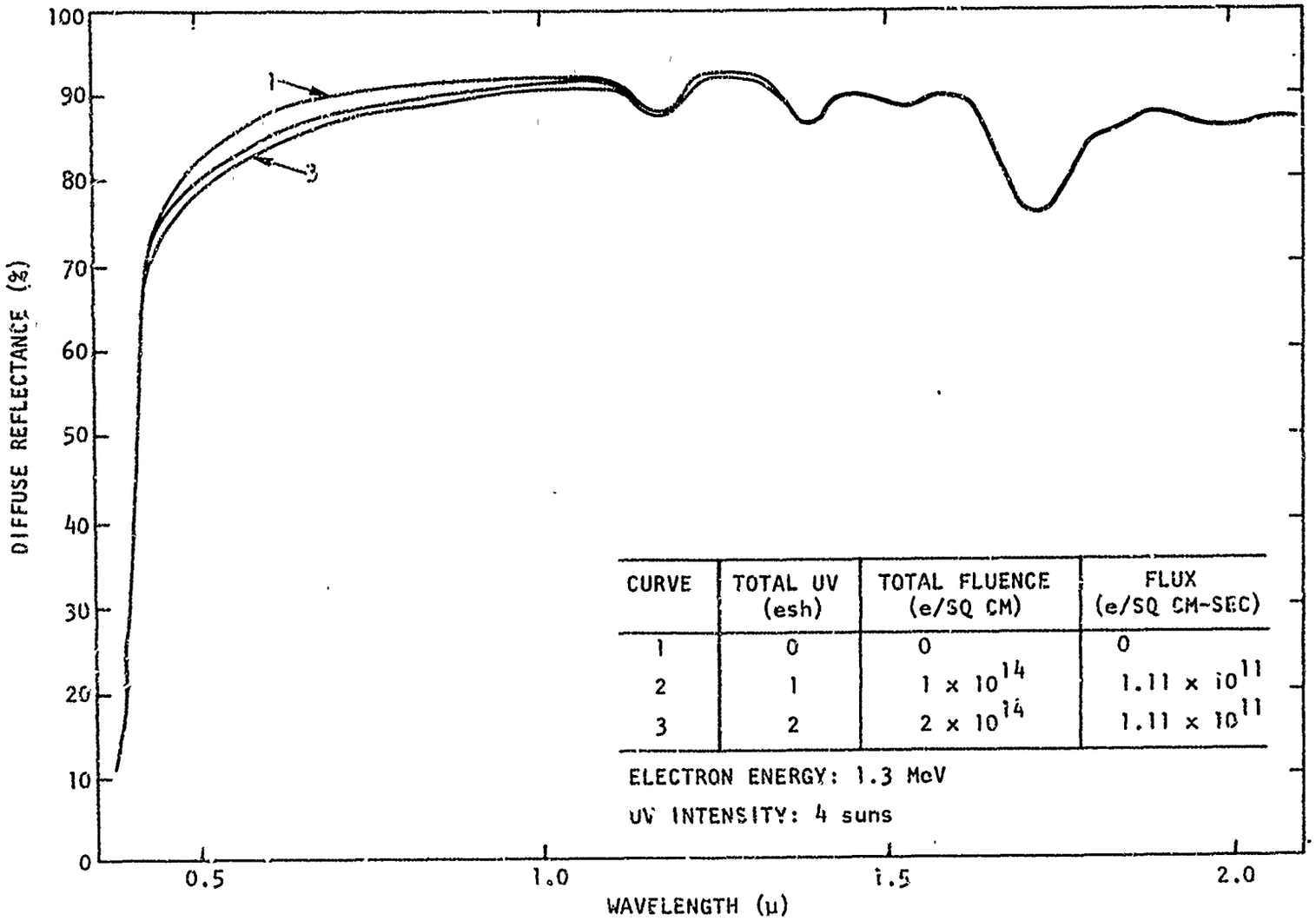

Figure 29. Effect of Simultaneous UV and Electron Irradiation (TiOx-031-G2B, RTV Binder)

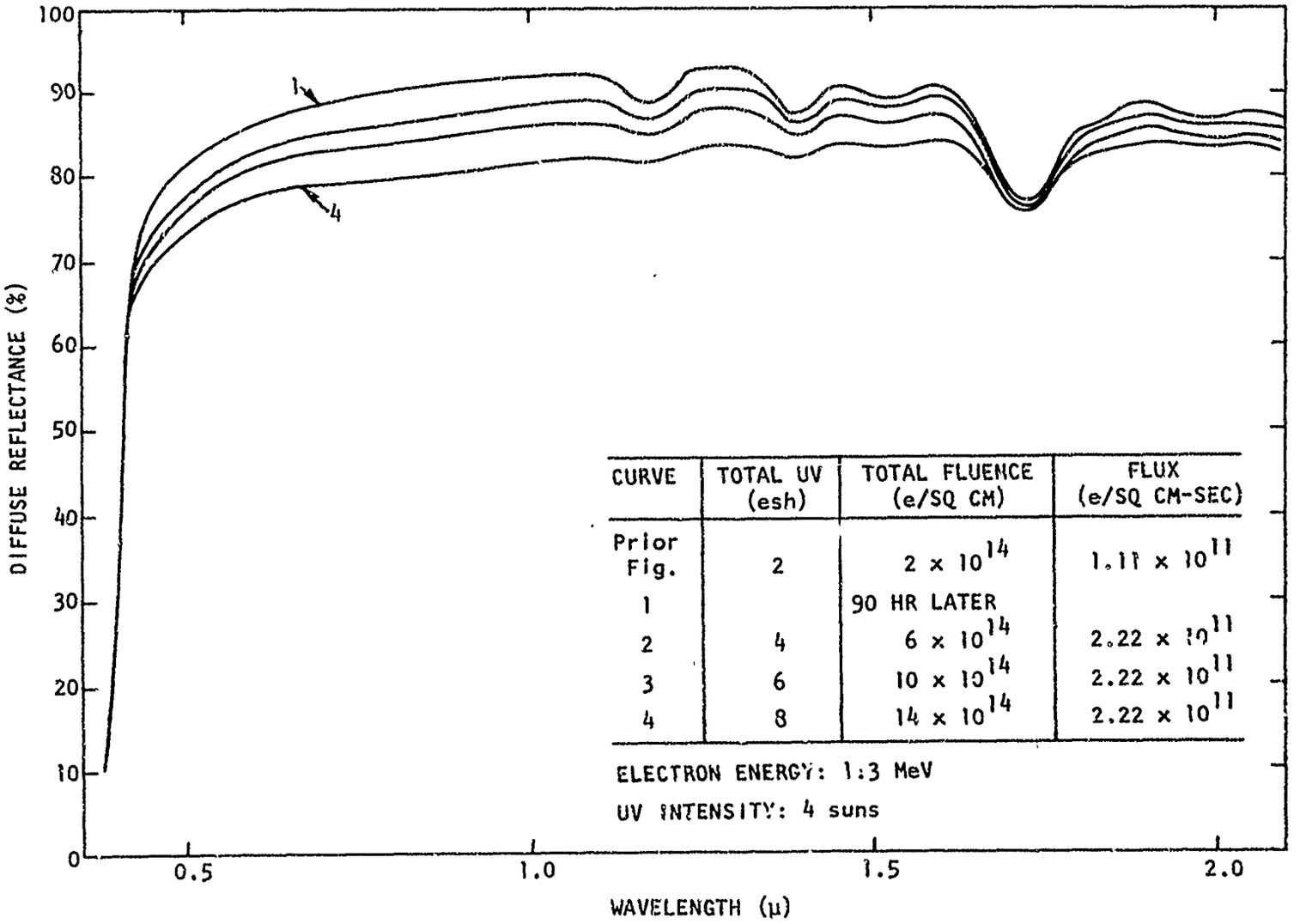

Figure 30. Effect of Further Simultaneous UV and Electron Irradiation after Recovery for 90 Hr (TiOx-031-G2B, RTV Binder)

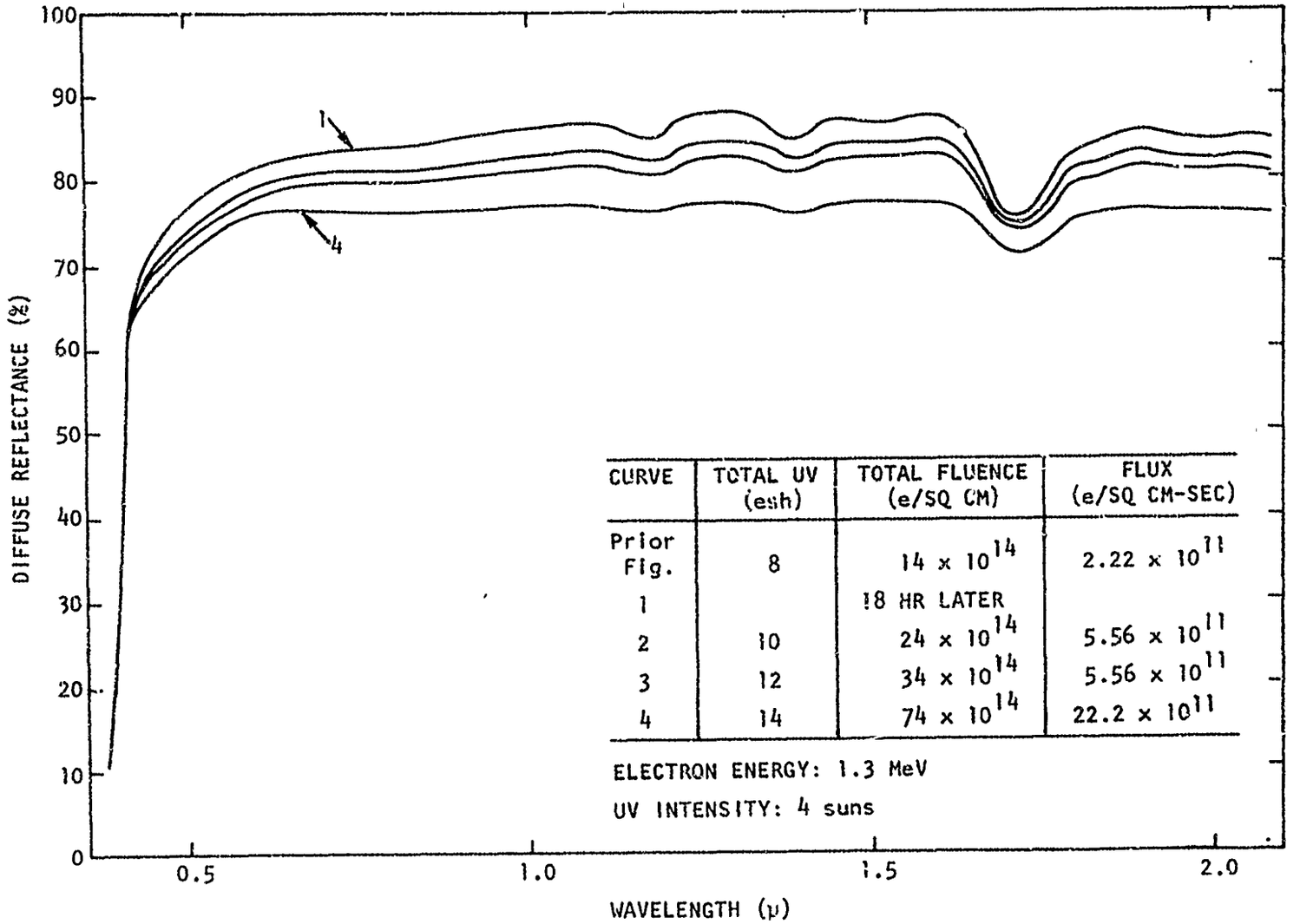

Figure 31. Effect of Further Simultaneous UV and Electron Irradiation after Recovery for 18 Hr (TiOx-031-G2B, RTV Binder)

degradation between curves 3 and 4 may well have resulted from using the larger electron fluence, coupled with the higher flux level, while the uv exposure increment was kept constant.

After a recovery period of 19.5 hr, continuing the simultaneous uv exposure but at the increased electron flux level gave spectra shown in Figure 32. It appears that degradation continues more slowly but uniformly across the spectrum once the IR degradation has caught up with the initially enhanced sensitivity in the visible and near-IR regions. With curve 4 of Figure 32, an end irradiation state equivalent to the separate uv and electron irradiations had been reached, and the experiments were stopped at that point.

Recovery Characteristics

Recovery of irradiated specimens was observed under a variety of conditions. First, there is the possibility of a rapid coating system recovery, say on the order of seconds to minutes. Although the residual vacuum in the system was often only in the 10^{-6} torr region, there seems to be some evidence that fast vacuum recovery is absent. In our experimental apparatus, this recovery would be difficult to observe. Spectral curves were started after uv exposure at times varying from minutes to 1 hr, but in no case were any drastic changes in the recovery characteristics observed during the spectral scanning time. When electron irradiation was involved, necessitating a 30-sec wait for the gamma flux in the experimental area to fall to acceptable levels on the radiation monitors so that the room where the in-situ apparatus is located could be entered, the shortest time before a spectrum could be started was about 5 min. Again, there was no evidence of a prompt recovery with a time constant of minutes; this does not preclude considerably faster recovery effects but sets a limit.

The next time scale for which recoveries were measured was over periods of hours. Spectra were monitored between irradiations or treatments at convenient intervals to permit the study of subsequent recovery.

Recovery from Ultraviolet Exposure

The recovery spectra for the TiO_2-RTV specimen which had been exposed to 22 esh of uv are shown in Figure 33. The initial reflectance characteristic in vacuum is shown by curve 1 (dashed). The maximum extent of degradation is indicated by curve 2, and recovery spectra in vacuum at indicated times are represented by curves 3 through 7.

All specimens were ultimately vented, first by admitting dry helium gas, which was then diluted by not more than 1 percent of dry nitrogen. This mixture was replaced by dry nitrogen, which in turn was then replaced by oxygen and, subsequently, by air. Spectra for some specimens were measured during vent-up. For the specimen represented in Figure 31, recovery had stopped sometime between 155 and 306 hr in vacuum at a level indicating persistent residual reflectance degradation. This spectral response did not change through vent-up but recovered to nearly its original vacuum characteristic

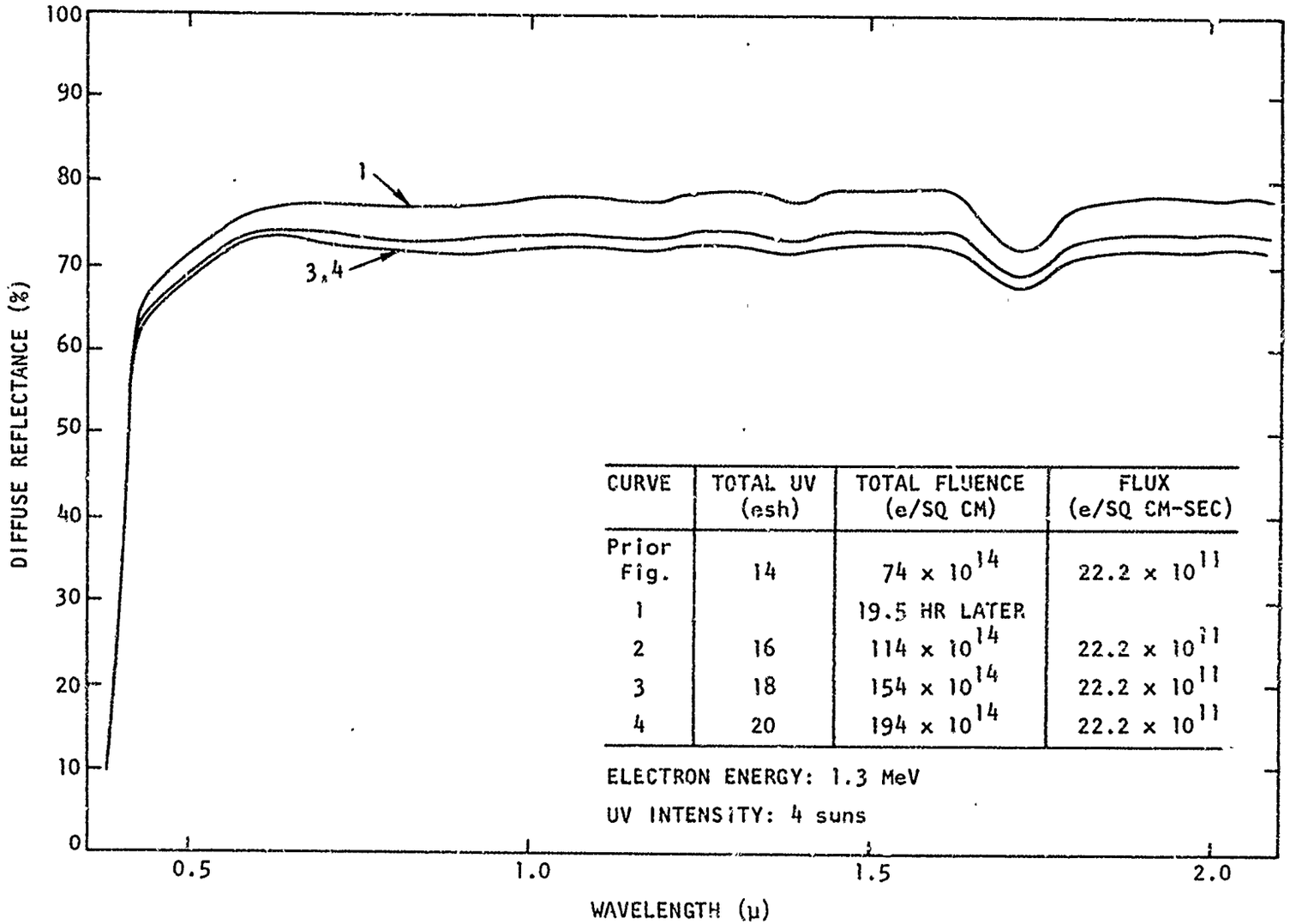

Figure 32. Effect of Further Simultaneous UV and Electron Irradiation after Recovery for 19.5 Hr (TiOx-031-G2B, RTV Binder)

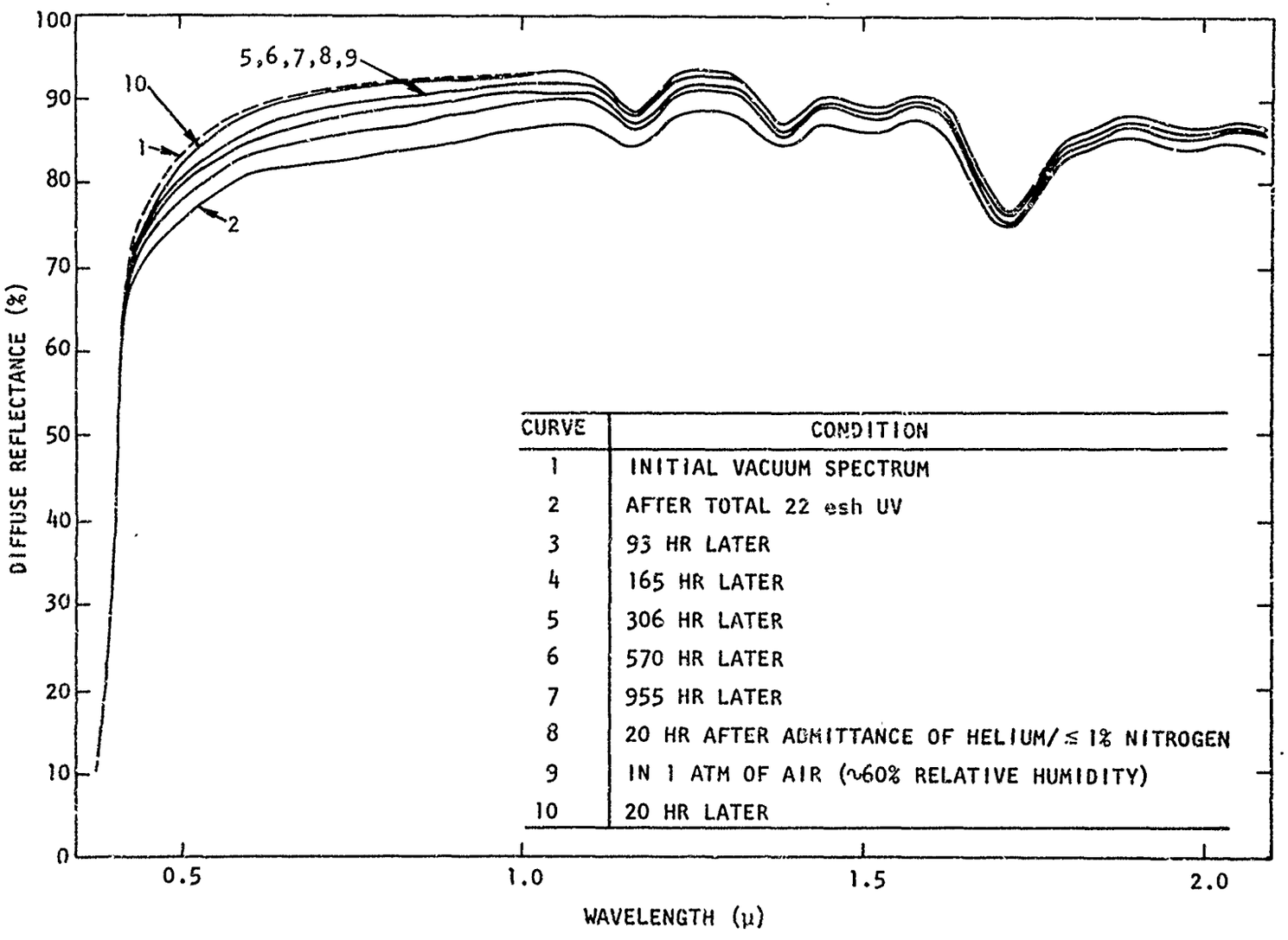

Figure 33. Recovery after Total Exposure of 22 esh UV (TiOx-033-G2, RTV Binder)

within 20 hr after air was finally admitted (with about 60 percent relative humidity). The slight discrepancy shown in Figure 33 may be due to experimental error. However, as mentioned earlier, the degradation observed from the "as-prepared" in air measurement, as compared with the stabilized preirradiation vacuum level, is irreversible.

Recovery from Electron Irradiation

Recovery for the specimen which was irradiated with electrons to a total fluence of 52 x 10^{14} e/sq cm is shown in Figure 34. Until after vent-up, recovery in vacuum remains incomplete; then within 20 hr, recovery becomes complete to the initial vacuum condition.

Recovery for the specimen which received an electron irradiation to a total fluence of 170 x 10^{14} e/sq cm is shown in Figure 35. Recovery had taken place from the maximum degradation shown by curve 2 to the final vacuum recovery indicated by curve 4. This specimen represents a special case for which the response was monitored during vent-up. There was no discernible change at 2 micrometers during actual vent-up with dry helium. Recovery within an hour of vent-up with dry helium is represented by curve 5. An attempt was made to displace the helium in the in-situ chamber by flushing with dry nitrogen but proved unsuccessful because of the experimental arrangement. The sample chamber was then isolated for about 20 hr; it is believed that the nitrogen concentration mixed with the helium was less than 1 percent. After subsequent evacuation of the chamber, it was backfilled first with nitrogen and later with oxygen. The spectrum obtained for the oxygen backfill is shown by curve 7 of Figure 35. Immediately after removal of the oxygen and subsequent backfilling with air, the characteristic had not changed: curve 8 overlays curve 7. However, after the specimen had been in air for 20 hr, slow recovery had continued as indicated by curve 9. Finally, as shown by curve 10, sometime during 554 hr of exposure to air, the specimen recovered completely back to its preirradiation vacuum condition.

Recovery from Simultaneous Ultraviolet and Electron Irradiation

For the binderless specimens, recovery after simultaneous uv and electron irradiation was very rapid in the IR and very slow in the visible region. To provide a comparison with this behavior, the early recovery characteristics of the TiO_2-RTV specimen after exposure to 2 esh of uv and 2 x 10^{14} e/sq cm are shown in Figure 36. Degradation had been almost exclusively in the visible and near-IR regions and was relatively small in magnitude. Recovery did take place, but even after 90 hr in vacuum the sample had not recovered to its preirradiation value. The irradiation sequence was then resumed, and after a total exposure of 20 esh of uv and 200 x 10^{14} e/sq cm, the sample exhibited the recovery characteristics shown in Figure 37. Vacuum recovery had come to a virtual standstill within a couple of hundred hours with less than half the damage recovered over most of the spectrum.

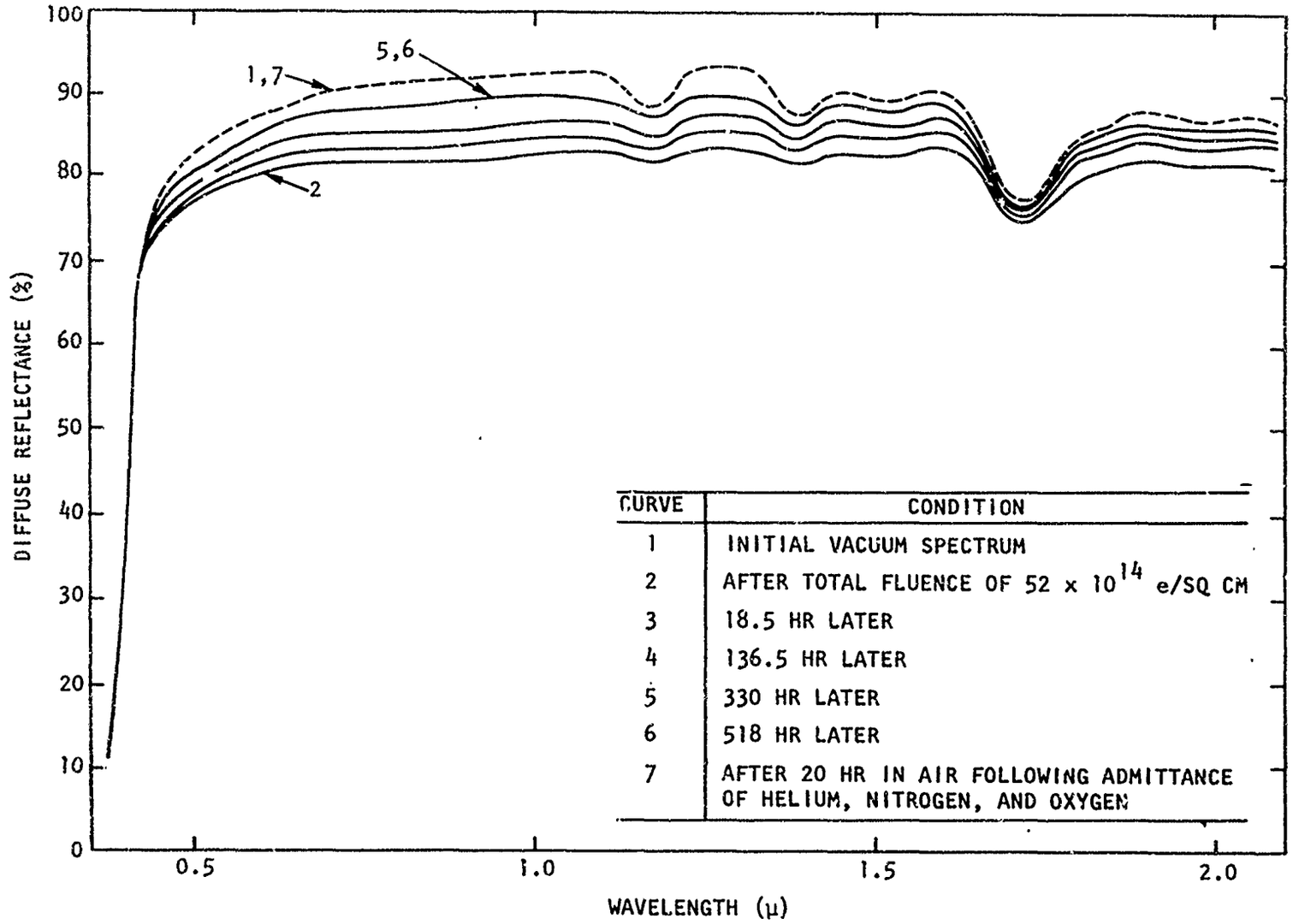

Figure 34. Recovery after Total Fluence of 52 x 10^{14} e/sq cm (TiOx-034-G2B, RTV Binder)

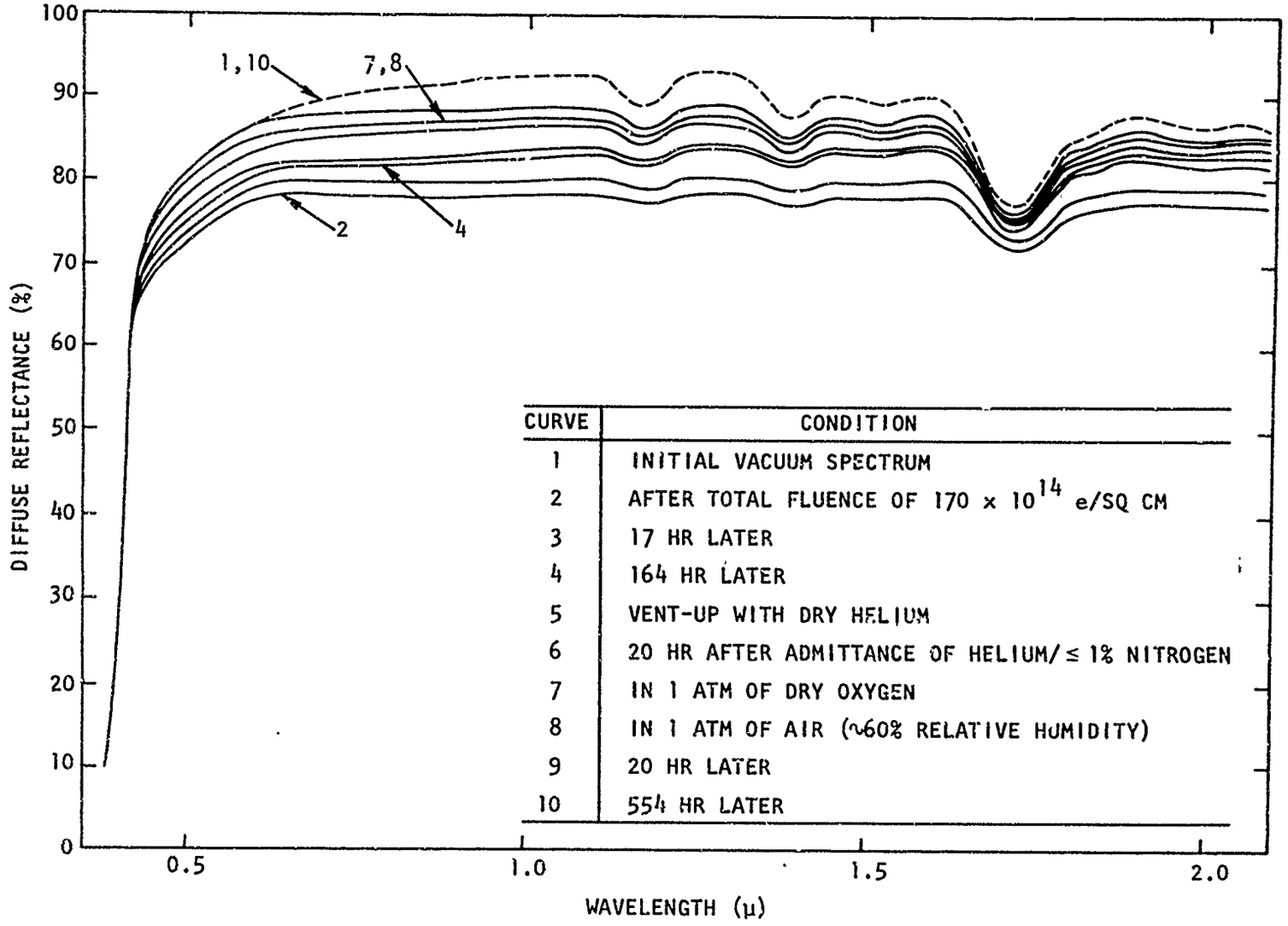

Figure 35. Recovery after Total Fluence of 170 x 10^{14} e/sq cm (TiOx-032-G2B, RTV Binder)

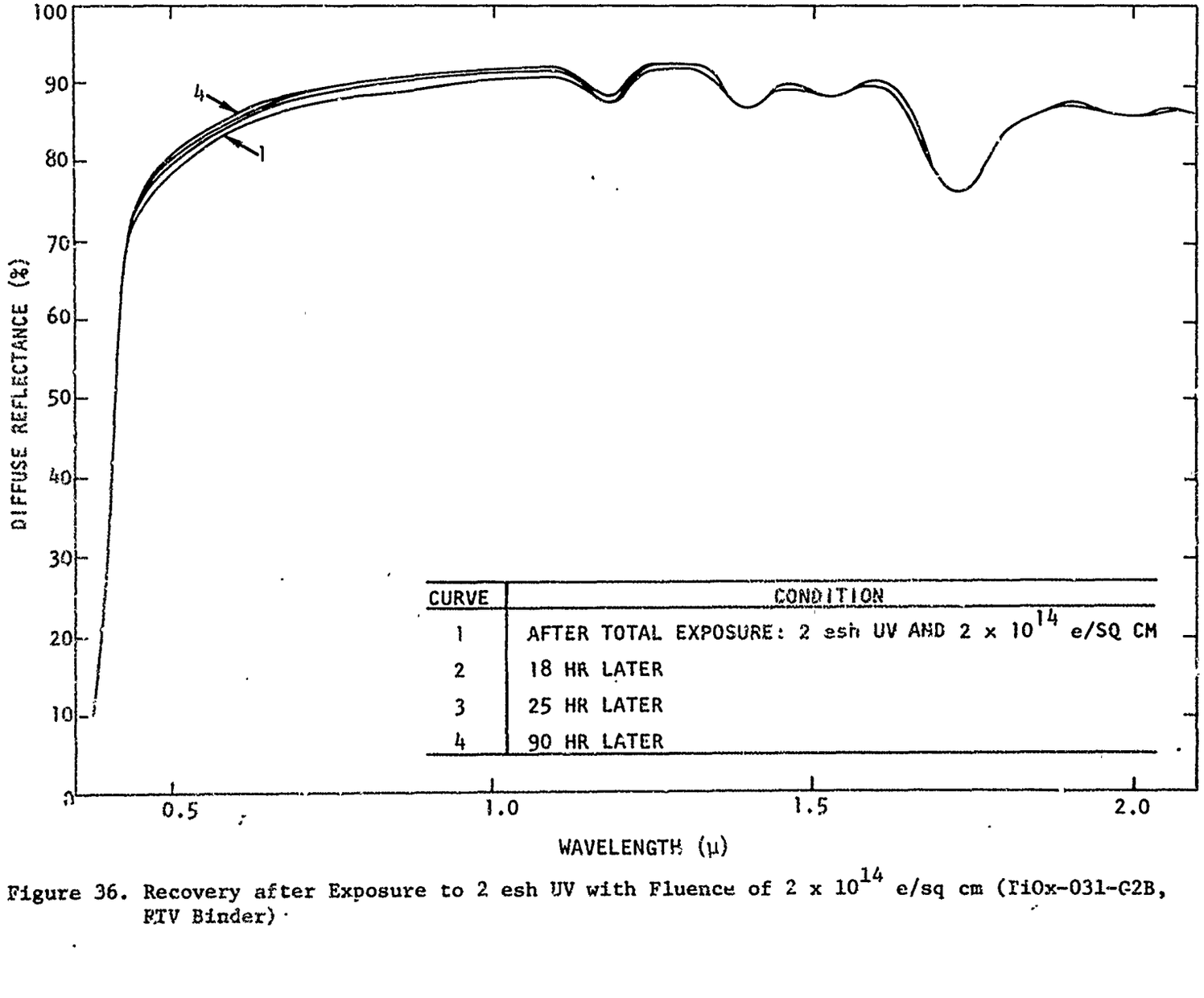

Figure 36. Recovery after Exposure to 2 esh UV with Fluence of 2 x 10^{14} e/sq cm (TiOx-031-G2B, RTV Binder)

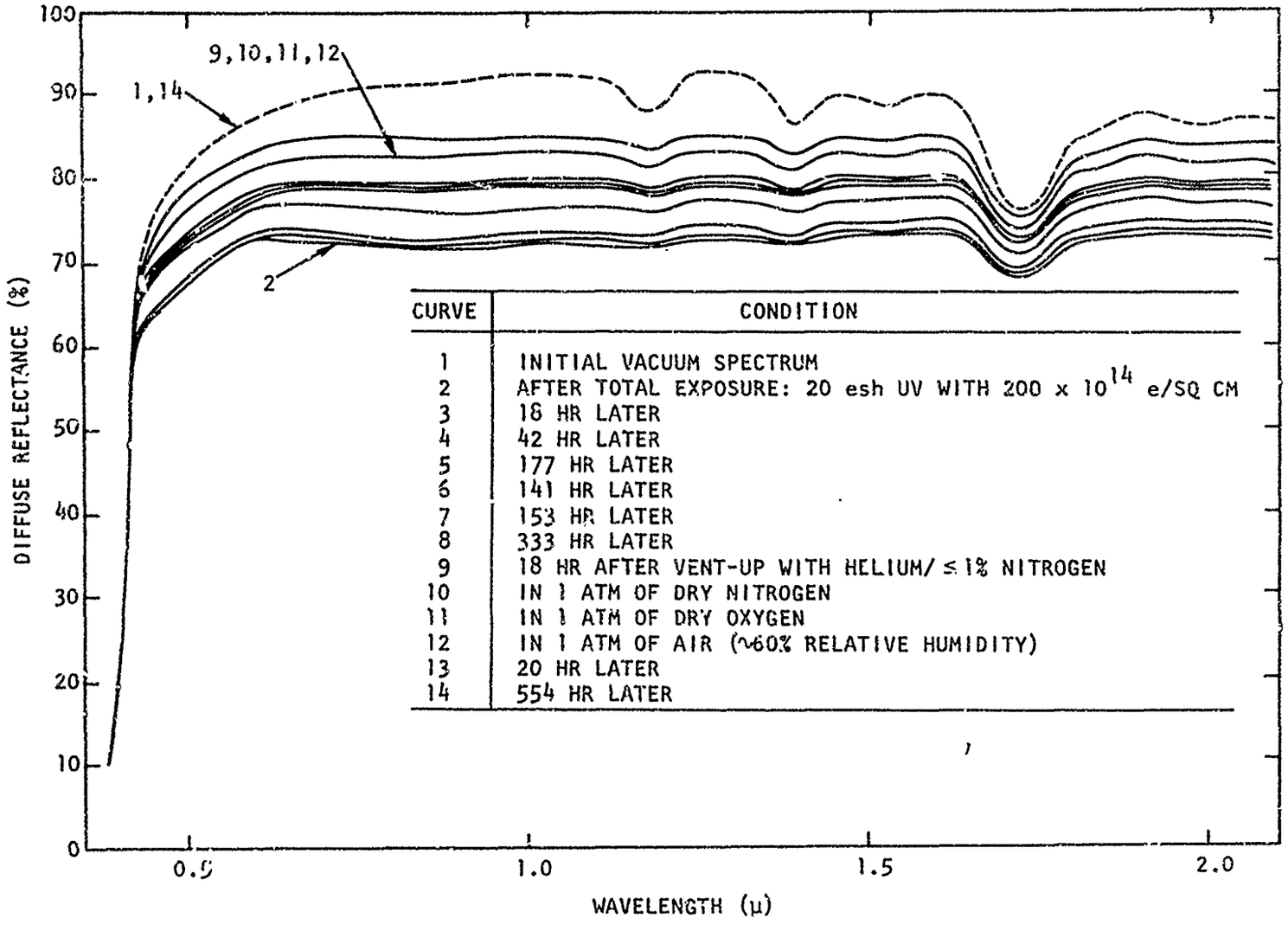

Figure 37. Recovery after Exposure to 20 esh UV with Fluence of 200 x 10^{14} e/sq cm (TiOx-03i-G2B, RTV Binder)

Vent-up and exposure through the various gases resulted in renewed recovery as shown by curves 9 through 12 of Figure 37. However, recovery was far from rapid as can be seen from curve 13, which was taken 20 hr after the sample had been exposed to air. Complete recovery was achieved again during a 554-hr period, at the end of which the specimen yielded a spectrum essentially identical to the original vacuum characteristic.

Reflectance Degradation Analysis

In the foregoing sections, the sets of spectra obtained following uv, electron, and combined irradiation have been presented. Such curves present a useful overall view of the damage, but plots of the reflectance of a particular wavelength versus exposure time, exposure rate, or recovery time are more pertinent to analysis. The curves in the foregoing sections indicate that the spectra can be divided into two regions, the visible and the IR, for purposes of analysis. An attempt has therefore been made to represent these regions by arbitrarily selecting two wavelengths along which to make analytical crosscuts. It appeared that the "visible" region would be least artificially distorted in its representation if 0.8 micrometer was chosen; in the IR, 2.0 micrometers is unaffected by the pair of adjacent absorption bands of the binder. Data reduction was undertaken using these values. For comparative purposes, corresponding data were obtained for the dry-pressed binderless specimens whenever possible.

Ultraviolet Exposure Dependence

The reflectance degradation at 0.8 and 2 micrometers as a function of uv exposure is shown in Figures 38 and 39. The data for the binderless dry-pressed specimen are connected by the dashed lines. The change in reflectance during recovery is indicated by vertically connected pairs of data points. The data points for the individual exposure sequence have arbitrarily been adjusted by the increment of the recoveries. As can be seen, the guide lines, fit by eye, appear to give a reasonably smooth functional dependence. This seems to justify this approach to data correlation.

For both wavelengths, the binderless specimen shows considerably more sensitivity to the mild, initial uv exposures (see Figures 38 and 39). The magnitude of damage for both specimens is greater in the visible than in the IR. Both specimens show saturation, the binderless specimen reaching its apparent final level at about half the exposures necessary for the silicone binder specimen. However, both specimens ultimately reach approximately the same saturation level.

Fluence Dependence

The reflectance degradation crosscuts for electron irradiation to 52×10^{14} e/sq cm of the TiO_2-RTV specimen are given in Figures 40 and 41. The reflectance scale on all figures in this section is the same, so direct comparisons can be made between them. The fluence scale for

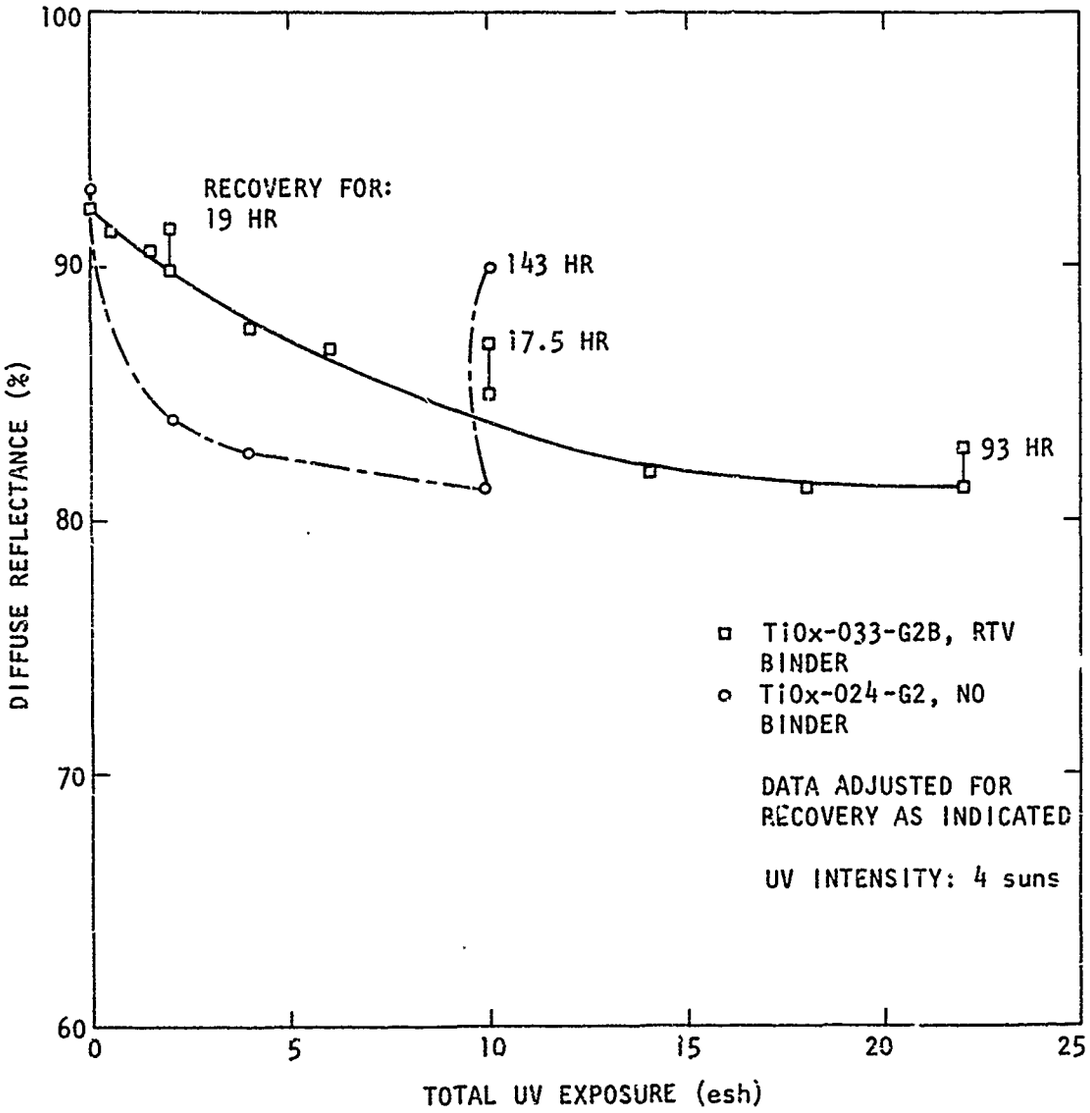

Figure 38. Reflectance at 0.8 Micrometer Versus UV Exposure (TiOx-033-G2B, RTV Binder; TiOx-024-G2, No Binder)

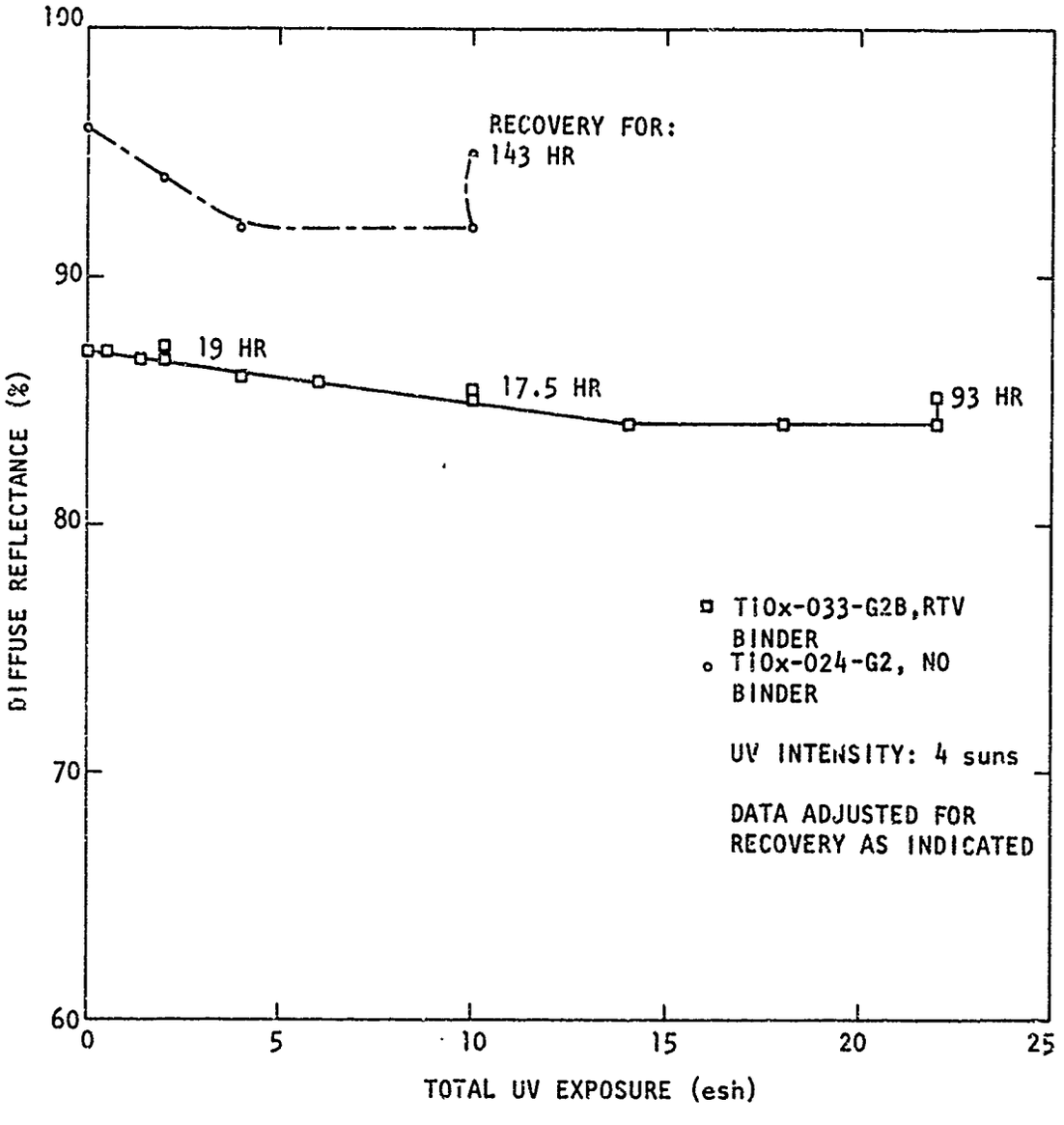

Figure 39. Reflectance at 2.0 Micrometers Versus UV Exposure (TiOx-033-G2B, RTV Binder; TiOx-024-G2, No Binder)

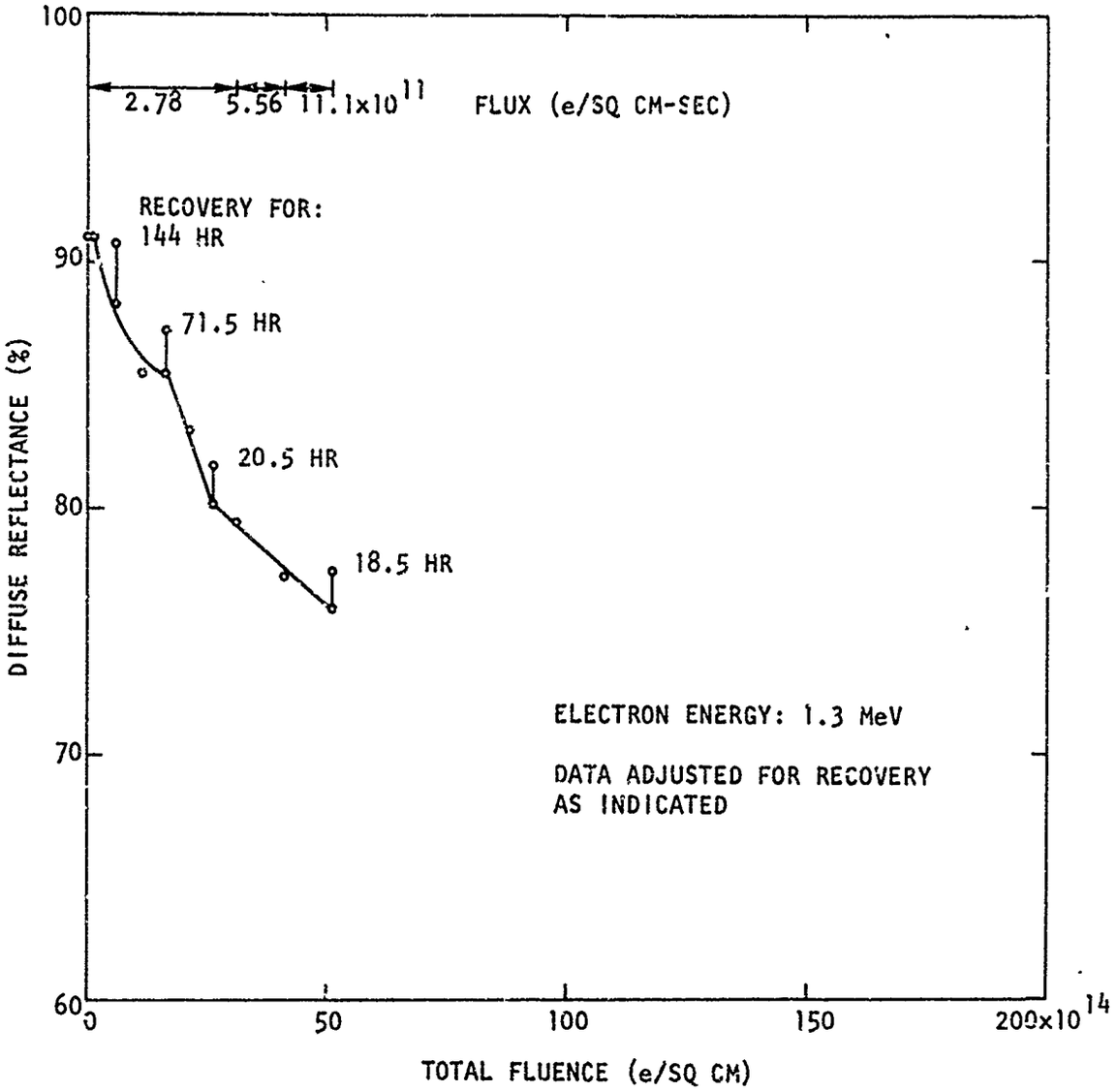

Figure 40. Reflectance at 0.8 Micrometer Versus Electron Irradiation (TiOx-034-G2B, RTV Binder)

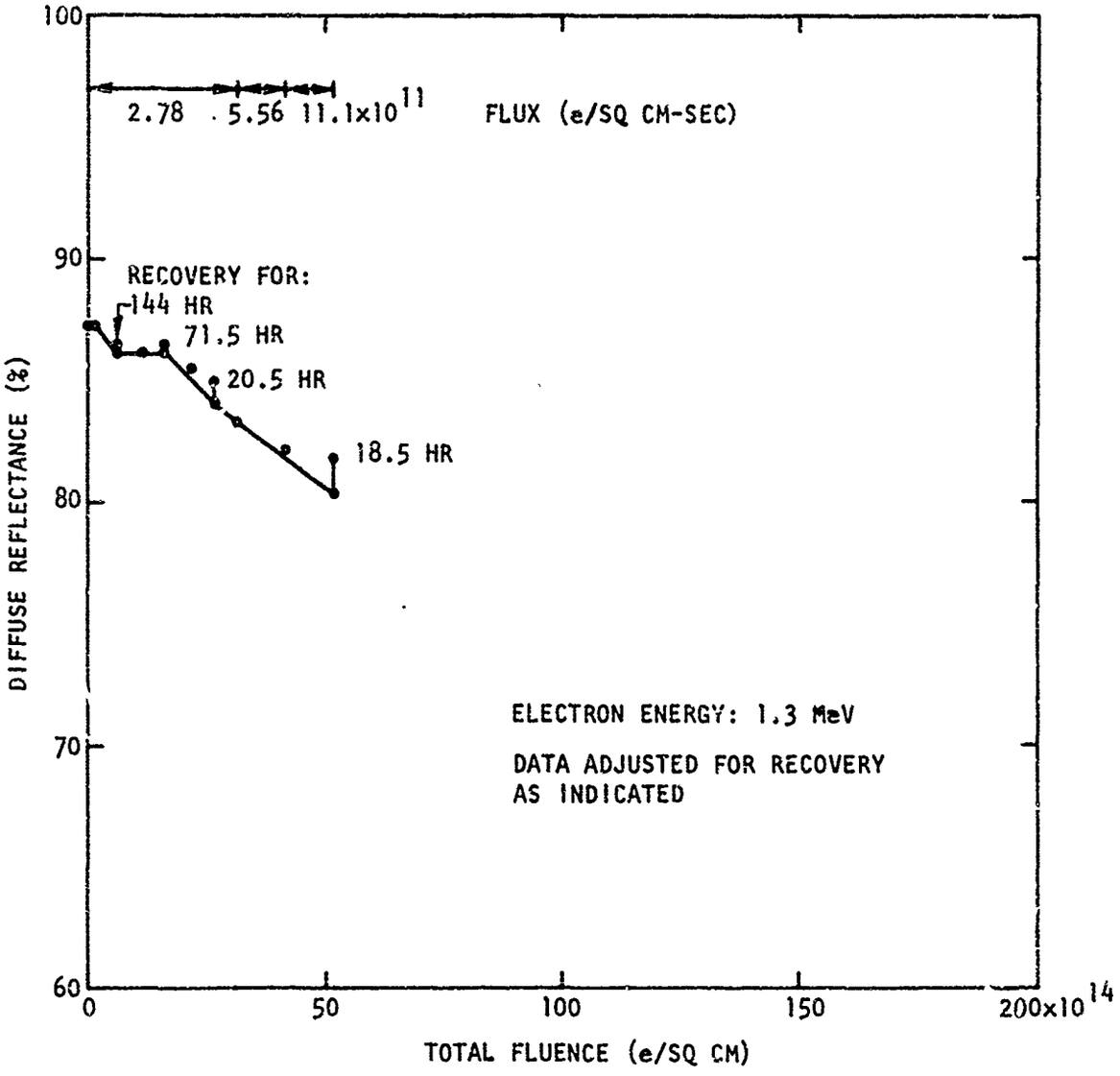

Figure 41. Reflectance at 2 Micrometers Versus Electron Irradiation (TiOx-034-G2B, RTV Binder)

Figures 40 and 41 was chosen to allow later direct comparison with larger values discussed below. The flux used for the various irradiations is indicated for the appropriate range. Recovery effects are treated as before. In contrast to the uv-only case, degradation in the IR is about half that in the visible instead of being a small fraction. For both the 0.8- and the 2.0-micrometer data, there is a cusp at about 20×10^{14} e/sq cm. The reason for this cusp is not clear. It may be an artifact of the experiment.

The corresponding degradation crosscuts for the binderless specimen are shown in Figures 42 and 43. These data were taken with constant flux and also show a scalloped saturation tendency, which is, however, considerably more pronounced. The degradation of the TiO_2-RTV specimen due to electron irradiation is greater than that of the binderless specimen. This result is in contrast to the case of uv exposure, where the TiO_2-RTV specimen is less sensitive than the binderless specimen.

The reflectance degradation for the binder specimen which was exposed to a variety of electron flux conditions is given in Figures 44 and 45. Although the general behavior is similar to that of the other specimen, it appears that larger fluxes are less effective in degrading the specimen at the same fluence level; for the conditions shown here about three times the number of electrons are required to degrade to about the same damage level. There also appears to be a fluence dependence in that the degradation rate is lower at higher fluences. There is definitely a flux-fluence interaction affecting the damage; the specimens had almost identical histories, and they had been in the same overall environment.

Simultaneous Ultraviolet and Electron Irradiation Dependence

The reflectance degradation crosscuts for simultaneous uv exposure and electron irradiation of the TiO_2-RTV specimen is shown in Figures 46 and 47. The reflectance at 0.8 micrometer is very strongly sensitive to electron density. Both regions show a transition to a saturation behavior at the higher fluence levels. The overall absolute degradation is about 25 percent larger for exposure to 50×10^{14} e/sq cm than for the separate electron treatment, but there is no obvious synergistic effect such as that noted for the binderless specimens. This difference might be an indication of different conditions at the pigment interfaces.

For the binderless specimen, the crosscuts obtained using simultaneous uv exposure and electron irradiation are shown in Figures 48 and 49. In addition to the 0.8-micrometer cut illustrated by Figure 48, crosscuts at 0.6 and 0.5 micrometer were taken, since the spectrum in the visible fell particularly rapidly. This low wavelength roll-off was very definite, and this strong degradation is decidedly absent for the binder specimen. If this effect is uv-related, requiring however the presence of electrons or their interaction energy, it is conceivable that the binder acts as a neutralizer, or passivation medium.

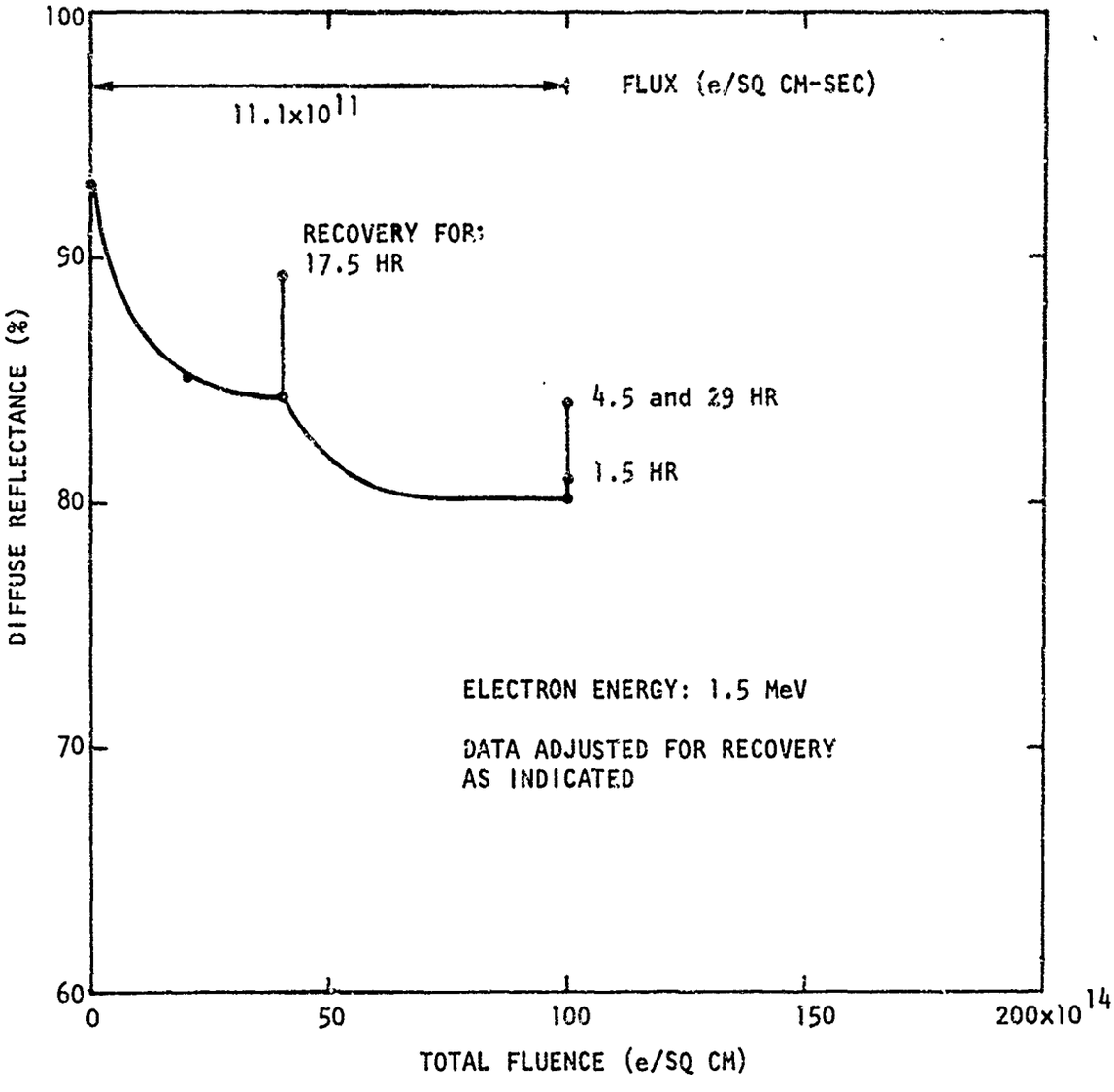

Figure 42. Reflectance at 0.8 Micrometer Versus Electron Irradiation (TiOx-028-G2, No Binder)

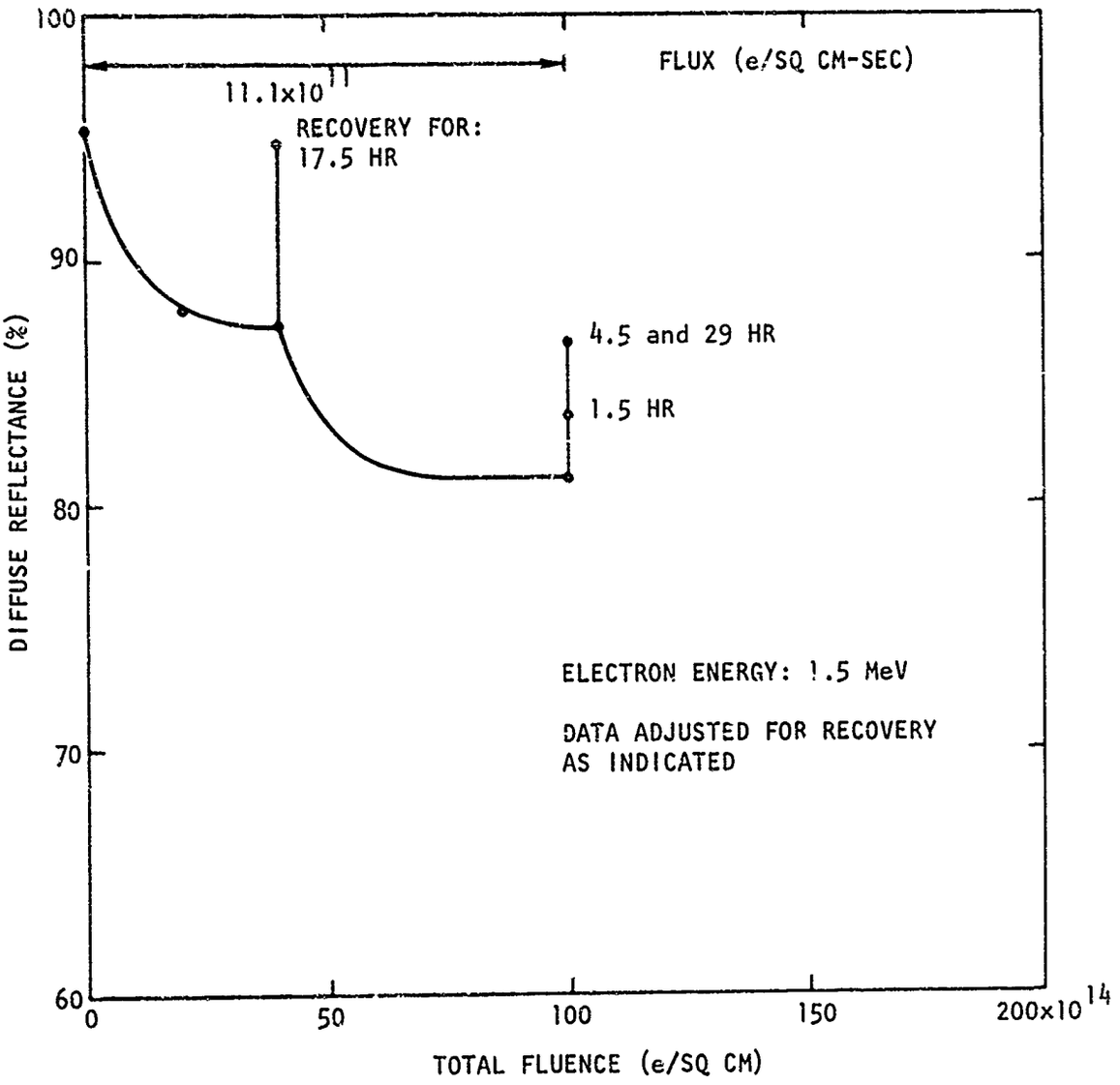

Figure 43. Reflectance at 2 Micrometers Versus Electron Irradiation (TiOx-028-G2, No Binder)

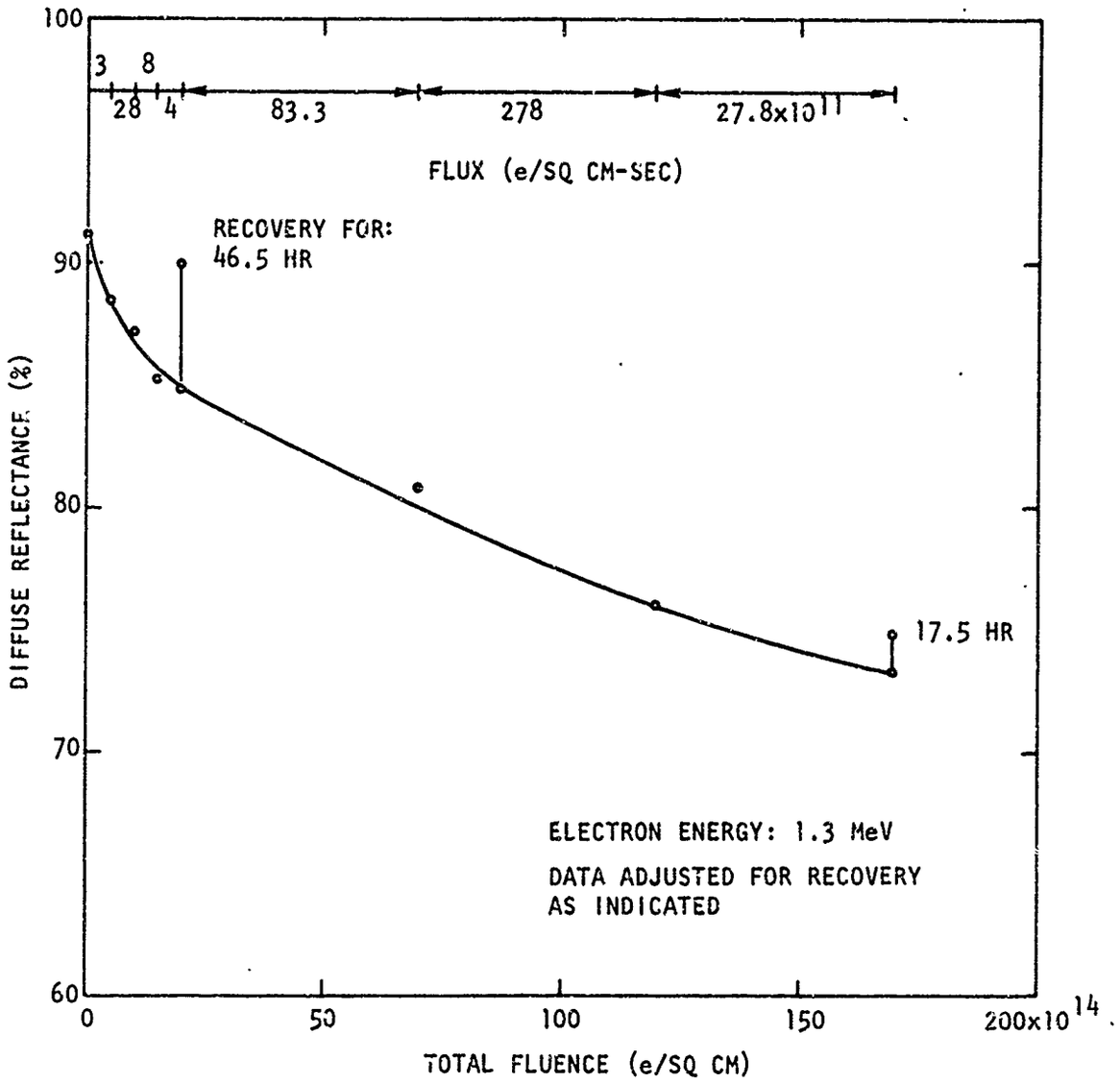

Figure 44. Reflectance at 0.8 Micrometer Versus Electron Irradiation Performed with Constant Fluence and Different Fluxes (TiOx-032-G2B, RTV Binder)

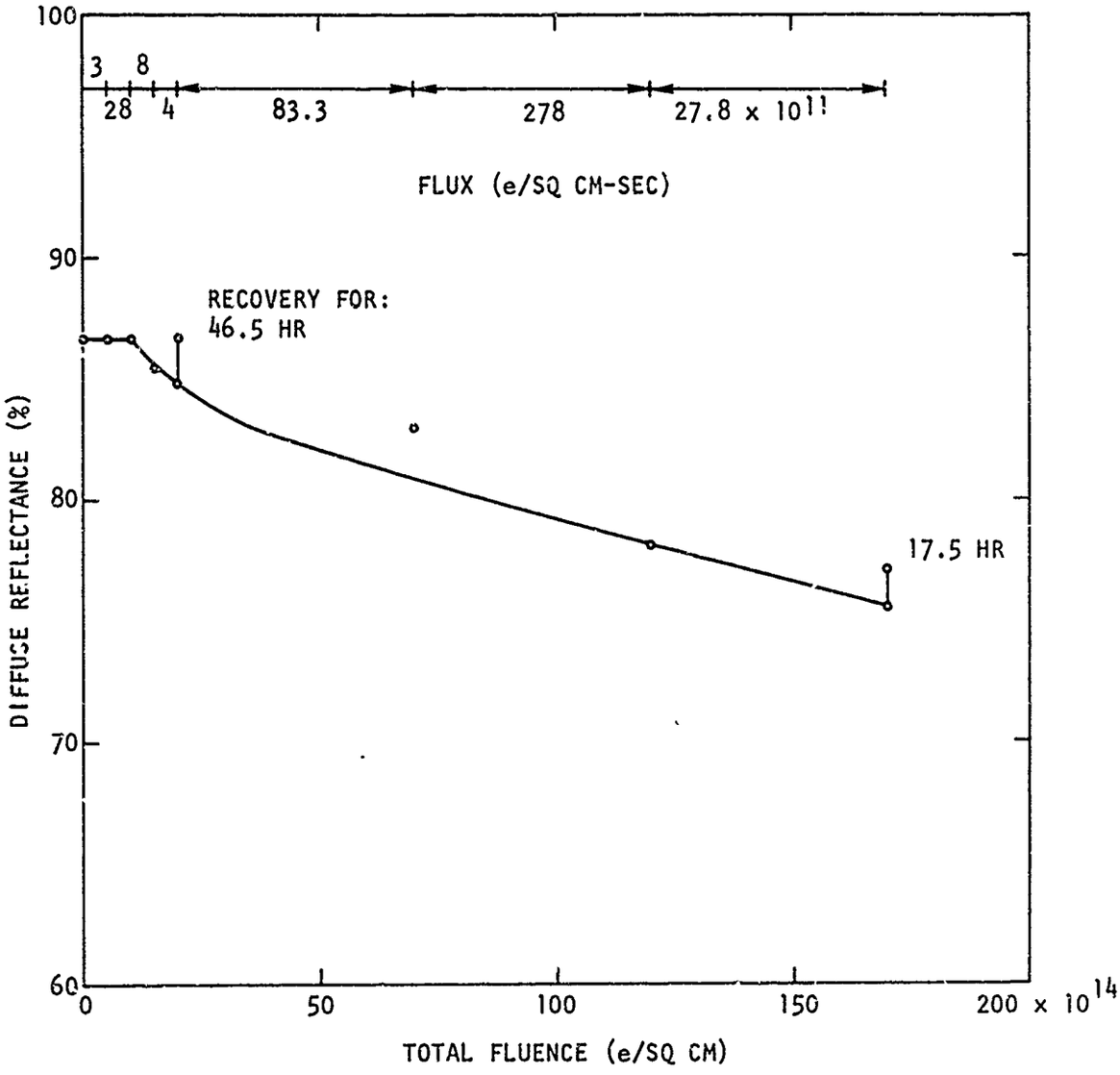

Figure 45. Reflectance at 2 Micrometers Versus Electron Irradiation; Constant Fluence with Different Fluxes (TiOx-032-G2B, RTV Binder)

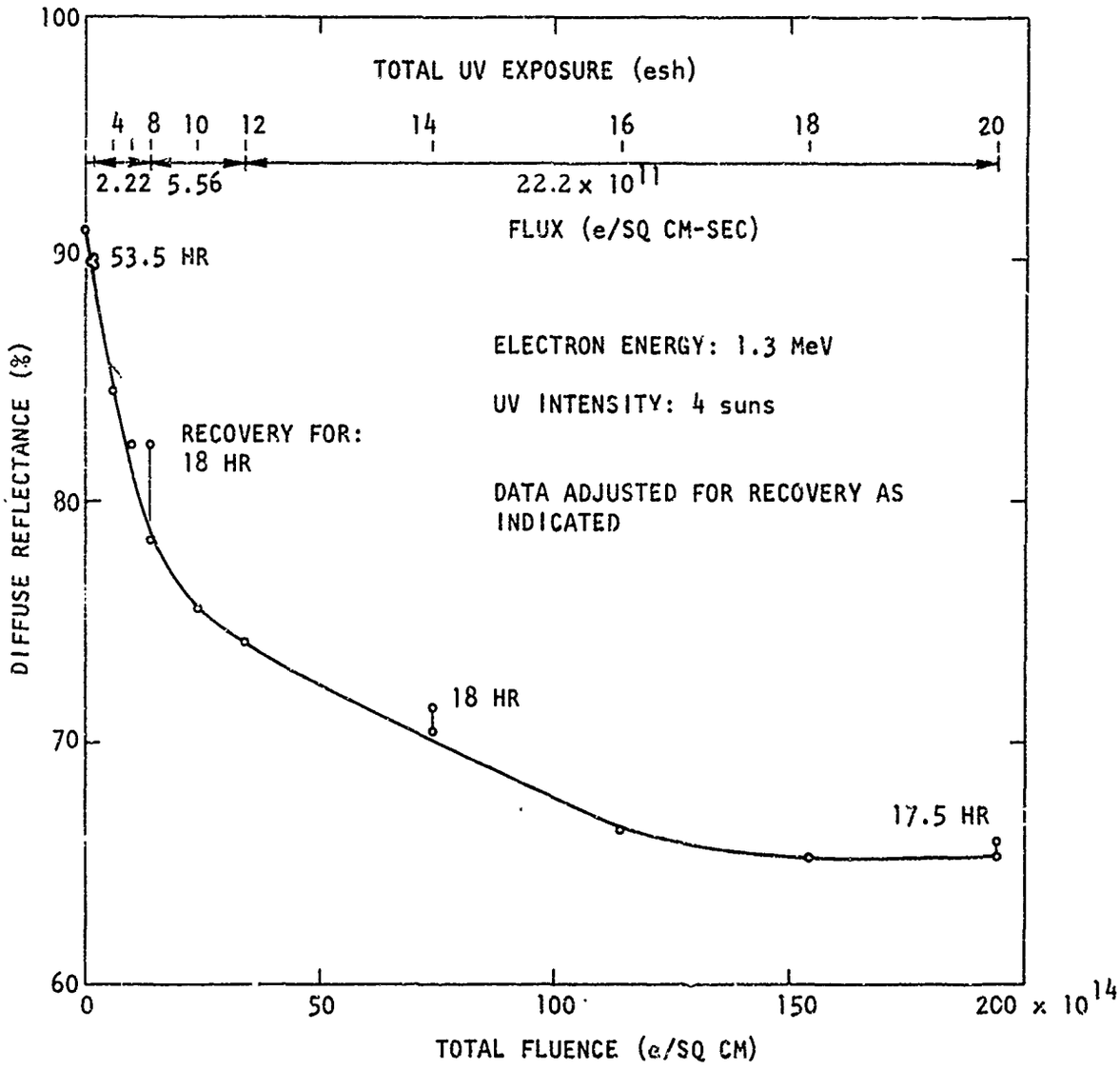

Figure 46. Reflectance at 0.8 Micrometer Versus Simultaneous UV and Electron Irradiation (TiOx-031-G2B, RTV Binder)

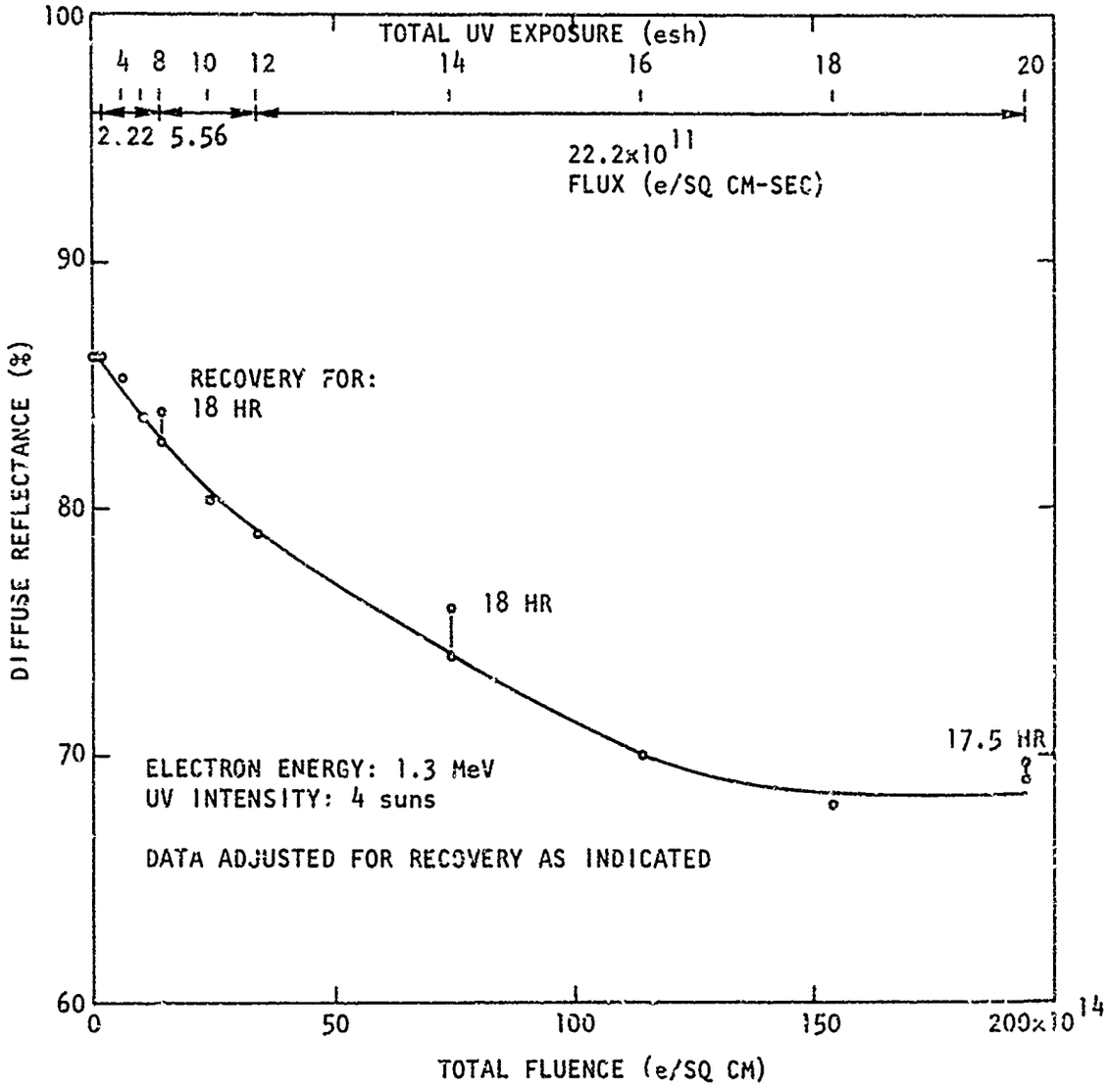

Figure 47. Reflectance at 2 Micrometers Versus Simultaneous UV and Electron Irradiation (TiOx-031-G2B, RTV Binder)

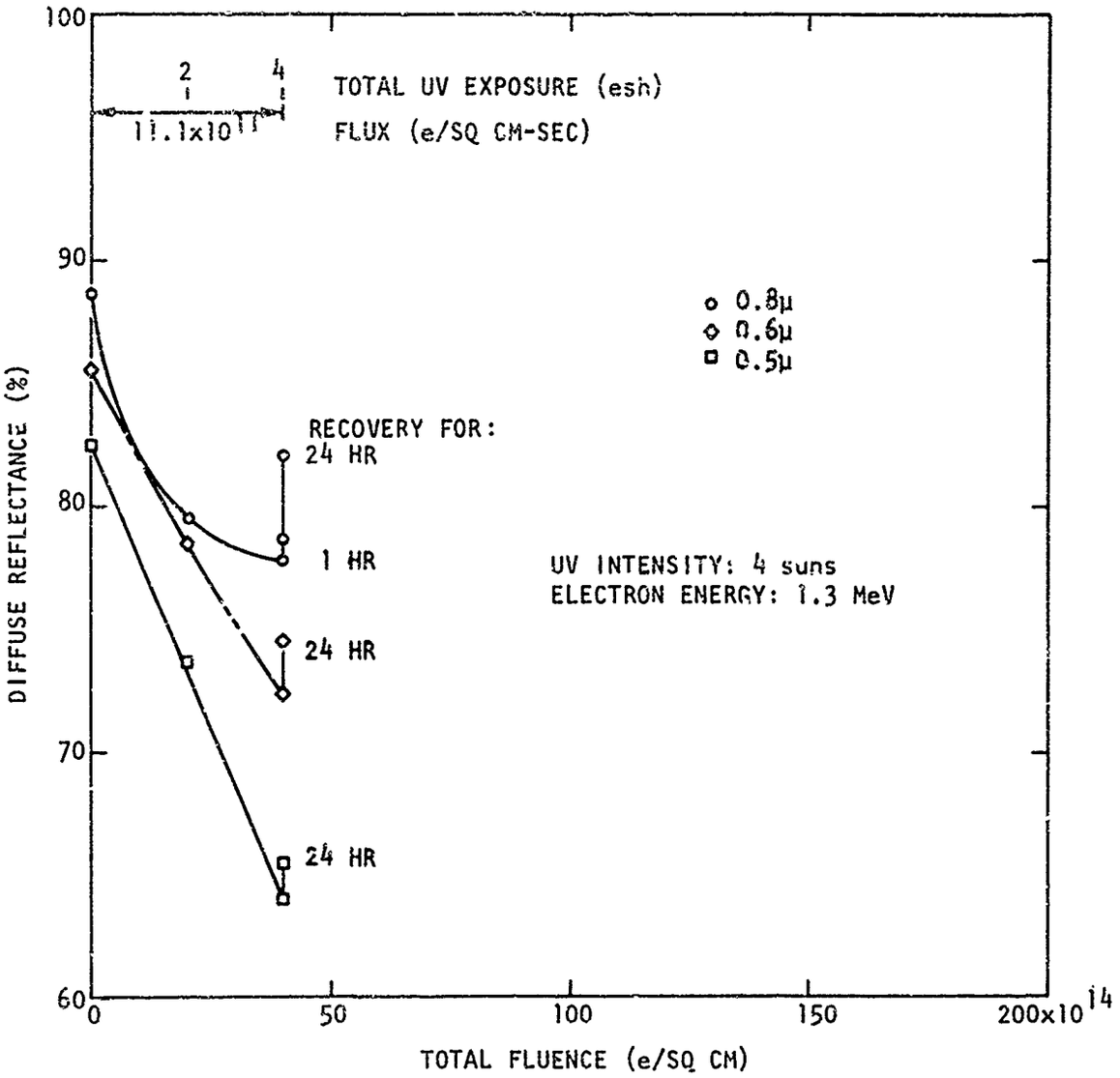

Figure 48. Reflectance at 0.8, 0.6, and 0.5 Micrometer Versus Simultaneous UV and Electron Irradiation (TiOx-026-G2, No Binder)

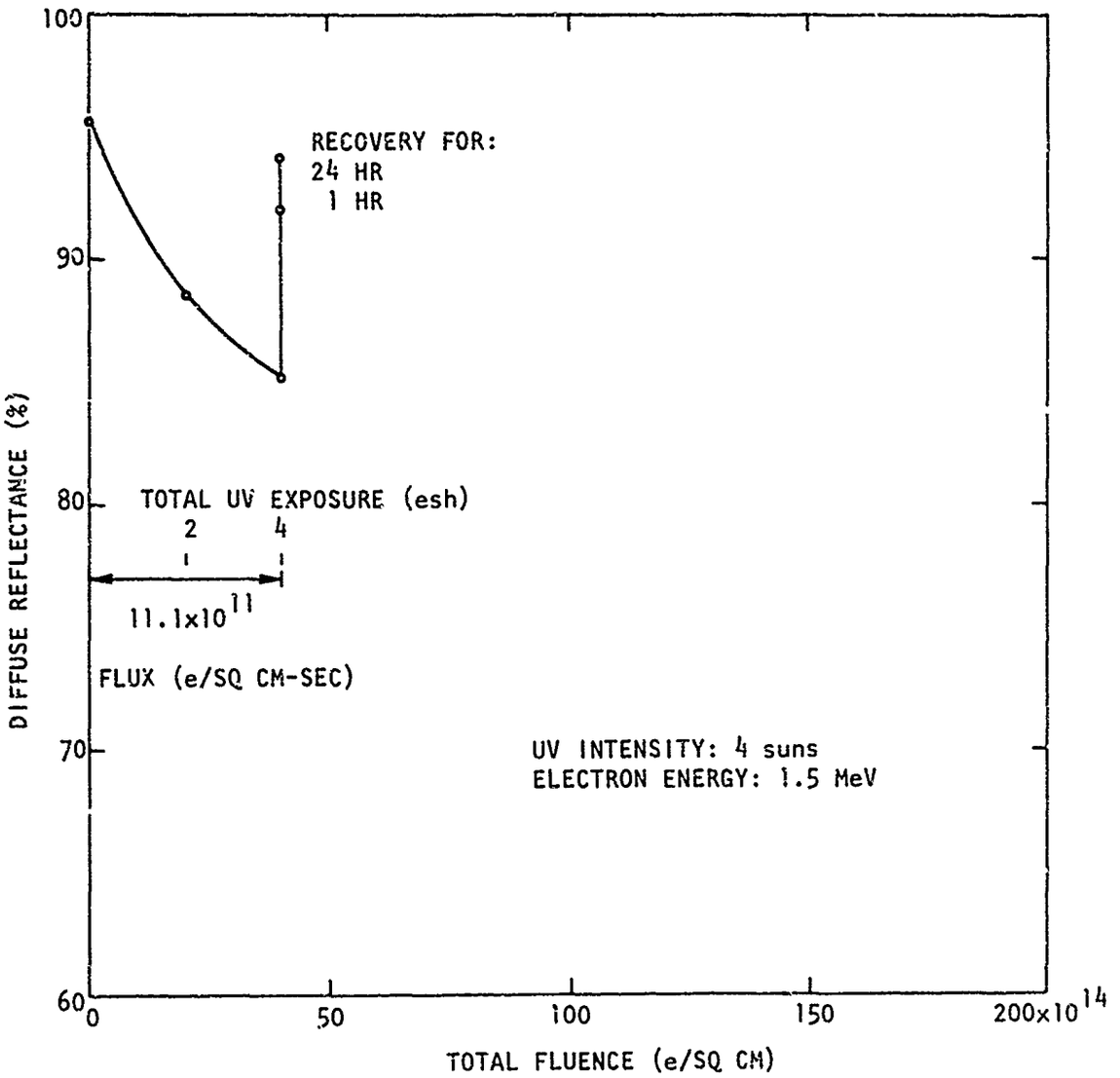

Figure 49. Reflectance at 2 Micrometers Versus Simultaneous UV and Electron Irradiation (TiOx-026-G2, No Binder)

Fluence Dependence of Reflectance Degradation

It was observed that at large fluences, the degradation per fluence unit appears to decrease. However, since large fluences usually imply large fluxes, the electron irradiation data were analyzed to attempt to separate the fluence and flux dependences. To unambiguously separate the effects, samples would have to be damaged at different fluxes to the same value of fluence. Then a different set of samples would have to be damaged at constant fluence. Since sufficient time was not available for this problem to be attacked in this way, the results are not unambiguous. However, the dominant effect was established. The results are shown in Figure 50, where the percent change in reflectance for an increment of 5×10^{14} e/sq cm is plotted versus total fluence. The points are numerically coded in the order in which they were taken. These points have been plotted versus flux as well, but a clearcut dependence on flux is not as apparent as the fluence dependence. In fact, the flux dependence is not sufficiently clear to permit the direction of the flux dependence to be determined. Points 2, 3, and 4 seem to indicate that a higher flux produces more degradation, while points 5, 6, and 7 indicate the opposite. If the points reflect flux-dependent competing processes (such as a stabilization dependent upon one type of carrier and an annealing dependent upon the other), a crossover in behavior may be occurring. Because of the importance of this point to simulation procedures, it should be further investigated.

Recovery Kinetics and Ambient Effects

Various attempts were made to obtain an analytic relationship for the recovery spectra presented earlier. In particular, the annealing of defects after irradiation, while still in a vacuum, was examined. Taking the fractional recovery as a function of time would fit neither a simple exponential annealing law nor a bimolecular model satisfactorily, even though the range of variables and number of good experimental points is not large. The curves can be fit fairly well to a $(t)^{1/2}$ plot, where t is the recovery time. The percent reflectance degradation which still needs to be recovered as a function of time (or ambient) is plotted unnormalized in Figure 51. In no case is recovery in vacuum completed. The recovery limit for electron-irradiated specimens seems to be fluence dependent. The recovery from uv exposure parallels the lower-fluence electron irradiation recovery. The behavior of the specimen which had been exposed to simultaneous uv and electron irradiation shows an inverted curvature in the recovery: at the start the recovery is slow; it then accelerates and is more rapid than the recoveries from the separate treatments. Recovery stops apparently quite abruptly at about half the degradation level, as if pinned to that value.

Upon vent-up, all specimens tend almost linearly to complete recovery, which they apparently reach in rather short order. It is particularly interesting to note that admission of oxygen, for example, <u>does not</u> make these binder specimens recover in minutes as some other pigment-binder systems apparently have done. Ultimate recovery may require an ambient

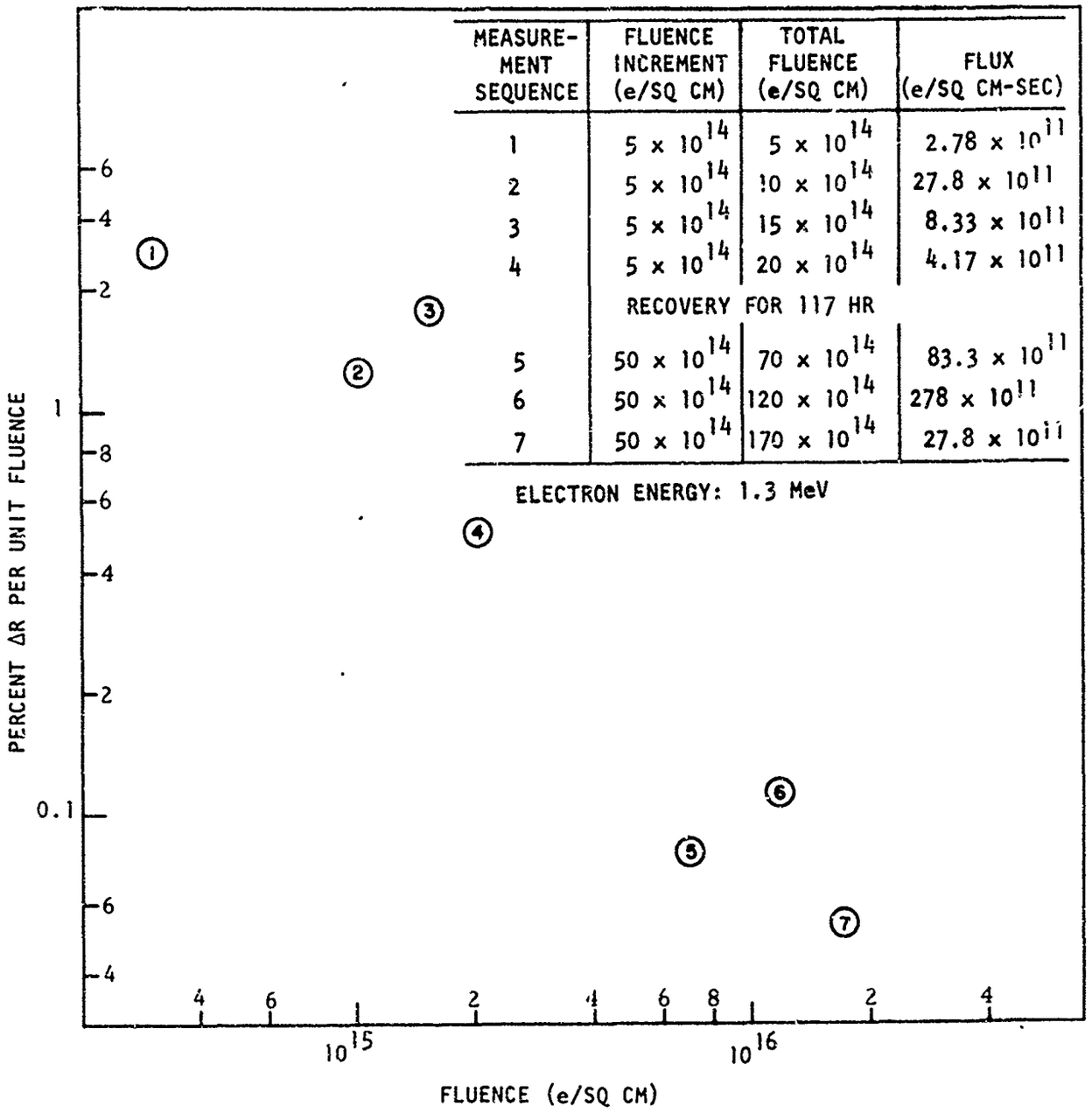

Figure 50. Degradation per Unit Fluence at 0.8 Micrometer Versus Electron Fluence; Unit of Fluence for Vertical Scale Is Taken as 5×10^{14} e/sq cm (TiOx-032-G2B, RTV Binder)

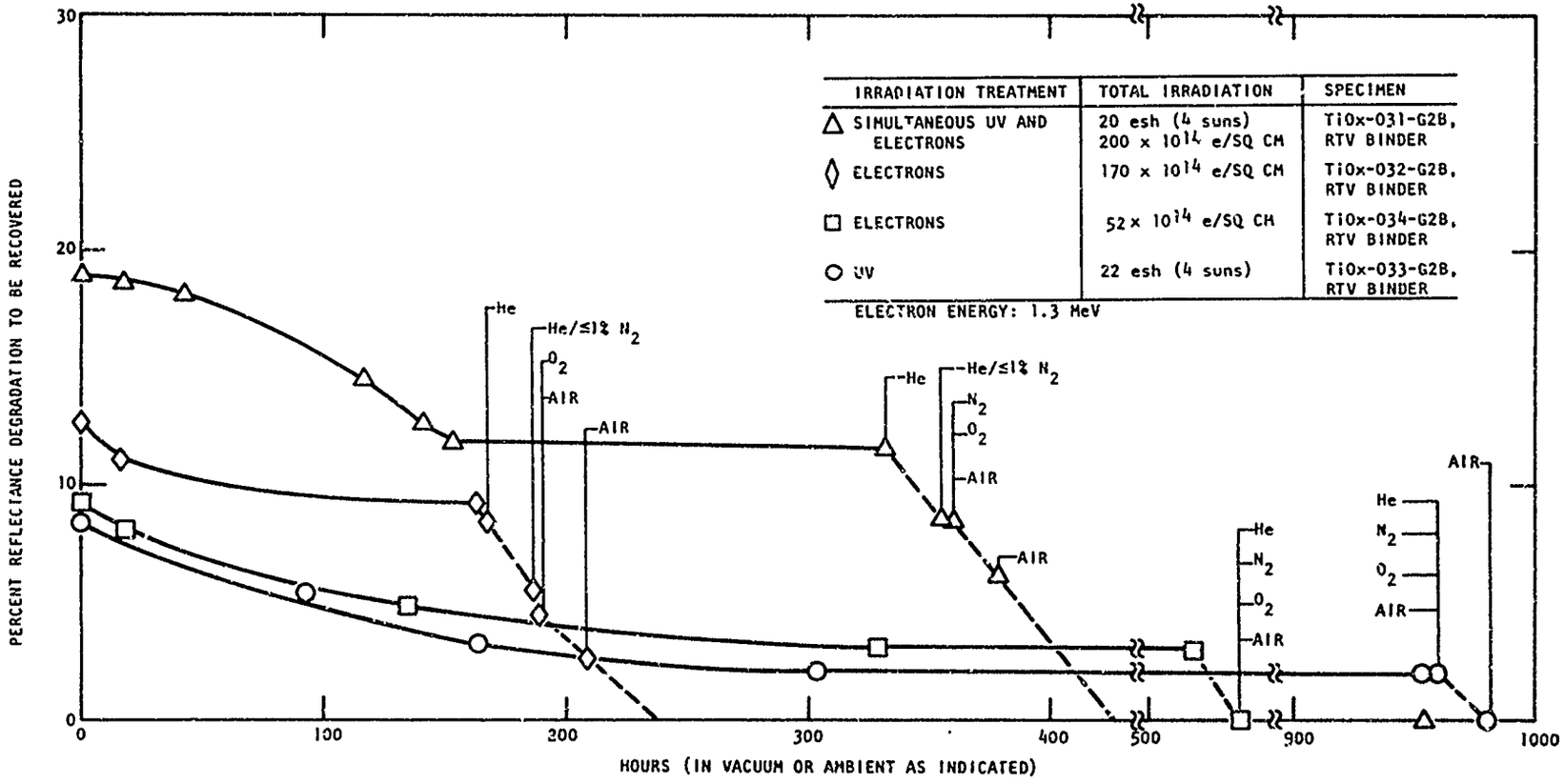

Figure 51. Percent Reflectance Degradation To Be Recovered Versus Time and Vent-Up to Various Ambients (TiOx-031-G2B, TiOx-032-G2B, TiOx-033-G2B, TiOx-034-G2B; All with RTV Binder)

oxidizing atmosphere capable of reaching effective damage centers via a diffusion process. This mechanism may be further ascertained by observing the temperature dependence of the recovery.

SECTION V

SUMMARY AND DISCUSSION

The following conclusions may be drawn from a comparison of the binderless specimens with those having binders:

1. For both types of specimens, the magnitude of the damage induced by uv exposure is much greater in the visible than in the IR. Both types of specimens show saturation behavior with uv irradiation, with the binderless specimens reaching an apparent final value of reflectance at about half the exposure necessary for the silicone binder specimens. Both types of specimens ultimately reach approximately the same saturation level.

2. The degradation induced by electron irradiation is greater at a given fluence for the TiO_2-RTV specimens than for the binderless specimens. The specimens with binders show no saturation behavior in the degradation with fluence, whereas the binderless specimens saturate at exposures below 5×10^{15} e/sq cm.

3. When simultaneously exposed to electron and uv irradiation, the specimens with binders do not show the saturation behavior found in the binderless samples. The marked synergistic effects observed with the binderless samples are not so apparent, if indeed they are present, in the samples with binders; added exposure with uv only increases the degradation by about 25 percent over that obtained with exposure to electrons only to a level of 5×10^{15} e/sq cm.

4. There is a large fluence effect in the rate of degradation for the silicone-binder samples, but the flux dependence is not as great.

5. All of the samples recover after degradation in vacuum, but the binderless samples recover more rapidly than the silicone-binder samples. In no case is the recovery in vacuum (10^{-6} torr) observed to be complete; i.e., the recovery ceases after a time. The recovery limit for electron irradiation seems to be fluence-dependent, while the recovery from uv damage parallels the lower-fluence electron recovery. The recovery from the simultaneous electron and uv exposure has a different curvature than the recovery from either exposure alone. The recovery after electron or uv exposure can be fit to a $(t)^{1/2}$ plot. Complete recovery does take place upon exposure of the specimens to air, but the recovery takes place less rapidly for the silicone-binder samples than for the binderless samples.

Perhaps the most striking aspect of the results reported here is the amount of evidence which points to the surface as one of the prominent controlling factors. The reflectance changes that occur when the binderless specimens are placed in a vacuum; the changes in reflectance, gas evolution, and low-frequency conductivity which result from heating in an inert atmosphere; and the relatively lower rate of degradation and recovery in the silicone binder samples all indicate the importance of the surface.

The fact that the degradation in binderless pigments that takes place under simultaneous electron and uv irradiation does not reach a definite saturation level is also interesting. Since the difference between the electron or the uv environment alone and the combined environment is a higher level of ionization, the lack of saturation suggests that some of the defects are stabilized by charged carrier capture. (Such a mechanism is not unknown in radiation damage processes in solids, and numerous examples can be found in reports of semiconductor studies; see, for example, Ref. 3.) Thus, the number of defects observed is enhanced as the local level of ionization increases.

However, it is probably not the ionization level alone which controls the number of defects observed, as can be seen from the flux dependence experiment. Although the flux dependence revealed by these results is not clear-cut, it has been shown that an increase in the flux level by an order of magnitude in the electron irradiation of the silicone-binder samples does not significantly increase the amount of damage per unit fluence. Thus, the fact that the surfaces of the pigments are coated by the binder apparently results in suppression of the defect stabilization by charge capture.

Based on the comparison of the degradation rates of the samples, with and without a binder, the apparently small flux dependence of the silicone-binder samples, and the lack of marked synergistic effects during simultaneous electron and uv irradiation of the samples having a binder, it can be concluded that the binder has a passivating effect on the pigment surface.

Since the study of the surface reactions is so important for determinations of the mechanisms involved in the degradation, the recovery data can be expected to yield useful information. Although not enough time was available during this investigation for a thorough study of the recovery kinetics, some information was obtained. The $(t)^{1/2}$ dependence which seems to be followed by the recoveries following either electron or uv exposure alone suggests diffusion-limited kinetics (Ref. 4). The fact that the recovery following simultaneous uv and electron irradiation does not follow such a curve suggests that diffusion of species from the surface to the defect sites is not adequate to explain the recovery in this case, and that perhaps more than one kind of annealing process is taking place. This explanation implies either multiple sinks for defects or multiple species of defects. More kinetic studies are necessary to resolve this question.

The above conclusions, based on the limited sampling of data obtained, are to be regarded as more suggestive than firm. The results obtained in this study point up the importance of a carefully controlled surface and the methods of monitoring surface reactions in mechanisms studies. These findings also suggest that a properly passivated surface may result in minimized or at least controlled degradation. The need for further studies on fluence dependence, on recovery kinetics, both in vacuum and while monitoring gas takeup, and on passivation techniques is clearly indicated.

REFERENCES

1. Compton, D. M. J., T. E. Firle, and J. T. Neu, Mechanisms of Degradation of Polymeric Thermal Control Coatings. Part I, Investigation on Degradation of Thermal Control Coating Materials, Air Force Materials Laboratory Report AFML-TR-68-334, Gulf General Atomic Incorporated, January 1969 (AD-686-448).

2. Saltsburg, H., Studies in Zinc Oxide Photoconductivity, Final Technical Report, U. S. Army Engineer Topographic Laboratories Report GA-8431, Gulf General Atomic Incorporated, December 1967.

3. Vook, F. L. (ed.), Radiation Effects in Semiconductors, Plenum Press, New York, 1968.

4. Waite, T. R., "Diffusion-Limited Annealing of Radiation Damage in Germanium," Phys. Rev. 107, 471 (1957).

APPENDIX

THEORETICAL CONSIDERATIONS

The predictability of the degradation of a thermal control coating in a radiation field hinges upon the ability to scale the relevant effects in the coating as the environment is altered. Thus, from the appropriate scaling laws, the effects of mixed environments can be predicted from a limited number of measurements in specific environments. For example, the effects of a wide range of intensities of UV plus particulate radiation of various energies can be predicted from a measurement of the effects of one intensity of UV plus electrons at a single energy. Such laws are also clearly useful in establishing simulation requirements.

To begin a formulation of such scaling laws, we make the following assumptions.

1. The stabilizing reaction for the reflectance degradation occurs at the polymer-pigment interface. Thus, charge or chemical species must be transported to the surface for degradation to occur.

2. The description appropriate to the effects of ionizing radiation on materials is the van Lint-Nichols[1] model, which states:

   a. The incident particle or photon produces a column of ionization in the material, the radius of which is approximately equal to the range of the secondary electron generated in the ionization process;

   b. The charge transport effects of the ionization depend on the total local (within the track) energy deposition and on the lifetime of the ionized particles before recombination.

Each of these assumptions is based on some physical evidence and will be further tested by future experiments to establish scaling laws.

These assumptions lead to the following picture for degradation:

GENERATION OF CARRIERS AND IONS → DIFFUSION TO SURFACE → STABILIZING REACTION AT SURFACE

For the first step, the rate of generation of carriers is given by

$$\dot{n} = \frac{\dot{Y}\,\rho}{E_p} \quad , \tag{1}$$

where

$\dot{n}$ = number of free electrons (or holes) generated per unit volume per sec,

$\dot{Y}$ = rate of energy deposition per gram from the irradiating beam,

E_p = average amount of energy lost by the irradiating particle in producing an electron-hole pair,

ρ = density.

The rate at which the charges (assumed for the sake of argument to be holes) reach the surface is

$$\dot{N}_s = \int dV\, \dot{n}(\vec{r})\, P(\vec{r},L) \quad , \tag{2}$$

where

$P(\vec{r},L)$ = probability that a carrier generated at the point $\vec{r}$ will reach a surface,

L = diffusion length for hole.

The arguments given for the functions in Eq. 2 emphasize the fact that both $\dot{n}$ and P are functions of position. The diffusion length is a function of the free-carrier lifetime. The lifetime is determined by the occupancy of the charge-capturing centers in the vicinity of the free carrier. Local ionization generated by an irradiating particle or photon changes the occupancy of some of the traps which are within a secondary electron range of the path of the ionizing particle or photon. This occupancy change persists for some time (called the trap relaxation time) before the trap reverts to normal (by emitting the captured carrier or by capturing a carrier of the opposite type). Thus, the lifetime of a free carrier and, hence, its probability of escape to the surface depend on the total local dose deposited in times comparable to the trap relaxation time.

Let us now consider a single region of either pigment or binder. For an irradiating particle whose range is much greater than the distance between

binder-pigment interfaces, the energy deposition in a region between interfaces is uniform and

$$\dot{N}_s = \frac{\rho \dot{Y}}{E_p} \int dV \, P(\vec{r},L) \quad . \tag{3}$$

For irradiation which is more strongly absorbed

$$\dot{n} = \frac{1}{E_p} \frac{dE}{dx} \quad , \tag{4}$$

where E is the energy flux. If we can write

$$E = E_o \, e^{-\alpha(E) \, \vec{k}\cdot\vec{r}} \quad , \tag{5}$$

where

$\alpha(E)$ = absorption coefficient per unit path length,

$\vec{k}$ = propagation vector of the irradiating particles,

E_o = incident energy flux,

then

$$\dot{N}_s = \frac{1}{E_p} \int dV \, e^{-\alpha(E)(\vec{k}\cdot\vec{r})} \, P(\vec{r},L) \quad . \tag{6}$$

To evaluate $P(\vec{r},L)$, consider an ionization event at the point $\vec{r}$. Assume that the electron is rapidly trapped, but that the hole follows a random walk until it is either captured by a hole trap in the bulk or reaches the surface.

In a random walk in a cubic crystal, a particle travels a vector distance R after n jumps, each a distance λ, where

$$R = \sqrt{n} \, \lambda \quad , \tag{7}$$

The time required to make n jumps is

$$t = \frac{n}{\Gamma} \quad ,$$

where Γ is the jump frequency. Each jump in the random walk for a carrier begins and ends with a carrier-scattering event. A reasonable time to take as the time between scattering events is the mobility relaxation time τ, which is related to the mobility through

$$\mu = \left(\frac{e}{m}\right) \tau \quad , \tag{8}$$

where μ is the mobility and e/m is the charge-to-mass ratio. Thus, the time to make n jumps is

$$t = \frac{n\mu m}{e} \quad ,$$

or, using (7),

$$t = \frac{R^2}{\lambda^2} \frac{\mu m}{e} \quad . \tag{9}$$

The probability that a carrier will "walk" for a time t is $\exp[-t/\tau_h]$ where τ_h is the bulk hole lifetime. Thus, the probability that the hole will "walk" a distance R is

$$P_R = \exp - [(R^2/\lambda^2)(m/e)(\mu/\tau_h)] \quad . \tag{10}$$

It is of interest to evaluate the "e-folding" distance for this probability. We do this in the following way. From Eq. A8, λ can be computed.

$$\mu = \frac{e}{m} \frac{\tau}{v} = \frac{e}{m} \frac{\lambda}{\sqrt{3\ kT/m}} \quad , \tag{11}$$

where v is the thermal velocity. Measurements on single crystals indicate that a mobility of 10 cm^2/volt-sec can be considered typical for materials

of interest for thermal control applications. Then $\lambda = 6.7$ Å at 300°K. The hole-trapping time is estimated from

$$\tau = \frac{1}{Nv\sigma} \quad , \tag{12}$$

where N is the concentration of trapping centers, σ is the hole capture cross section, and v is the thermal velocity. Taking $N = 10^{18}$ (approximately 20 ppm hole traps), $\sigma = 10^{-15}$ cm^2, and $v = 10^7$ cm/sec (300°K), we have

$$\tau = \frac{1}{10^{18} \cdot 10^{7} \cdot 10^{-15}} = 10^{-10} \text{ sec} \quad .$$

Then the "e-folding" distance is

$$R = (\lambda^2 \epsilon \tau_n / m\mu)^{\frac{1}{2}} \quad ,$$

which is 880 Å for the above parameters. Harrity[2] computes 1040 Å for the average trapping distance in single crystal Al_2O_3 from electrical conductivity data, so the agreement with experiment is reasonable.

This formulation contains the possibility of synergistic effects, since the probability that a hole will reach the surface does depend upon the degree of ionization it encounters in its diffusive path. As pointed out in Ref. 1, the mean carrier lifetime is determined by the ionization density in the path of the irradiating particle and not by the average ionization density throughout the crystal. At low doses and dose rates where the paths of two irradiating particles do not overlap in a time comparable to the trap relaxation time, one path does not influence the other and the effects of different paths are additive. At higher doses, the trapped carriers in one path may change the trap occupancy for a subsequent path that traverses the same region. Hence, the response to a given dose rate may change as the dose accumulates. In addition, the formulation accounts for the fact that the more strongly absorbed radiations produce more carriers near the surface.

These considerations allow us to write Eq. 3 in a simpler form

$$\dot{N}_s = F(\gamma,s)\ \dot{\gamma} \quad , \tag{13}$$

where

F = an empirical function which is a constant at low doses,

γ = dose received in a trap relaxation time,

s = ratio of ionization per unit length produced by irradiating particle to ionization per unit length of high-energy electron or gamma ray (called the specific ionization).

Thus, for highly penetrating radiation, the number of holes reaching the surface is linear in dose rate for dose rates such that the mean time for track overlap exceeds the trap relaxation time. At higher dose rates, the function F must be evaluated empirically.

The next steps to be taken in the development of the scaling laws are to:

1. Take a suitable integral over the particle volume to compute the probability that the particle reaches the surface. This integral need not be evaluated completely, but the dependence on particle size should be determined.

2. Carry out an evaluation of the effect of previous irradiation on τ_h, since each electron created becomes a hole trap.

3. Perform an approximate calculation of the energy absorption for the evaluation of Eq. 6. This brings us to light-scattering theory. A semi-empirical approach, such as the one taken by the workers at Hughes Aircraft Company,[3] seems most promising on a short term.

4. Account for the possibility of rate-limiting at the surface.

The development of approximate scaling laws which are based on a fundamental understanding of the physical processes occurring in the pigments and which are useful for practical prediction does not seem to be an insurmountable or interminable task.

REFERENCES

1. van Lint, V. A. J., and D. K. Nichols, IEEE Trans. Nucl. Sci. NS-13, 119 (1966).

2. Harrity, J. H., Radiation Effects in Dielectric Materials, Final Report on Contract DAAB07-69-C-0033, U.S. Army Electronics Command Report TR-ECOM-0033-F, Gulf General Atomic Incorporated, December 1969.

3. Levin, H., V. Harrold, and C. Berggren, Study of Color Center Formation in White Powder Compounds, National Aeronautics and Space Administration Report NASA-CR-73337, Hughes Aircraft Company, July 1969.

ACKNOWLEDGMENTS

The research was under the direction of Dr. D. M. J. Compton from 1 September 1968 until his resignation from Gulf General Atomic in May 1969. After 5 May 1969, the work was directed by Dr. T. M. Flanagan, with Dr. Compton serving as consultant for the remainder of the research.

Under a subcontract, irradiations and measurements utilizing in-situ apparatus were performed by General Dynamics, Convair Division, under Gulf General Atomic direction. This work was supervised by Dr. J. T. Neu; most of the irradiations were carried out by R. T. Murray, who was responsible for the Convair accelerator facility.

The major portion of the Gulf General Atomic experiments were implemented and executed by B. D. Kitterer, who also participated in some of the design aspects and data reduction of this investigation.

UNCLASSIFIED
Security Classification

DOCUMENT CONTROL DATA - R & D

(Security classification of title, body of abstract and indexing annotation must be entered when the overall report is classified)

1 ORIGINATING ACTIVITY (Corporate author)	2a. REPORT SECURITY CLASSIFICATION
Gulf General Atomic Incorporated P. O. Box 608 San Diego, California 92112	Unclassified 2b. GROUP

3 REPORT TITLE

MECHANISMS OF DEGRADATION OF POLYMERIC THERMAL CONTROL COATINGS.
PART II, EFFECTS OF RADIATION ON SELECTED PIGMENTS

4 DESCRIPTIVE NOTES *(Type of report and inclusive dates)*

Final report for the period 1 September 1968 through 30 November 1969

5 AUTHOR(S) *(First name, middle initial, last name)*

Tomas E. Firle and Terry M. Flanagan

6. REPORT DATE	7a. TOTAL NO. OF PAGES	7b. NO. OF REFS
December 1969	104	4

8a. CONTRACT OR GRANT NO.	9a. ORIGINATOR'S REPORT NUMBER(S)
F33615-69-C-1055 b. PROJECT NO.	GA-9853
c.	9b. OTHER REPORT NO(S) *(Any other numbers that may be assigned this report)*
d.	AFML-TR-68-334, Part II

10 DISTRIBUTION STATEMENT

This document has been approved for public release and sale; its distribution is unlimited.

11 SUPPLEMENTARY NOTES	12. SPONSORING MILITARY ACTIVITY
	Air Force Materials Laboratory Air Force Systems Command Wright-Patterson AFB, Ohio 45433

13. ABSTRACT

An investigation has been conducted on the mechanisms of degradation of pigments and polymeric coatings for thermal control applications exposed to ultraviolet (uv) and electron irradiation. The materials investigated were rutile (titanium dioxide) and strontium titanate ($SrTiO_3$). The effects of treating the pigments by heating in various gas ambients at elevated temperatures were studied using gas chromatography and electrical conductivity measurements. Significant changes in the surface characteristics were found to result from these treatments. A comparison was made between the reflective degradation in binderless pigments and silicone-binder coatings exposed to uv light, to energetic electrons, and simultaneously to uv light and electrons. Evidence for stabilization of defect sites by charge capture was discovered in the binderless pigment experiments. This mechanism for defect stabilization does not appear as prevalent in the silicone-binder coatings, since the binder apparently passivates the pigment surface to some extent. The fluence dependence of the degradation and the recovery of the damage in vacuum and in the presence of various gas ambients was also studied.

DD FORM 1 NOV 65 1473

UNCLASSIFIED
Security Classification

14 KEY WORDS	LINK A		LINK B		LINK C	
	ROLE	WT	ROLE	WT	ROLE	WT
Thermal control coatings						
Ultraviolet						
Titanium dioxide						
Strontium titanate						
Optical degradation						
Electron irradiation						
Chemical reduction						
Carbon dioxide						
Adsorption						
Desorption						
Electrical conductivity						
Annealing						